UNIVERSITY OF LONDON
IMPERIAL COLLEGE OF SCIENCE AND TECHNOLOGY
DEPARTMENT OF CHEMISTRY

Gas Scattering from Metal Surfaces

by

Karol Senkiw, B.Sc

Submitted for the Degree of Doctor of Philosophy
JUNE 1979

ABSTRACT

The scattering of a helium beam from the (110) surface of a tungsten single crystal has been investigated under various surface conditions. Auger Electron Spectroscopy (AES) and Low Energy Electron Diffraction (LEED) were used to characterize surfaces. The spatial distribution of the scattered gas from the clean surface showed a sharp, intense specularly reflected beam but following the adsorption of overlayers of oxygen on the surface the spatial distribution changed markedly yielding several well-defined peaks. Analysis of the scattering data showed that thepositions of these peaks were consistent with a diffractive process. The symmetries of the adsorbed overlayers were obtained by LEED and could be compared to the symmetries indicated by the atom scattering data. For low coverage oxygen layers, having p(2x2), p(2x1) and (1x1) overlayer structures, agreement between the two sets of results is clearly observed but for more complicated overlayer structures the complexity of the scattering distributions makes comparison more difficult.

A small number of experiments were performed using deuterium as the incident gas. Elastic diffractive scattering was again observed from overlayer structures but additional structure appeared in the angular distributions which is tentatively attributed to scattering in which there is energy transfer between translational and rotational modes of the deuterium molecule. In helium scattering inelastic processes are confined to energy transfer between the translational modes of the helium and the vibrational modes of the solid. Some indication that such processes do occur can be obtained from the scattering distributions.

ACKNOWLEDGEMENTS

I wish to thank the Chemistry Department, Imperial College for the provision of laboratory facilities and the Science Research Council for the award of a research studentship.

I wish to thank in particular my supervisor, Dr D.O. Hayward, for his guidance and encouragement throughout the course of this work. I am also indebted to Mr Bernard Hanks for the expert advice he gave during the design of the molecular beam system. I should also like to thank the technical staff of the Chemistry Department for their assistance in the construction of parts of the apparatus.

Finally I wish to express my gratitude to Miss T. Richardson for her careful and excellent typing of the manuscript.

Karol Senkiw

C O N T E N T S

		Page No:
Abstract		2
Acknowledgements		3
Chapter 1:		7
1.1	INTRODUCTION	7
Chapter 2:	NOTATION AND BASIC PRINCIPLES	12
2.1	Scattering Geometry and Diffraction	12
2.2	The Interaction Potential	15
2.3	Quantum Theory of Scattering	18
2.4	The Debye-Waller Factor	20
Chapter 3:	LITERATURE SURVEY	23
3.1	Experimental	23
3.2	Theoretical	33
Chapter 4:	EXPERIMENTAL	37
4.1	The Apparatus	37
	The Work Chamber	39
	(i) General	39
	(ii) The Substrate Assembly	39
	(iii) The Detector System	42
	The Molecular Beam Section	44
	(i) The Service Well	46
	(ii) The Dosing Line	47
4.2	Experimental Procedures	50
	(i) Attainment of Ultra High Vacuum	50
	(ii) Measurements of Low Pressures	50
	(iii) Target Preparation and In Situ Cleaning	52
	(iv) The Gas Scattering Experiment	54

		Page No:
Chapter 5:	MOLECULAR BEAM GENERATION	58
5.1	Introduction: Outline of Nozzle Source Arrangement	58 60
5.2	An Outline of Nozzle Beam Theory	60
	(i) Beam Energy	60
	(ii) Beam Flux	65
Chapter 6:	SURFACE CHARACTERIZATION	66
6.1	Introduction	66
6.2	Basic Principles of LEED	66
6.3	The LEED System	69
6.4	The Auger Process: Basic Principles	71
6.5	The Auger Electron Spectrometer	75
Chapter 7:	RESULTS	77
7.1	Preparation of Ordered Surface Layers	77
	(i) Ordered Carbon Overlayers (ii) Ordered Oxygen Overlayers	84 84
7.2	Scattering on Clean and Contaminated Surfaces	87
7.3	Scattering from the Carbide Surface	90
7.4	Helium Scattering from Adsorbed Oxygen Layers	96
7.5	Deuterium Scattering from Ordered Oxygen Layers	107
7.6	Helium Scattering from High Coverage Oxygen Layers	112
Chapter 8:	DISCUSSION	115
	(i) Helium on Clean Metals	115
	(ii) Helium, Deuterium and Neon on Carbided Surfaces	119
	(iii) Helium Scattering from Oxygen Covered Surfaces	124
	(iv) Inelastic Effects in Helium Scattering	126

		Page No:
Chapter 8:	(v) Analysis of Inelastic Interactions of Helium	130
	(vi) Inelastic Scattering of Molecular Deuterium	134
	Summary	138
References		141

CHAPTER ONE

INTRODUCTION

1.1

As a result of improvements in vacuum technology there has been in the last two decades a vast amount of research performed into many aspects of surface physics and chemistry. Much of this research has been devoted to developing surface analytical methods, which for the most part identify the chemical constituents of the surface layers of a material, e.g. Auger Electron Spectroscopy (AES), X-ray Photoelectron Spectroscopy (XPS) and Appearance Potential Spectroscopy (APS). Other techniques, principally Low Energy Electron Diffraction (LEED), yield information on the surface geometry of materials.

The work described in this thesis was primarily an investigation of the scattering of helium atoms by a W(110) surface. This type of experiment is commonly called a molecular beam scattering experiment. Investigations of this type consist essentially of observing the spacial distribution of a well-defined incident beam of atoms/molecules which have been scattered by a target. Experiments of this type have become more frequent during the past decade without becoming as commonplace or routine as AES, LEED or XPS studies. The reasons for this are essentially that the vacuum requirements are probably more stringent than for most other studies and also that any successful

molecular beam investigation really requires one or more surface analytical techniques to be available in order to properly define experimental conditions. It may be said therefore that molecular beam scattering experiments are still in their infancy.

The observations made in the course of this work are a continuation of the molecular beam experiments of my predecessors in this laboratory (Chappell 1971, Walters, 1973). The actual aims of the experiments and indeed the apparatus on which the observations were made,were however totally different. My predecessors both used an all glass vacuum system. Their results, in keeping with other results of the same period (reviewed by Smith 1974),demonstrated the need to have surface analytical techniques available. At the commencement of this study therefore it was decided to design and have built a stainless steel vacuum system incorporating LEED and AES facilities. A further change in technique was made in order to improve the energy spread in the incident beam. Chappell and Walters had both used an oven source yielding a Maxwellian distribution of velocities in their incident beams and it had been recognised for some time that this situation could be improved upon with the aid of a nozzle source (Anderson, 1965). This procedure demanded a much larger pumping capacity in the molecular beam chambers, a problem which is far more easily coped with in a stainless steel system than in a glass system. Descriptions of the vacuum chamber and molecular beam arrangement are given in Chapters 4 and 5.

The aim of the present study was to observe the scattering of gases from a metal surface; W(110) was in fact chosen as the target. The work of Walters and Chappell and others (reviews of Smith 1974, Toennies 1974) had demonstrated that apparently clean metal targets did not give rise to diffraction phenomena for incident beams of gas atoms/molecules under the available experimental conditions, which generally involved the use of Maxwellian incident beams and targets at room temperature or above. While at the onset of this work it was not thought that diffraction would be found from a clean W(110) target it was felt that diffraction phenomena could occur from ordered overlayers. Merrill and Weinberg (1971) had reported this phenomena for a surface carbide grown on a W(110) crystal during the cleaning procedure. In particular it was felt that ordered adsorbed layers of oxygen on W(110) would be an adsorbate system worthy of study. This system had been studied by many workers using a variety of techniques (see Chapter 7) and was known to give rise to a number of different overlayer structures at coverages less than one monolayer.

An important factor in the scattering of thermal energy atom beams is that the incident atoms cannot penetrate below the surface of the target. This should make the technique sensitive only to the surface and should not involve any averaging of surface properties over several layers, as is the case with electron spectroscopies and LEED. The implications of this are further discussed in

Chapters 8 and 9. Molecular beam scattering experiments may also be capable of yielding information concerning surface vibrations.

Perhaps the most important aspect of gas-surface scattering experiments is that they are used to determine the gas-surface interaction. An outline of the manner in which this may be achieved is given in the following chapter. This chapter also contains brief details on the mathematical notation and approaches used in quantum mechanical descriptions of the gas-surface interaction. It is generally accepted that a quantum mechanical theory is desirable in order to explain the scattering of atoms by surfaces, although qualitative agreement with the results of gas/metal systems has been achieved by using classical methods. As the gas-surface interaction gives rise to strong scattering the first-order distorted wave Born approximation (kinematic theory) has been shown to be inappropriate in gas-surface scattering. Solutions of the Schrödinger equations must be sought via more powerful numerical methods.

As was remarked earlier, molecular beam scattering experiments, both practically and theoretically, are at an early stage. Many improvements are still to be made in improving experimental techniques, especially in the energy analysis of both incident and scattered beams. Many concepts utilised in the discussion of gas-scattering experiments, e.g. Debye-Waller factors and coherence widths, have been introduced following their use in LEED, neutron scattering and X-ray scattering but the appropriate-ness of these concepts in gas-surface scattering analysis

is not at present fully confirmed. In order for improved methods to develop in gas-scattering experiments it would appear that an expansion in the range of systems studied must first take place. To date the bulk of the detailed research has been directed toward the helium/alkali halidesurface systems. It is hoped that the study outlined in the present work will provide an indication of the wide range of situations that may be studied.

CHAPTER TWO

NOTATION AND BASIC CONCEPTS

2.1 Scattering Geometry and Diffraction

The scattering geometry is outlined in Figure (2.1). The surface is assumed to consist of a periodic array of atoms.

Elastic diffraction by a periodic surface can be described by the two conservation laws:-

$$\text{(i)} \quad \frac{\hbar^2 k_i^{\,2}}{2m} = \frac{\hbar^2 k_f^{\,2}}{2m} \qquad \text{Conservation of Energy} \qquad (2.1)$$

$$\text{(ii)} \quad \underline{K}_f = \underline{K}_i + \underline{G} \qquad \text{Conservation of Parallel Momentum} \qquad (2.2)$$

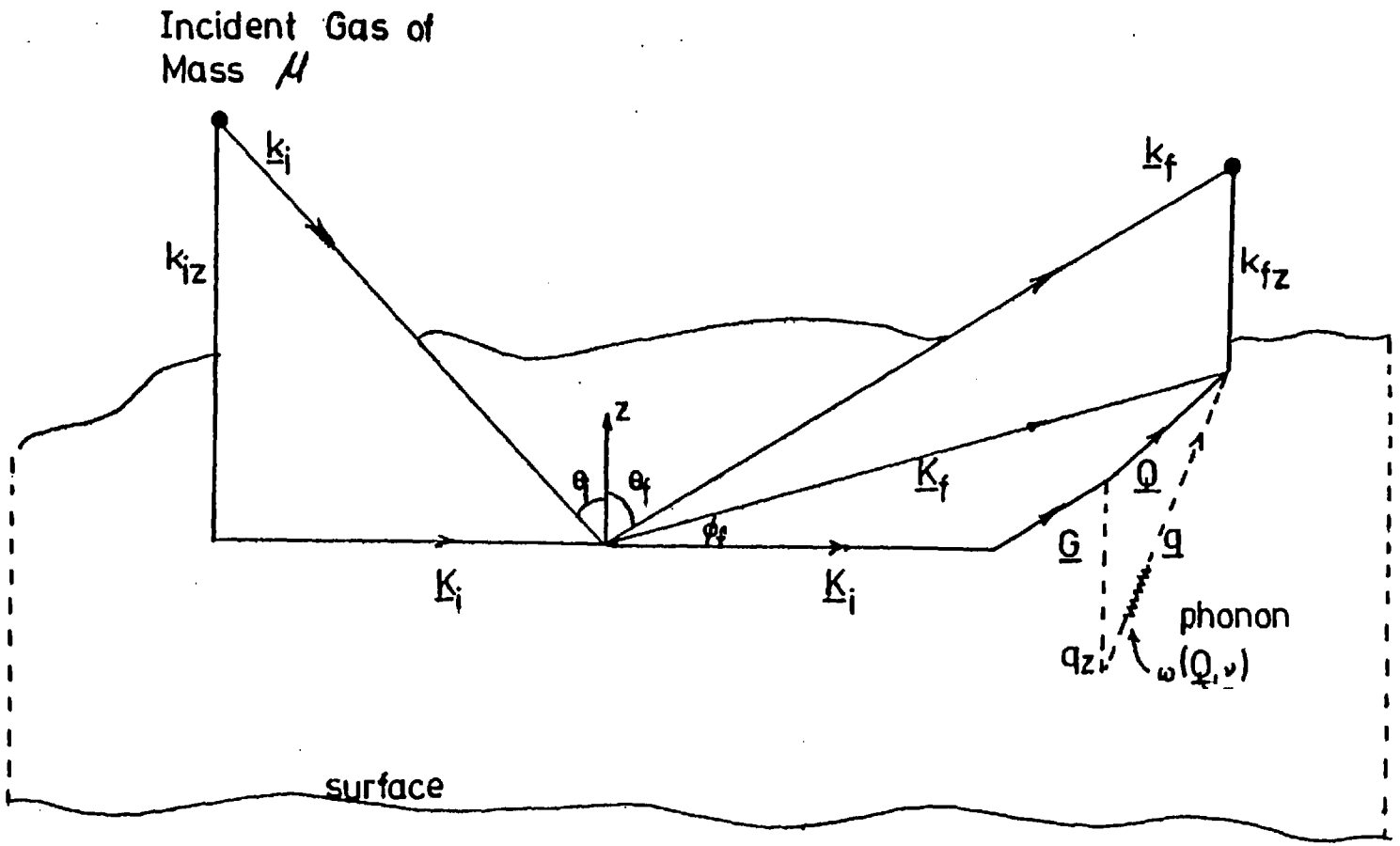
where $\underline{k}_i$ is the incident wave vector

$\underline{k}_f$ is the scattered wave vector

$\underline{K}_i, \underline{K}_f$ are the projections of these wave vectors in the surface plane

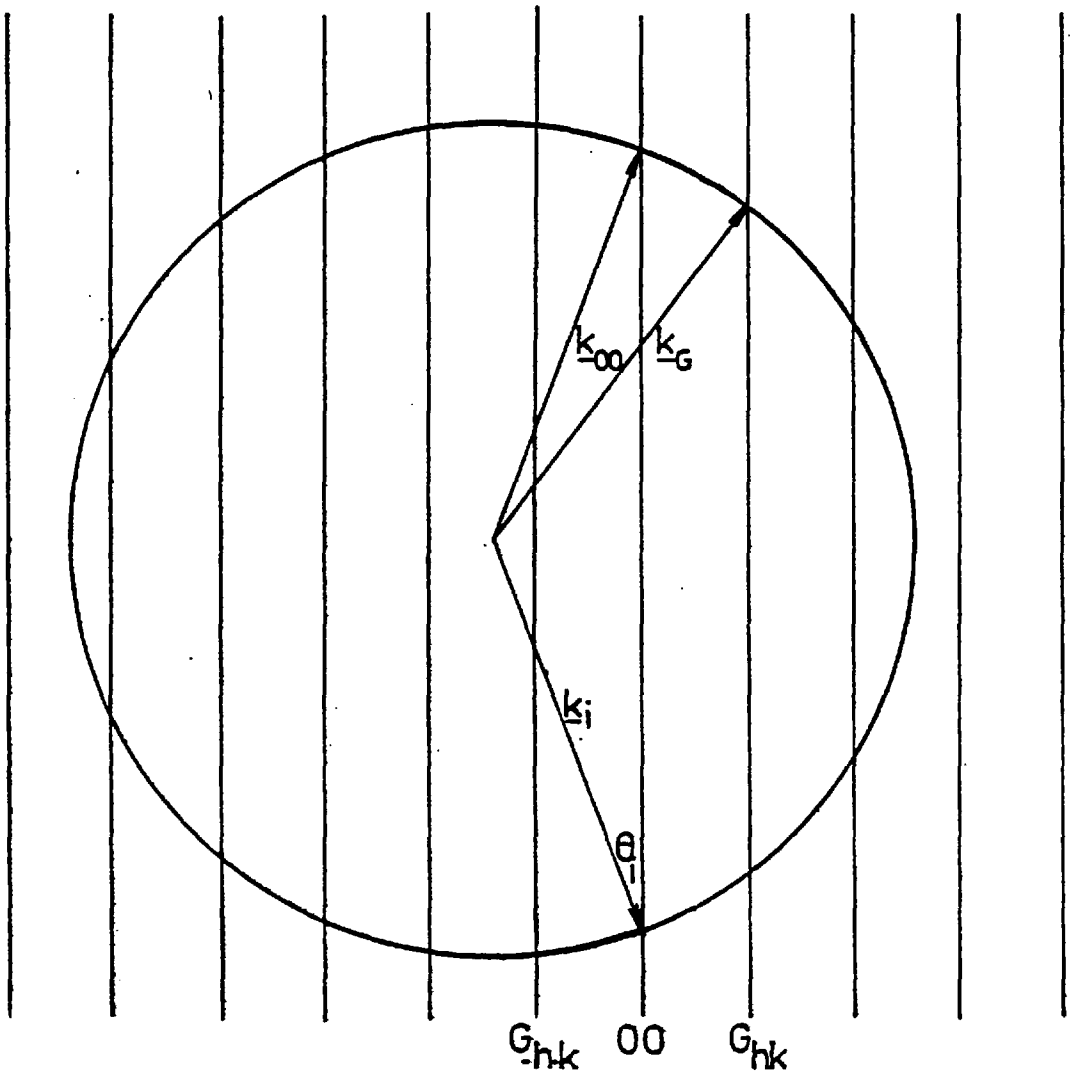
$\underline{G}$ is a surface reciprocal lattice vector.

As in the case of x-ray, neutron and electron scattering the diffraction conditions can be depicted by an Ewald construction. Scattering by a two-dimensional lattice removes restrictions on diffraction in the plane perpendicular to the surface, as is shown by equation 2.2, therefore the diffraction conditions are fulfilled by considering the intersection of the Ewald sphere with rods drawn in reciprocal space and not with reciprocal



SCATTERING GEOMETRY

FIG. 2.1



EWALD CONSTRUCTION
FOR $\theta_i = 20°$

FIG. 2.2

lattice points. This construction is drawn in Figure (2.2). The circle has radius $|\underline{k}_i|$ and the reciprocal lattice rods are separated by the distance $\frac{2\pi}{d}$, where d is the row spacing.

2.2. The Interaction Potential

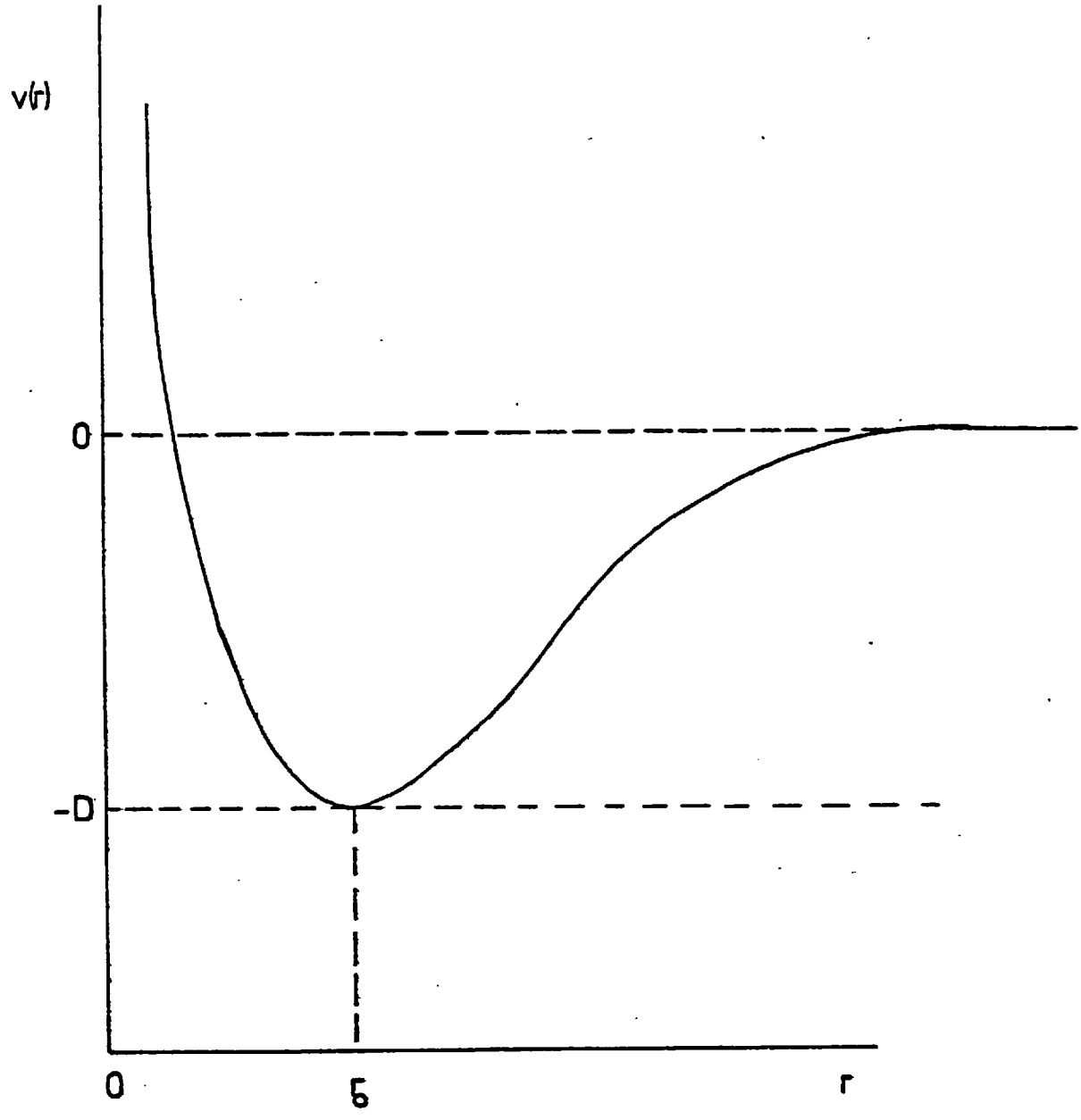
In the neighbourhood of a surface a gas molecule experiences forces originating from the electromagnetic interactions of the nuclei and electrons. The interaction energy V(R,z) will determine the scattering properties of the system. For a gas atom, of incident energy E, and a perfectly rigid crystal surface the Schrödinger equation may be written as

$$\left| -\frac{\hbar^2}{2\mu} \nabla^2 + V(\underline{R},z) - E \right| \psi(\underline{R},z) = 0 \qquad (2.3)$$

In calculating the scattering properties of a system it is necessary to propose an interaction potential. The precise nature of interaction potentials are unknown, although it is recognised that at 'long range' atoms attract one another and at 'short range' they repel one another. This situation is indicated in the interaction potential curve shown in Fig. (2.3).

For a pair of single neutral atoms a non-vanishing force of attraction exists at long range which can be described by a potential energy relationship of the form

$$\phi(r) = \frac{-c}{r^6} - \frac{c'}{r^8} - \frac{c''}{r^{10}} \qquad (2.4)$$



THE INTERACTION POTENTIAL ENERGY CURVE V(r) FOR TWO ATOMS WHOSE CENTRES ARE SEPARATED BY A DISTANCE r

FIG. 2.3

where c, c', c'' are constants. The first term arising from instantaneous dipole-dipole interaction, the second from the instantaneous dipole-quadrupole interaction and the third from instantaneous quadrupole-quadrupole interaction.

At 'short range' the overlap of the electron clouds produces a repulsive interaction obeying an exponential law such as

$$\phi(r) = D \exp(2a(r_0-r)) \text{ where } r/r_0 \ll 1 \qquad (2.5)$$

D is a positive energy,

a is a positive parameter, of dimension length^{-1}

It is customary to calculate the potential energy of a gas atom near a solid surface by summing the pairwise potentials $v(\underline{r})$ of the solid, viz.

$$V(\underline{r}) = \sum_j v(|\underline{r}-\underline{r}_j|) \qquad (2.6)$$

where $|\underline{r}-\underline{r}_j|$ is the distance from the gas atom to the j^{th} solid atom.

The validity of this expression is questionable, especially for metals, which have conduction electrons. For a surface showing perfect periodicity in the x and y directions the gas-surface interaction can be expressed in a Fourier expansion.

$$V(\underline{r}) = \sum_{\underline{G}} V_{\underline{G}}(z) \exp(i\underline{G}.\underline{R}) \qquad (2.7)$$

where $\underline{R}$ is a vector in the surface such that

$$\underline{r} = (\underline{R}, z) \tag{2.8}$$

One important aspect of gas scattering experiments is that they are capable of yielding information concerning the interaction potential. An outline of the manner in which this information is obtained is given in a later section.

2.3. Quantum Theory of Scattering

This section outlines the general approach of the present day quantum-mechanical treatments. A brief description is given of the formulation of some basic equations but there is no detailed discussion of how these equations are solved. The discussion is limited to elastic scattering from a periodic surface.

The Schrödinger equation

$$H\psi = E\psi \tag{2.9}$$

can be written in the form

$$\left| -\frac{\hbar^2 \nabla^2}{2\mu} + V(\underline{r}) \right| \psi(\underline{r}) = \frac{\hbar^2 k^2}{2\mu} \psi(\underline{r}) \tag{2.10}$$

where $V(\underline{r})$ and $\psi(\underline{r})$ may both be expanded as shown in equation (2.7) and below

$$\psi(\underline{r}) = \sum_{\underline{G}} \psi_{\underline{G}}(z) \exp[i(\underline{G}+\underline{K}).\underline{R}]. \tag{2.11}$$

Substitution and rearrangement gives the set of equations

$$\left|\frac{d^2}{dz^2} + k_{\underline{G}z}^2 - \frac{2\mu}{\hbar^2} V_0(z)\right| \psi_{\underline{G}}(z) = \frac{2\mu}{\hbar^2} \sum_{\underline{G}' \neq \underline{G}} V_{\underline{G}-\underline{G}'}(z) \psi_{\underline{G}'}(z) \tag{2.12}$$

where

$$k_{\underline{G}z}^2 = k_i^2 - (\underline{K}+\underline{G})^2. \tag{2.13}$$

As $z \to \infty$, the interaction potential is nearly zero, hence for all $\underline{G}$'s

$$(\frac{d^2}{dz^2} + k_{\underline{G}z}^2)\psi_{\underline{G}}(z) = 0. \tag{2.14}$$

The solutions of this equation are

(i) $$\psi_{\underline{G}}(z) \xrightarrow{z\to\infty} k_z^{-\frac{1}{2}} \exp(ik_z z)\delta_{\underline{G},0} + k_{\underline{G}z}^{-\frac{1}{2}} A_{\underline{G}} \exp(ik_{\underline{G}z} z) \tag{2.14a}$$

for all $\underline{G}$'s with $k_{\underline{G}z}^2 > 0$, i.e. the open channels.

(ii) $$\psi_{\underline{G}}(z) \xrightarrow{z\to\infty} \kappa_{\underline{G}z}^{-\frac{1}{2}} A_{\underline{G}} \exp(-\kappa_{\underline{G}z} z) \tag{2.14b}$$

for all $\underline{G}$'s with $k_{\underline{G}z}^2 < 0$, i.e. the closed channels $\kappa_{\underline{G}z} = (-k_{\underline{G}z}^2)^{\frac{1}{2}}$.

Various computational techniques have been devised to calculate the $A_{\underline{G}}$ terms from which the diffraction intensities $P_{\underline{H}}$ can be obtained, where $\underline{H}$ is a member of the set of reciprocal lattice vectors $\underline{G}$ obeying condition (i). The $P_{\underline{H}}$ are related to the $A_{\underline{H}}$ terms by

$$P_{\underline{H}} = |A_{\underline{H}}|^2 \tag{2.15}$$

For elastic scattering $\sum_{\underline{H}} P_{\underline{H}} = 1$ the unitary condition (2.16)

A summary of the quantum-mechanical treatments of the atom-surface scattering phenomena is given in the

historical section.

The presence of the potential well ensures that there will be at least one eigenenergy E_n in the range $0>E_n>-U$. When one of the bound states has this value, E_n, associated with its motion in the z direction then

$$\frac{\hbar^2 k_{Gz}^2}{2\mu} = E_n \qquad (2.17)$$

and 'selective adsorption' occurs (Lennard-Jones and Devonshire, 1935). This phenomena is observed experimentally as a variation in the scattered intensities of diffracted beams with change in incident energy, incident angle or azimuthal angle. These variations show sharp minima and maxima. A knowledge of the eigenvalues E_n of a potential subsequently allows the interaction potential to be determined.

2.4. The Debye-Waller Factor

The Debye-Waller factor is used to estimate the total fraction of the scattering cross-section that is elastic, i.e. it accounts for inelastic collisions due to the thermal motion of the lattice. In earlier experiments this factor has been used to estimate surface Debye temperatures. The account given here makes use of the relationships established from x-ray, electron and neutron scattering experiments, but as will be seen in the discussion of scattering from clean metal surfaces (Chapter Eight) these relationships are not conclusively established in gas-surface scattering.

The Debye-Waller factor is defined as $\exp(-2w)$

where $2w = \langle(\Delta\underline{k}.\underline{u})^2\rangle$ (2.18)

$\Delta\underline{k} = \underline{k}_f - \underline{k}_i$ being the total momentum transferred to the crystal

$\underline{u}$ is the displacement vector

$\langle\ \rangle$ represents a thermal average.

Normally $\underline{u}^2$ is averaged rather than $(\Delta\underline{k}.\underline{u})^2$ with the result that

$$2w = [\Delta k_z(\theta_i,\theta_f)]^2 \langle u_z^2(T_s)\rangle \tag{2.19}$$

In the specular case the momentum transferred might be expected to be $2k_{iz}$, however Beeby (1971) has shown that it is probably necessary to account for the acceleration of the gas-atom by the attractive well of the interaction potential. Assuming only the normal component of motion is affected

$$(\Delta k_z)^2 = \frac{8\mu E_i}{\hbar^2}\left(\cos^2\theta_i + \frac{D}{E_i}\right) \tag{2.20}$$

where D is the well depth

$\langle u_z^2\rangle$ is generally calculated from a Debye continuum model, with a characteristic temperature θ_c

$$\langle u_z^2\rangle = (3\hbar^2/2M_s k_B\theta_c)\int(\theta_c/T_s) \tag{2.21}$$

In the high temperature limit $\langle u_z^2\rangle = \dfrac{3\hbar^2 T_s}{M_s k_B \theta_c^2}$ (2.22)

Combining (2.20) and (2.22)

$$2w = \frac{24\mu E_i T_s}{k_B \theta_c^2 M_s} \left(\cos^2\theta_i + \frac{D}{E_i}\right) \qquad (2.23)$$

If the above derivations were realistic it would be expected that gas surface scattering would prove to be more useful in investigating mean square displacements of surface atoms than LEED where multiple scattering and the effects of several surface layers will have to be accounted for.

CHAPTER THREE

LITERATURE SURVEY

3.1. Experimental

Detailed accounts of previous molecular beam work can be found in an article by Senkiw & Hayward (1979) and in a previous Ph.D. thesis (Walters, 1973). Other general reviews of gas-surface scattering have been given by Smith (1973), Toennies (1974) and Somorjai & Brumbach (1974). A comprehensive discussion of the subject has been given in the book by Goodman & Wachman (1976). The recent trends in molecular beam studies (non-reactive type) will be discussed below with emphasis placed on topics that are directly relevant to the experimental work performed in this project.

Since previous research in this laboratory was completed (Walters, 1973) few experiments on the scattering of molecular beams from metal surfaces have been performed.

The reason for this probably stems from the fact that clean metals have, until recently, failed to show diffraction phenomena. An exception to this statement was demonstrated in the results of Tendulkar & Stickney (1971), who worked on the (112) face of tungsten. This crystal surface is unusual amongst the low-index crystal faces in that it contains deep corrugations, Fig. (3.1). Tendulkar & Stickney showed that diffraction was observed but only for beams incident along the $\langle 1\bar{1}0 \rangle$ azimuth and not for beams incident along the $\langle 11\bar{1} \rangle$ azimuth. Recently,

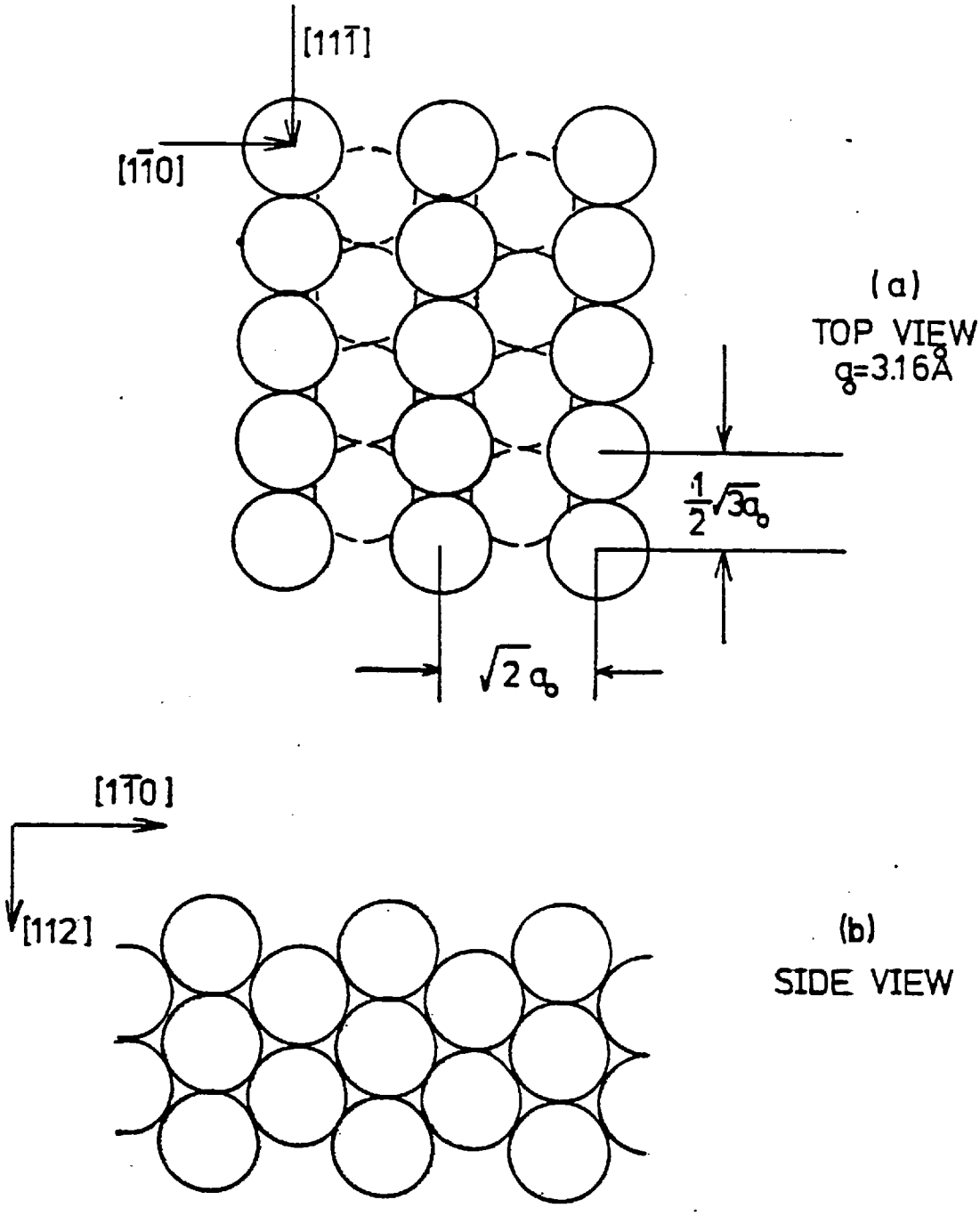


FIGURE SHOWING THE ATOMIC STRUCTURE OF THE (112) FACE OF A TUNGSTEN SINGLE CRYSTAL

FIG. 3.1

further studies on metal surfaces have begun. These have been conducted under somewhat superior experimental conditions to previous studies. Boato et al (1976b) claimed to observe diffraction of both He and H_2 from Ag(100) when the surface was cooled to 100K. This claim was supported by the work of Horne and Miller (1977). Lapujoulade & Lejay (1977) have recently observed diffraction of helium atoms from the stepped (117) surface of copper. In view of these results it seems probable that further studies on clean metals will be conducted. During the last few years there has been a gradual improvement in experimental apparatus resulting in better angular resolution, and improved vacuum conditions. Without these improvements it is doubtful whether the results of Boato and co-workers and Horne & Miller would have been obtained.

Similar improvements have been introduced in studies on alkali-halide crystals, from which diffraction of helium and hydrogen molecules had been observed in extensive work by Stern and co-workers, (Estermann & Frisch, 1930, 1931, 1933) and Johnson (1928, 1930, 1931). The improved procedures have enabled all of this earlier work to be repeated and much more detailed information concerning the gas-surface scattering process has been obtained. Modern research has investigated the following topics, in connection with scattering from alkali-halide:-

(a) Gas-surface interaction potential

(b) Inelastic scattering

(c) Surface geometry and the effects of overlayers

As was shown in Chapter 2 interaction potentials can be estimated by observing the variation in diffracted beam intensities with angle of incidence or azimuthal angle. From this information 'bound state' energies can be derived. Recent observations began with the work of O'Keefe (1970a,b) on the scattering of ^3He, ^4He, H_2 and D_2 from (100) LiF at room temperature using an oven source.

Subsequent studies have been able to improve on the quantitative deductions of this work by the use of nozzle sources and lower surface temperature. Extensive investigations have been performed by Williams (1971a, 1971b), Boato et al (1976a) and Liva and Frankl (1976).

Other alkali-halide crystals have been studied, for example NaCl (Fisher and co-workers, (1974)) and NaF (Wood et al (1974)). An interesting feature of the latter work is the occurrence of a maximum in the diffraction intensity of the $(\bar{1}1)$ beam under incident conditions that produce a minimum for other beams including the (00). This result has been confirmed by Liva and Frankl (1976) and has been important in developing theoretical approaches which aim to calculate scattering intensities (Chow and Thompson, (1976b)). The variations in peak intensities are due to bound state effects and Frank et al (1977) have used such effects to measure the coefficient of expansion of the surface layer of LiF. They found this to be twice as large as the value for the bulk, a result that appears somewhat surprising and requires further investigation. Most studies on alkali-halide surfaces are now conducted at temperatures between 80K and 150K as this reduces

incoherent background scattering, due to the motion of the crystal lattice. Observations of the behaviour of scattering intensities with surface temperature allowed Bledsoe and Fisher (1974) to estimate that the surface Debye temperatures of LiF and NaCl (100) faces were 350 ± 50K and 250 ± 30K respectively.

The importance of surface temperature in determining the type of scattering observed when neon is used as the incident gas has recently been recognised. Studies on LiF (100) conducted by Boato et al (1976) and Williams (1971b) indicated that diffraction was occurring whereas the earlier studies of Smith et al (1970, 1971), conducted at room temperature, produced the rainbow scattering phenomena predicted by McClure (1970). Boato (1976) has pointed out that when the surface is lowered to extremely low temperature, about 10K, the adsorption of the residual gas in the scattering chamber gives rise to spurious results, notably the gradual decay in the (00) specular beam signal intensity.

Mason and Williams (1972, 1974) showed that it is possible to study the ordering of physisorbed layers on alkali halide crystals. LEED work is hindered here because of electron stimulated desorption effects. On LiF, overlayers of C_2H_5OH, H_2O, CCl_4 and C_6H_6 were studied. By observing the appearance and positions of fractional order peaks in the helium scattering distribution Williams and Mason determined that H_2O was adsorbed in registry with the surface whereas, C_2H_5OH was out of registry due to molecular size effects and CCl_4 did not appear to order, deduced by the absence of fractional peaks.

Further work was done on NaF, again by Williams and Mason, but on this occasion a nozzle source was used and it was found that many of the diffraction beams were split. This was thought to be related to a variation in surface concentration of the adsorbed layer across the surface. Williams and Mason also made estimates of activation barriers for diffusion and diffusion coefficients for the adsorbed molecules.

Williams (1971a, 1971b) also investigated inelastic scattering between incoming molecules and surface vibrational modes, a phonon being emitted or absorbed. As thermal energy incident beams have energies close to that of phonon energies they should be an ideal tool for studying surface phonons. Fisher (1972) had also conducted a study in which loss processes were investigated. Boato et al (1975) confirmed Williams observations.

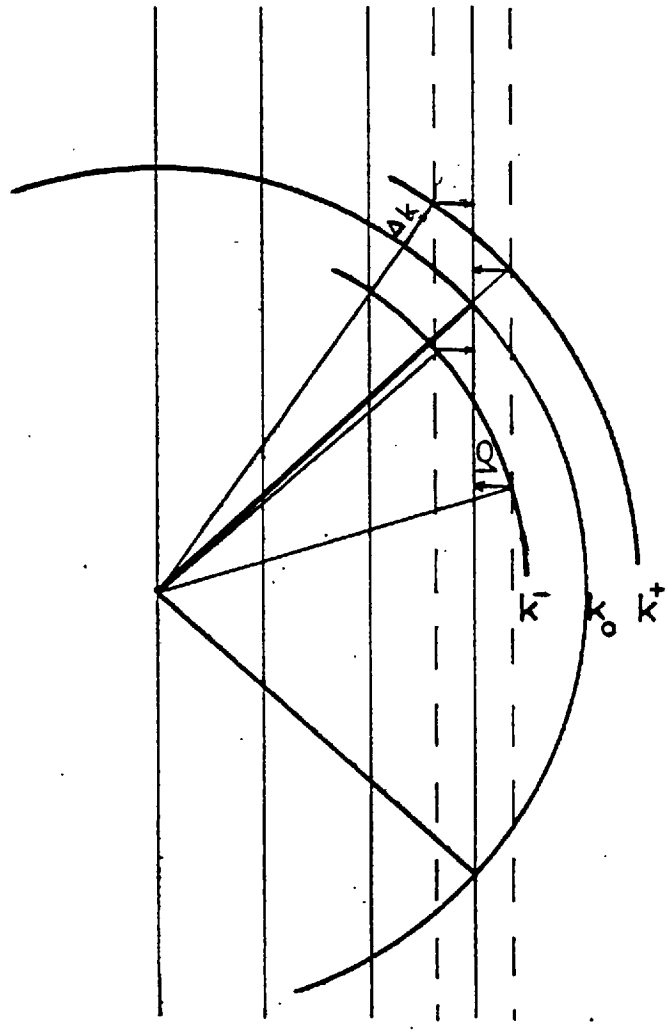
The inelastic processes result in additional structure being observed between the main diffraction peaks. The way in which this structure comes about is shown in the Ewald sphere diagram in Fig. (3.2). Williams discussed his results in terms of surface Rayleigh waves using the relation:-

$$\frac{\Delta k}{|\underline{Q}|} = \frac{v_s}{v_a}$$

v_s is the velocity of the surface wave

v_a is the velocity of the incoming atom.

Such an interpretation is not however universally accepted at the present time, Goodman (1974). The role of phonon processes in scattering of atomic beams has



EWALD CONSTRUCTION ILLUSTRATING THE INTERACTION OF SURFACE PHONONS [AFTER WILLIAMS (1971a, 1971b)]

FIG. 3.2

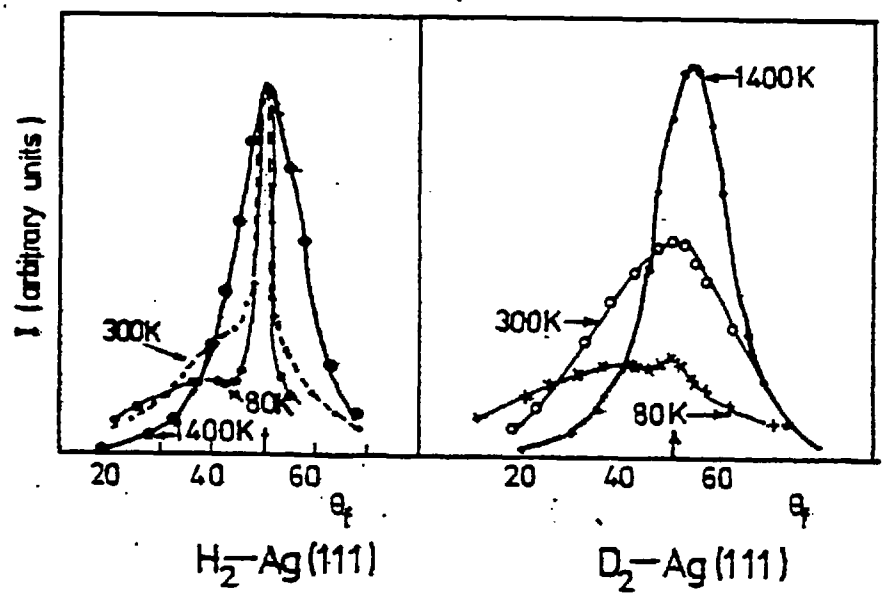
been discussed by Goodman (1972) and Beeby (1972a,b). There does not appear to be any general agreement at present as to whether inelastic encounters can be limited to single phonon events or whether multiphonon processes are occurring. Further it is not clear whether an explanation can be obtained using purely surface phonon modes or whether bulk phonon contributions occur. These conflicting opinions will only be resolved when much more experimental data is available.

Diatomic molecules may interact inelastically with surfaces by interchange of energy between phonon and rotational modes. This process has been observed for the scattering of D_2, H_2, and HD from LiF(100) (O'Keefe et al 1970a, 1970b),(Saltsburg et al 1967) and from Ag(111) (Sau and Merrill (1973). D_2 shows the more marked inelastic scattering behaviour, the specular peak being broadened considerably. Fig. (3.3) shows the results of some of these studies. It has been suggested in the case of the Ag(111) surface that the difference between the behaviour of the two isotopes was due to differences in the allowed rotational-state transitions. The selection rule for a rotational-state transition of a homogeneous diatomic molecule is $\Delta J = \pm 2$. For D_2 the energy change for the transition $J=0 \leftrightarrow 2$ is 250R J mol^{-1} whereas for H_2 for the same transition an energy change of 519R J mol^{-1} is required. Silver has a Debye temperature of 225K and energy exchange with H_2 will involve multiphonon processes whereas the interaction with D_2 may involve only a single phonon process. It was therefore concluded that D_2 would be more likely to show

(a) RESULTS of SALTSBURG et.al.

$T_s = 560K$

$\theta_i = 50°$

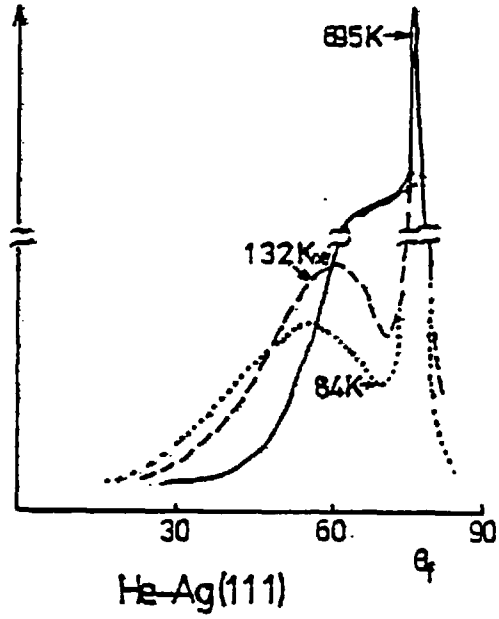


H_2—Ag(111) D_2—Ag(111)

(b) RESULTS of SUBBARAO and MILLER

$T_s = 560K$

$\theta_i = 77°$



He—Ag(111)

FIG. 3.3

rotational vibrational energy transfer than H_2.

An interesting comparison of H_2 scattering and the scattering of He from Ag(111) can be made. Fig. (3.3b) indicates that the scattering distribution for both shows a sharp specular peak accompanied by a broader lobe. Clearly helium has no rotational modes and any inelastic scattering involves energy transfer between the translational state of the helium and phonons of the crystal. The similarity of the two scattering distributions suggests that a similar explanation is applicable in the case of H_2 scattering and that multiphonon processes involving the rotational modes of H_2 do not occur.

Energy exchange between rotational and translational modes of the incoming molecules, i.e. a process which involves no net energy transfer between molecule and surface, has been investigated by Rowe and Ehrlich (1975), who have observed the scattering of HD, H_2 and D_2 from a MgO (001) surface. Extra structure was found in the scattering distributions between the elastic diffraction peaks as had previously been observed by Boato et al (1974) with LiF (001). Rowe and Ehrlich (1975) also worked on LiF(001) but found that the exchange processes were more readily observed on MgO, because of its higher surface Debye temperature. They also found that D_2 showed the effects more strongly than HD and H_2 and that it was more readily observed at high angles of incidence.

3.2. Theoretical

This section contains a brief literature survey of attempts to use quantum theory to explain gas-surface scattering phenomena.

Following the experimental work of (Estermann and Stern, 1929, 1930, 1931) initial attempts to develop a quantum mechanical explanation of diffraction phenomena were made by Jackson and Howarth (1933), and Lennard Jones and co-workers Devonshire and Strachan (1935, 1936, 1937). The latter developed a perturbation approach (essentially a first-order distorted-wave Born approximation) and applied it to the calculation of accommodation coefficients (see Goodman (1971) for review). The first-order distorted-wave Born approximation is not valid in cases where there exist strong diffraction beams. Recently a more realistic quantum method has been formulated, following the work by Beder (1964), Howsmon (1966, 1967), and Cabrera, Celli, Goodman and Manson (1970). Most work has been concerned with elastic scattering although attempts to develop methods for explaining inelastic scattering are now being put forward.

In the absence of perturbation theory the solution of the Schrödinger equation, takes the form of a set of coupled differential equations, which for the elastic case are

$$\left|\frac{d^2}{dz^2} + k_{\underline{G}z}^2\right|\psi_{\underline{G}}(z) - \frac{2\mu}{\hbar^2}\sum_{\underline{G}'} V_{\underline{G}-\underline{G}'}(z)\psi_{\underline{G}'}(z) = 0$$

The derivation of these equations was given in Chapter 2. Attempts to solve these equations are greatly dependent on the available computer time, which naturally has increased rapidly in the last decade. Numerical integration is necessary as analytical solutions are not possible. Accurate numerical evaluations depend upon the number of partial waves labelled by the G vectors used in the analysis. Wolken (1973) and Tsuchida (1969) have shown that the computer time needed increases rapidly with increase in the number of partial waves and this imposes a severe restriction on the accuracy of current calculations. Partial waves arising from reciprocal lattice vectors leading to allowed diffracted beams are sometimes termed 'open channels', while those associated with bound or evanescent states are termed 'closed channels'. The importance of including 'closed channels' in calculations was recognised by Wolken and Tsuchida, and recently Chow and Thompson (1976a, 1976b) have demonstrated that experimental observations of the scattering intensity variations with incident angle can be satisfactorily explained using a quantum approach based solely on elastic scattering but involving multiple scattering via bound states.

The earlier calculations of Cabrera, Celli, Goodman and Manson (1970) and Tsuchida (1969) had not allowed for such processes. In these earlier calculations bound states were introduced into discussions following the main calculations in order to explain the reasons for minima being observed in experimental observations of specular beam intensities whereas these were <u>always</u> present as maxima in the calculated scattering distributions. In such

discussions, bound states, by increasing surface residence times, were held to enhance the probability of inelastic collisions, thereby removing molecules from the elastic beam. The recent work of Chow and Thompson (1976b) appears to remove the need for such qualitative arguments. The use of large numbers of partial waves, up to 61 have been used, increases computing time markedly as has already been stated. This limits the usefulness of such calculations when the parameters of a particular potential function are being optimised, since it is very difficult for systematic variation of potential function parameters to be performed. Wolken (1974) and Goodman and Tan (1973) have commented on the role that less thorough calculations involving less partial waves, can play in investigating interaction potentials.

Wolken (1973) showed that the emergence of open channels should cause changes in the intensity of the diffracted peaks as the energy or angle of incidence of the beam is varied. Such phenomena, termed 'threshold behaviour', have not yet been observed experimentally.

Recent calculations by Garibaldi et al (1975) have demonstrated that the rainbow effect [predicted in the classical trajectory calculations of McClure (1970)] can be produced in a quantum treatment in the form of a modulating envelope superimposed on the diffraction peaks. Their calculation introduces some approximations in solving the set of equations (2.12), already mentioned.

One feature of the model is that it has a corrugated hard wall potential which, though somewhat unrealistic, simplifies calculation considerably and has been used frequently in first attempts to perform calculations using new approaches (see Chow & Thompson, (1976a), Garcia, (1976), and Beeby (1971)). The results of the calculations of Garibaldi et al have been compared with the experimental observations of Boato et al (1975) and there appears to be qualitative agreement.

CHAPTER FOUR

EXPERIMENTAL

4.1. The Apparatus

The overall layout of the stainless steel U.H.V. system used in this work is shown in Fig. (4.1). A detachable glass gas handling line is not shown in this figure. A more detailed layout of each section is shown in subsequent figures. The system may be divided into three distinct sections.

(i) The work chamber, in which the scattering experiment and surface analysis are performed.

(ii) The beam section, in which the incident gas is collimated to form a well-defined beam.

(iii) The service well, which lies directly beneath the work chamber and leads to the main diffusion pump.

Three oil diffusion pumps are used in the system; two to pump the beam chambers and one large pump to maintain U.H.V. conditions in the work chamber. In all three pumps the pumping fluid is Santavac 5, a polyphenylether. In order to obtain U.H.V. quickly the apparatus must be baked. The manipulative devices used to drive the bellows assemblies that rotate the crystal holder and the detector orifice have to be removed before bakeout. A set of elements mounted on the superstructure of the apparatus are used to heat the system when it is enclosed in its bakeout oven. The work chamber and service well can be heated to 525K and the beam section to 425K.

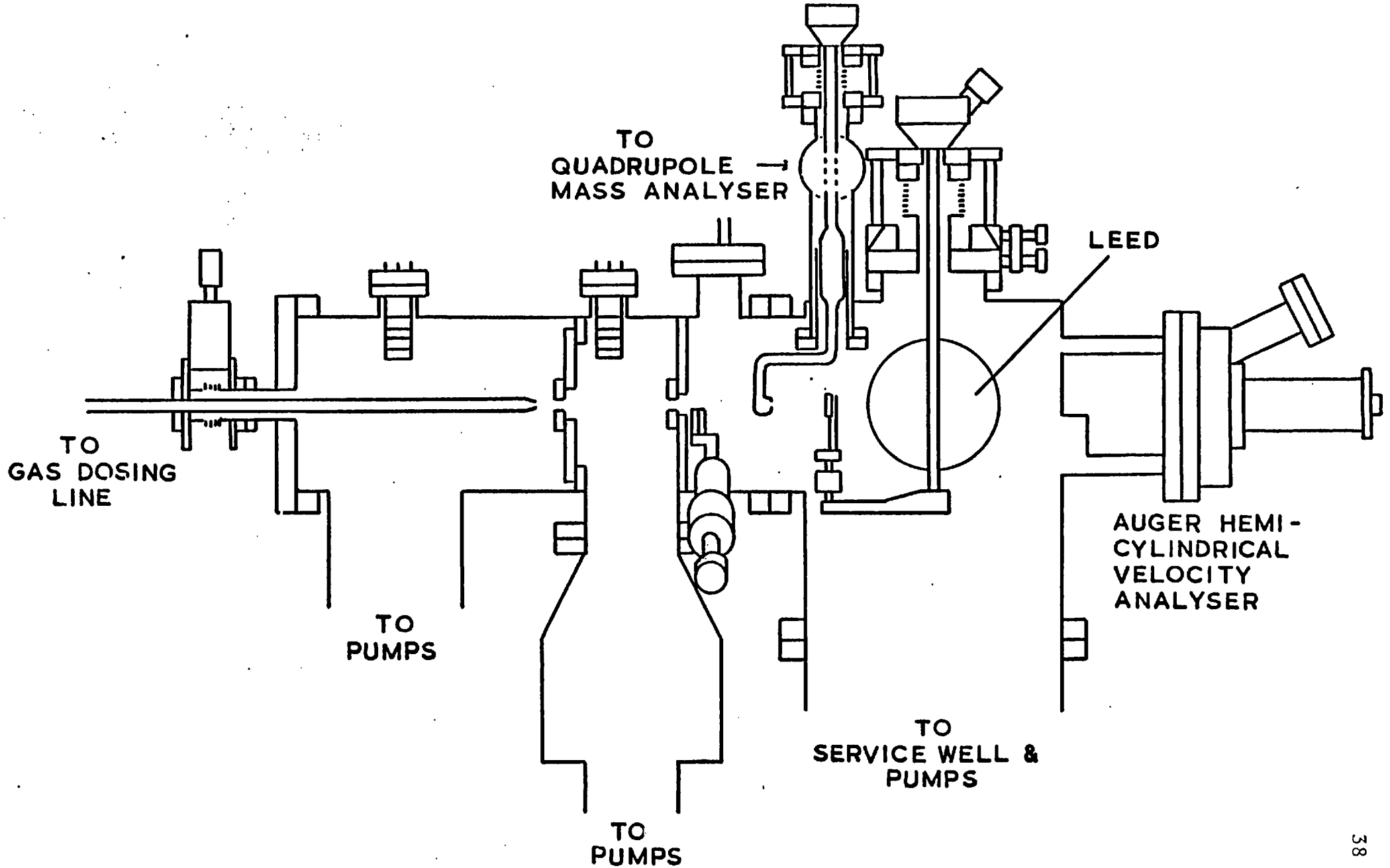


FIG. 4.1

MOLECULAR BEAM SYSTEM

The Work Chamber

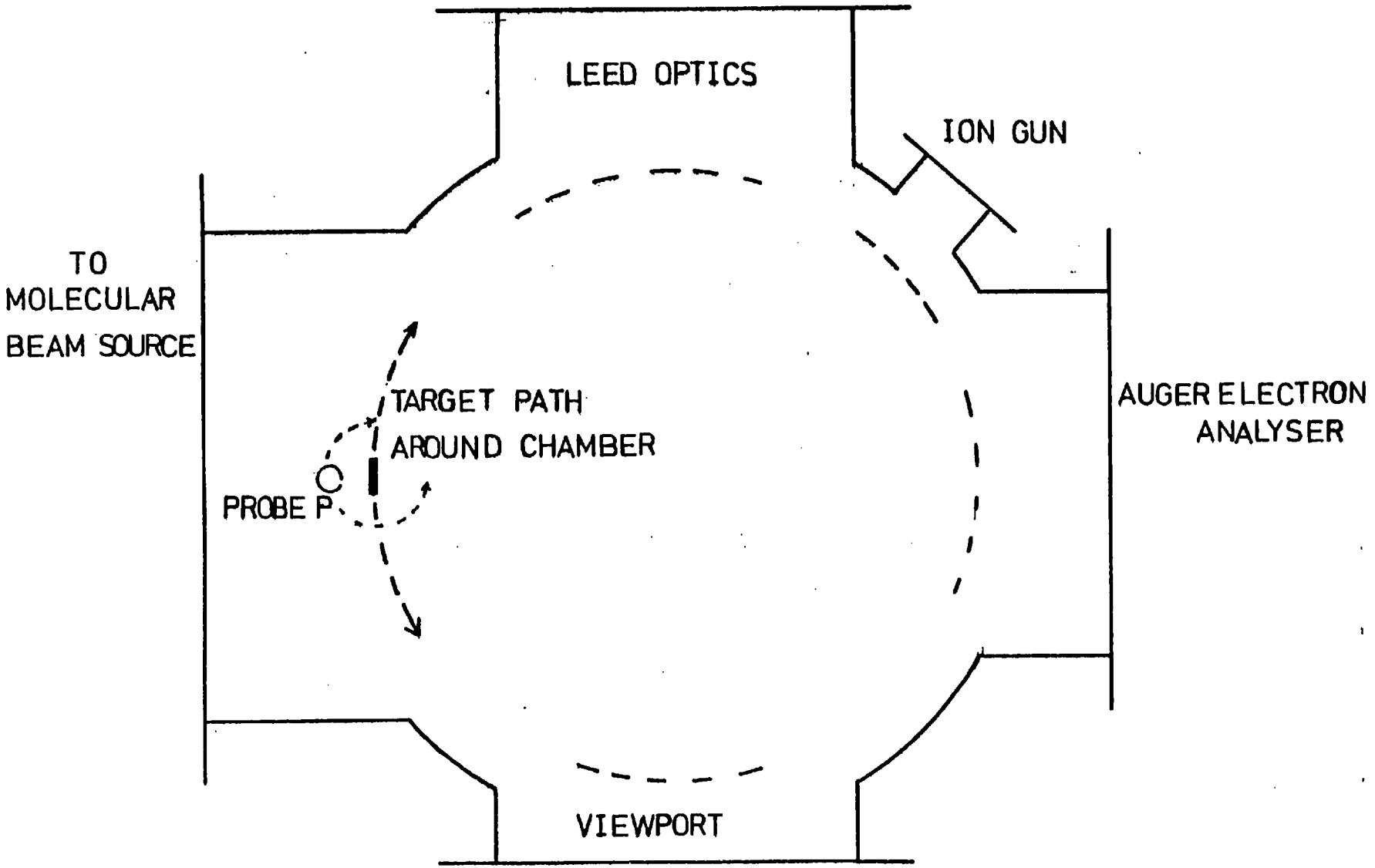
(i) General

The work chamber is drawn in Fig. (4.2). It is a 12" diameter stainless steel cylinder fitted with several side ports. The target holder is mounted on an arm, of radius 5", which rotates about the central axis of the work chamber by means of a bellows manipulator. This also provides some vertical motion and a second rotational movement that turns the target about its vertical axis. The first rotational movement allows the target to be moved in front of a number of ports where low energy electron diffraction, Auger electron spectroscopy, argon ion bombardment, electron bombardment and molecular beam scattering may be carried out.

The probe P is used to collect scattered gas through a 1mm orifice. Thegas is then analysed in the quadrupole mass spectrometer. The probe may be rotated through 360^{o} and can be moved vertically through distances of approximately ± 25mm.

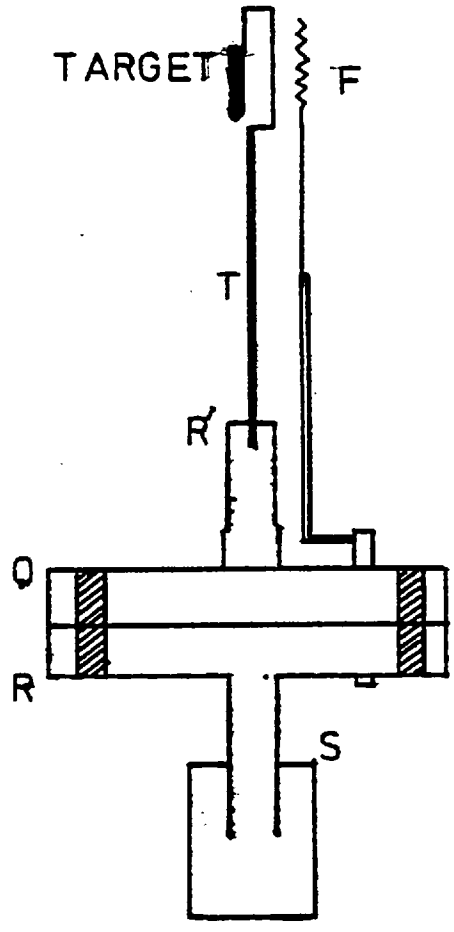
(ii) The Substrate Assembly (Fig. 4.3)

The crystal target is supported by a single piece of tungsten rod T which had been etched down to approximately 0.2 mm at one end. This was bent around the crystal to provide a fairly tight support. It was important to ensure that this support was sufficiently rigid to withstand temperatures of 2500K without distorting. The free end of the tungsten rod fits tightly into a hole bored in a stainless steel rod R'. This rod forms part of a cross piece which is



WORK CHAMBER

FIG. 4.2



SUBSTRATE ASSEMBLY

FIG. 4.3

bolted onto a quartz disc Q, which provides electrical insulation of the crystal. A second cross piece R is bolted to the underside of the disc and connects to a rotating mount S, on the arm of the manipulator. A tungsten-rhenium thermocouple was connected to the back of the crystal. The crystal was heated by electron bombardment from the filament F which was made from 0.3mm tungsten wire.

(iii) The Detector System

The detector system, drawn in Fig. (4.4), is connected to the work chamber via an internal, gold wire sealed flange F. The detector is a Q7B quadrupole mass spectrometer. An ion gauge is mounted on a side arm for calibration purposes. Molecules scattered from the target are sampled by the pyrex glass probe P, via the small orifice O (diameter 1mm), and are then channelled into the detector line. The detector line is isolated from the work chamber by the gold wire sealed flange and a ground glass seal S. This seal was formed by regrinding both the barrel and sleeve of a syringe to give a smooth, gas-tight seal, that allows the probe P to be rotated in the work chamber. Inside the detector line the barrel of the syringe is attached (via a glass-to-metal seal and a spring clip C) to the rod R. This rod is directly connected to a manipulator which provides rotational and vertical movement of the probe P. The spring clip and the small section of bellows attached to the sleeve of the syringe are protective measures to prevent fracture of the glass should there be any non-axial forces applied to the barrel of the syringe when the manipulator is used.

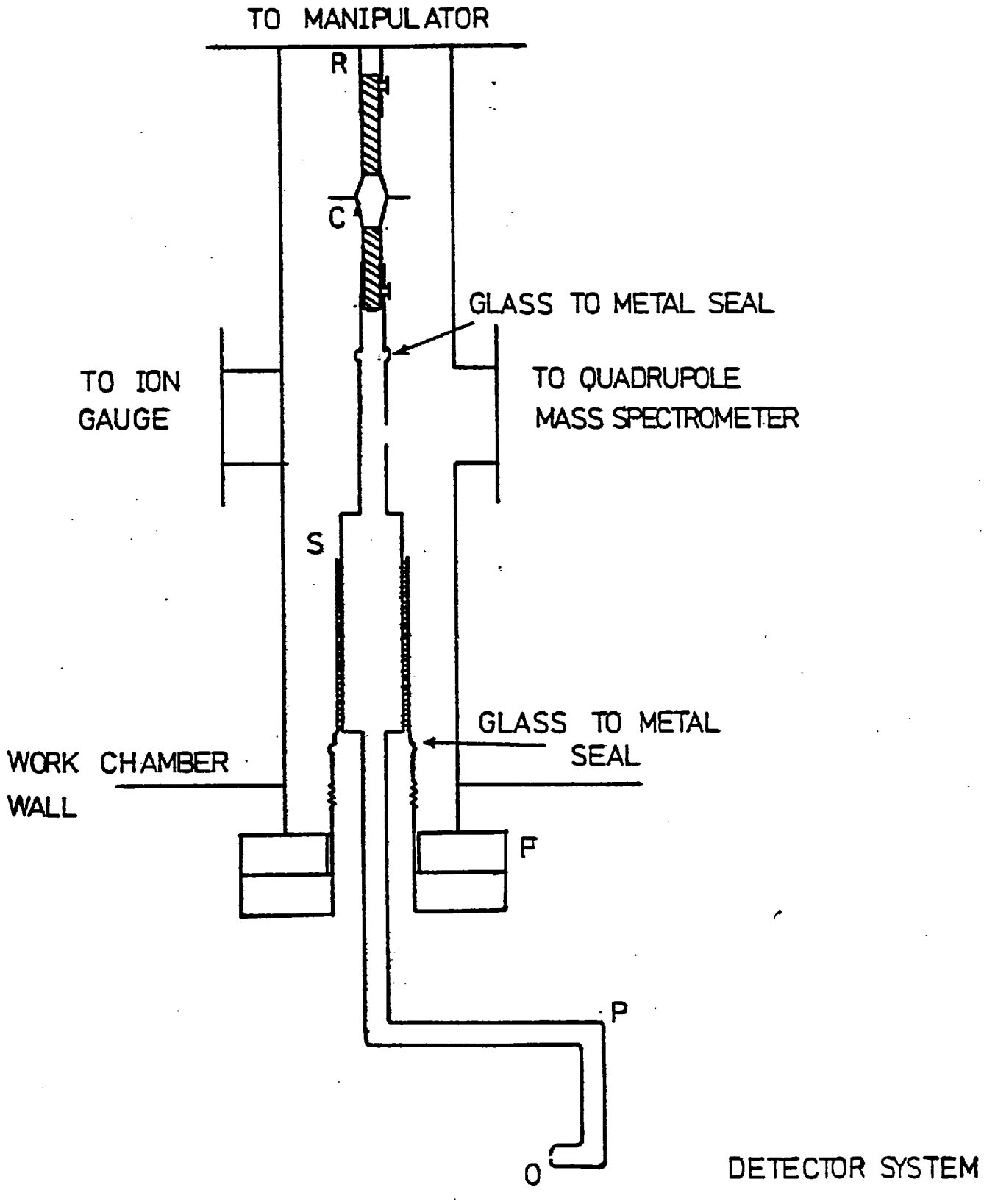
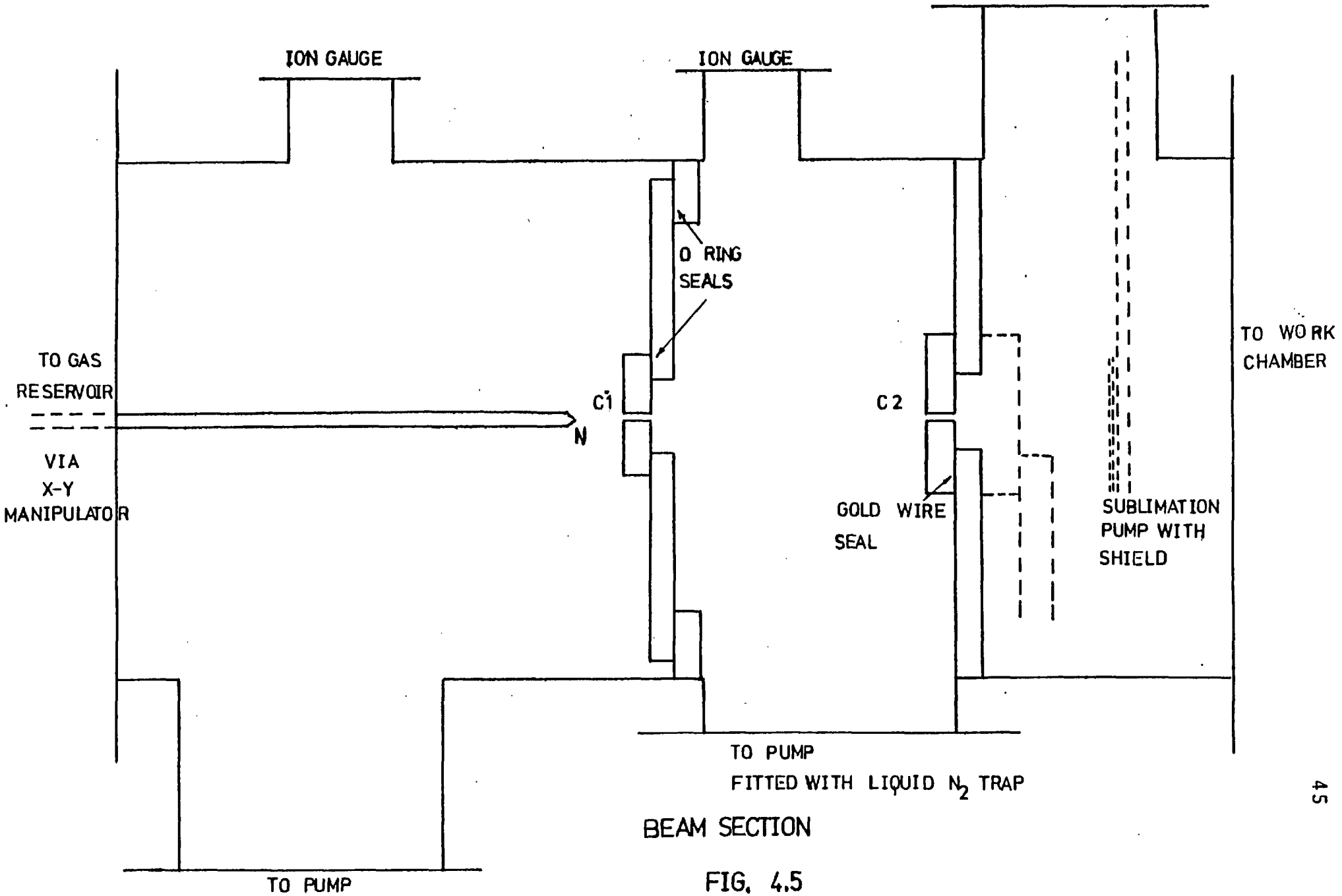

TO MANIPULATOR
R
C
GLASS TO METAL SEAL
TO ION GAUGE
TO QUADRUPOLE MASS SPECTROMETER
S
GLASS TO METAL SEAL
WORK CHAMBER WALL
F
P
O
DETECTOR SYSTEM

FIG. 4.4

The Molecular Beam Section (Fig. 4.5))

This section contains two differentially pumped chambers. The beam is generated in the first chamber from a nozzle N. The nozzle was made by drawing down thick-walled glass tubing until the end was sealed and then gradually grinding this end until a small hole was obtained. Several convergent nozzles were made in this way, the one selected for use having an exit orifice of 0.0075mm diameter. This diameter was measured by projecting a microscope image onto a ground glass screen and comparing the image size with a calibrated scale. Gas emerging from the nozzle is formed into a beam by two collimating channels C1 and C2. The first channel is situated approximately 1cm away from the nozzle exit and is 1cm long and 1mm in diameter. This first chamber is pumped by a 600 litre/sec. oil diffusion pump. A pressure of 1×10^{-7} torr can be obtained in this chamber when the beam is not operating. An ion gauge is mounted in the top of the chamber.

The second chamber is pumped by a 400 litre/sec. oil diffusion pump which has a liquid nitrogen trap attached and makes it possible to pump this stage to a pressure of 1×10^{-10} torr before the beam is operated. The second collimating channel is again of 1mm diameter and is drilled in a stainless steel plate that is attached to a second, fixed plate that separates the beam section from the work chamber. A gold wire seal is used between these two plates. A bakeable, all metal gate valve, fitted on the work chamber side of the separating plate, may be used to



BEAM SECTION

FIG. 4.5

completely isolate the beam chamber from the work chamber. A getter filament (titanium-molybenum alloy) with an evaporation shield is positioned between the target and the gate valve and is used to help to reduce the background pressure, due to random components in the beam, when active gases are used as incident gas. Thetotal distance from the nozzle to the target is 32cm.

Two limited motions are available to ensure accurate alignment of the nozzle with respect to the beam axis. The nozzle is attached to a bellows which enables the nozzle to be placed on the axis of the first collimator. This manipulation is made during beam operation and is monitored by observing beam intensity.

Before the nozzle was placed in the first chamber (also termed the exhaust chamber) the two collimators were accurately aligned by a line of sight method. A bright light was placed on the work chamber side of the second collimator and viewed with a telescope through the two collimators. The position of the first collimator was adjusted to give the brightest image. Slight adjustments in the position of this collimator were possible since the plate in which it was bored was connected to the wall separating the first and second chambers with bolts that fitted through eccentric holes. Viton-o-rings were used to provide the seals between the collimation chambers.

(i) The Service Well

The service well contains an ion gauge, a liquid nitrogen cooled baffle plate, a set of titanium getter filaments and a viton-o-ring sealed gate valve, which is

used to isolate the main diffusion pump (2500 litre/sec.). Gases can be admitted into the work chamber via a leak valve. The dosing line is attached to the leak valve by a long narrow bore (5mm) stainless steel line. This line can be pumped by the mercury diffusion pumps in the dosing section. The line contains three miniature valves that allow gases to be admitted directly from cylinders and provide a means of isolating the leak valve.

(ii) The Dosing Line

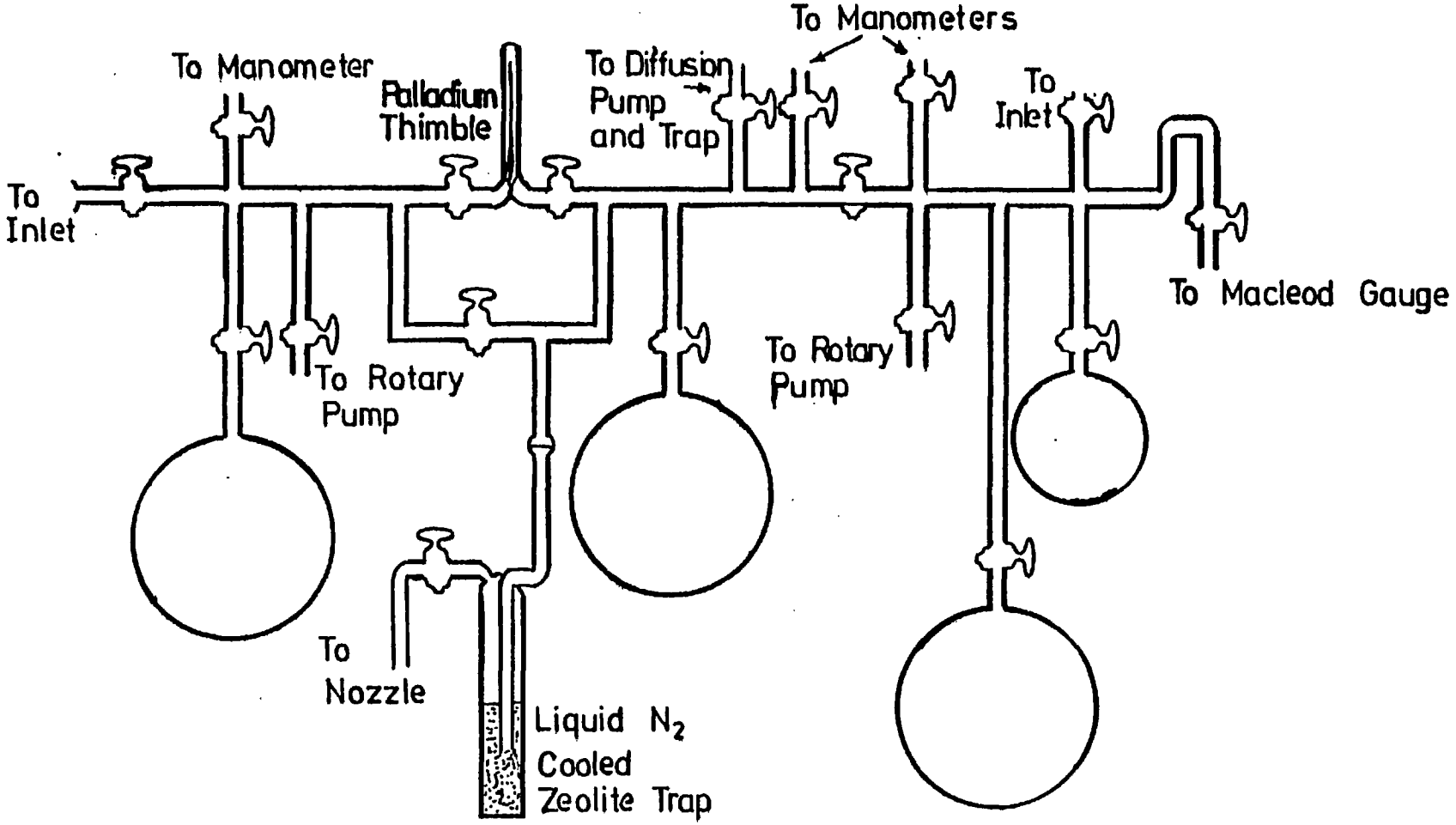
The line provides the gas reservoir for the nozzle. It was constructed from pyrex glass and may be pumped down to pressures of the order of 1×10^{-7} torr by two mercury diffusion pumps. Springloaded greased stop-cocks are used throughout the line as the greaseless valves available at the time were thought to be unreliable. Contamination of the incident beam by the grease is kept to a minimum by using a zeolite trap, held at liquid nitrogen temperature. This also allows cylinder gases to be cleaned sufficiently for use in the beam. The line is drawn in Fig. (4.6) and the main components are outlined below:

(i) 2 mercury diffusion pumps, and liquid nitrogen trap

(ii) Liquid nitrogen cooled zeolite trap

(iii) A Macleod gauge to measure the limiting pressure of the line

(iv) 3 mercury manometers, to measure gas storage pressure (at approximately one atmosphere).



SCHEMATIC DIAGRAM OF GAS DOSING LINE

FIG. 4.6

(v) 4 gas storage bulbs.

(vi) Inlets and outlets, to connect to gas cylinders and theline to the leak valve.

(vii) A ball and socket joint to connect the dosing line to the nozzle inlet. Accidental blockage of the nozzle by particles of dust or grit from the dosing section is prevented by a coarse sintered glass filter.

(viii) A palladium thimble, to purify hydrogen isotopes.

4.2. Experimental Procedures

(i) Attainment of Ultra High Vacuum

During the course of a scattering experiment it was important that the condition of the surface under investigation did not change. This required the use of ultra high vacuum conditions. The pressure in the work chamber during a scattering experiment was of the order of 2×10^{-10} torr. This pressure was achieved by using a 2500 $\ell\ s^{-1}$ oil diffusion pump with a nitrogen cooled trap. This pump was capable of pumping the chamber to below 5×10^{-11} torr when the molecular beam was not in operation. This low pressure was achieved following a 12-20 hr. bakeout of the system at 525K. The getter filaments in the service well were used during experiments in which deuterium was the incident gas and again background pressures of the order of 2×10^{-10} torr were maintained.

(ii) Measurements of Low Pressures

Total pressure was measured with ion gauges and partial pressures with a quadrupole mass spectrometer. Residual gas analysis in the work chamber was performed prior to any scattering experiments, but subsequently the quadrupole mass spectrometer was used as the detector in the scattering experiment. In this role a fixed mass/charge ratio was investigated and in order to operate under optimum conditions increased sensitivity at that particular mass/charge ratio was obtained at the expense of resolution by adjusting factory-set potentiometers in the control unit. In this

mode a residual gas spectrum could not be obtained.

Preliminary experiments were performed which showed that the mass spectrometer had a sensitivity of about 10A $torr^{-1}$. This is to be compared with the 100A $torr^{-1}$ quoted in the instrument manual. In its normal mode the sensitivity could not be increased above 10A $torr^{-1}$ even though the quadrupole was overhauled and a new electron multiplier fitted. However as only ratios of intensities were required in the present work an absolute value of the sensitivity was not required. The requirement of only ratios of intensities means that day-to-day variations in the sensitivity were not of great importance.

The quadrupole was pumped down to the work chamber pressure before use. A separate line to the diffusion pump through the rear of the quadrupole was available for this purpose as pumping through the small orifice of the detection probe was very slow. This pumping line was closed off by a metal valve when the quadrupole was used as a stagnation detector in scattering experiments.

The total pressure in various parts of the system could be measured by four ion gauges, one in each of the beam chamber sections, one in the detector line and one in the work chamber. In the beam chambers VIG 20 gauges fitted with tungsten filaments were used. These could measure pressures down to 1×10^{-10} torr. In the detector section and work chamber VIG 10 gauges fitted with lanthanum hexaboride filaments were used. These function accurately to pressures of 2×10^{-11} torr. The pressure limits are determined by the x-ray limits of the gauges (Redhead, 1968).

(iii) Target Preparation and In Situ Cleaning

The target used throughout this work was a 99.99% pure single crystal of tungsten cut to expose its (110) face. It was supplied in the form of a disc 1cm in diameter and 1mm thick, by Metals Research Ltd. It was stated to have been spark cut to within 2^{o} of the (110) face. Subsequent Laue x-ray analysis confirmed this and allowed the main azimuthal directions to be determined.

The crystal was prepared for the experiment by following well established techniques (Weinberg & Merrill, 1972a). First the crystal was mechanically polished on a lapping wheel. Nylon pads, coated with a series of diamond pastes of diminishing size (90μ, 60μ, 40μ, 25μ, 14μ, 6μ, 3μ, 1μ and ¼μ), were successively placed on the wheel. The crystal was cleaned ultrasonically in distilled water between each polishing grade to ensure complete removal of particles embedded in the surface. A mirror finish was obtained following the above procedure. The crystal was given a brief, chemical etch to remove the topmost layers, which would have been highly fragmented after polishing treatment. The etchant used was a solution containing, by volume, 67% lactic acid, 22% sulphuric acid and 11% hydrofluoric acid. (Weinberg & Merrill, 1972a). The crystal face was swabbed with the solution for about 5 sec. and then immersed in distilled water. This procedure was repeated several times. The crystal was fitted into its holder and the whole substrate assembly was cleaned ultrasonically, first in

iso-propyl alcohol and then in distilled water. Next the substrate assembly was mounted in the work chamber which was then pumped down to U.H.V. Prior to in situ cleaning an Auger spectrum of the target surface was obtained which showed peaks arising from oxygen and carbon but no clear indication of tungsten, reflecting the contaminated state of the surface following the polishing and etching procedures. At this stage no LEED pattern could be obtained. The crystal was then heated in vacuum to temperatures of about 2500K. Considerable outgassing occurred initially with increases in pressure of approximately 10^{-5} torr. Due to the frail nature of the crystal holder heating to these high temperatures was possible only for short periods of about 20 minutes. Some holders did, in fact, bend and distort and had to be replaced but as the main surface contamination had occurred during the crystal polishing and etching processes, exposure of the surface to the atmosphere during the remounting process did not produce a serious contamination problem. Carbon layers on the surface were removed by prolonged heating in oxygen at a pressure of 10^{-7} torr. Oxygen contamination was then removed by heating to high temperatures >2200K (see Chapter Seven). Once the contamination due to the preparation procedure had been removed the heating periods required to produce a clean surface or specific surface conditions were shorter and did not reach as high a temperature and it was possible to perform all the experiments described in this thesis using the same crystal holder.

The LEED and Auger techniques were used regularly to follow the progress of the cleaning cycle. The first LEED pattern obtained was not that of a clean tungsten (110) face but was a more complex pattern arising from a surface carbide, as observed by Weinberg & Merrill (1972b).

(iv) The Gas-Scattering Experiment

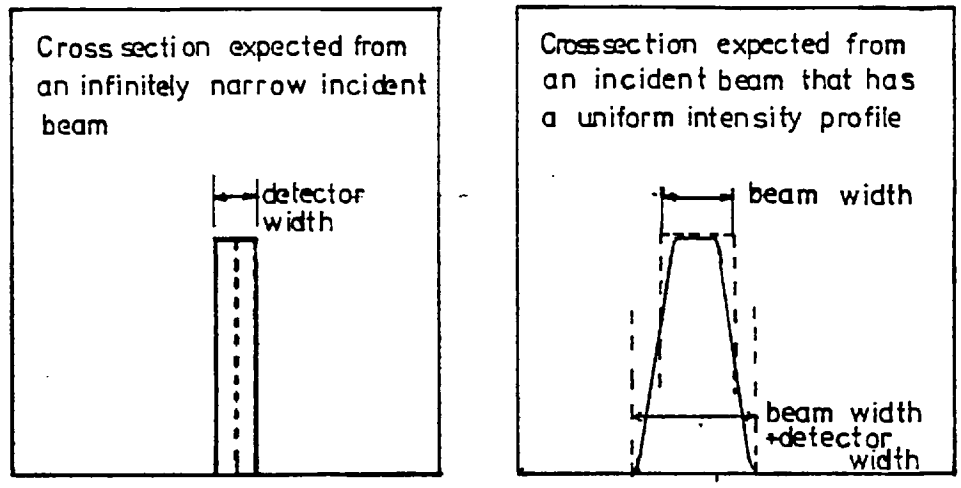
Before each run the system was calibrated by noting the maximum detector signal obtained when the beam entered the detector, the crystal having been moved out of the beam. This calibration provided a check on the beam performance and safe-guarded against:-

(i) partial blockage of the nozzle by foreign materials,

(ii) mis-alignment of the nozzle with respect to the collimation axis.

A plot of beam signal versus reservoir pressure was available for comparison. (This was made during the initial setting-up of the molecular beam). During an experiment it was undesirable to move the target out of the beam to check the beam intensity using the detector as it was difficult to reproduce the scattered beam signal exactly. As the reservoir pressure falls during the course of an experiment the plot of beam signal versus reservoir pressure was required in order to normalise the scattered signals to a constant incident beam. Any movement in the target resulted in slight changes in incident condition due mainly to backlash effects in the manipulator. For the same reason LEED and Auger spectra were only observed at the start and finish of a run.

When the maximum beam signal had been established and been found to be free from any of the effects mentioned earlier the position of the detector was noted as it was required in determining incident conditions. The angular position of the detector corresponding to maximum incident beam signal showed no variation throughout the course of the work (to within the limits of accuracy of the scale on the manipulator $\pm\frac{1}{2}^{o}$) but the vertical position was found to vary by ±1mm. This arose through the necessity of removing the manipulators during bakeout. The beam profile (cross-section) was obtained in the course of maximising the incident signal. A plot of the vertical cross-section is shown in Fig. (4.7). As the beam is cylindrical the angular cross-section is similar but as is mentioned elsewhere measurement of the angular position of the detector is not as accurate as the measurement of its vertical position and this profile is not shown. The plot shows the beam signal to be flat topped, the edge effects arising from the finite size of the detector orifice. Once the beam calibration was complete the surface was characterised by LEED and Auger spectroscopy and the crystal was then moved into the incident beam, the crystal manipulator tilt mechanism being adjusted to bring the crystal face almost perpendicular to the beam axis. The position of the specularly reflected gas was then determined by manoeuvering the detector until an intense narrow peak was found. Due to the sharpness of the peak it was difficult to find during the initial experiments, but once its position had been established, especially its vertical


Cross section expected from an infinitely narrow incident beam
detector width
Cross section expected from an incident beam that has a uniform intensity profile
beam width
beam width + detector width

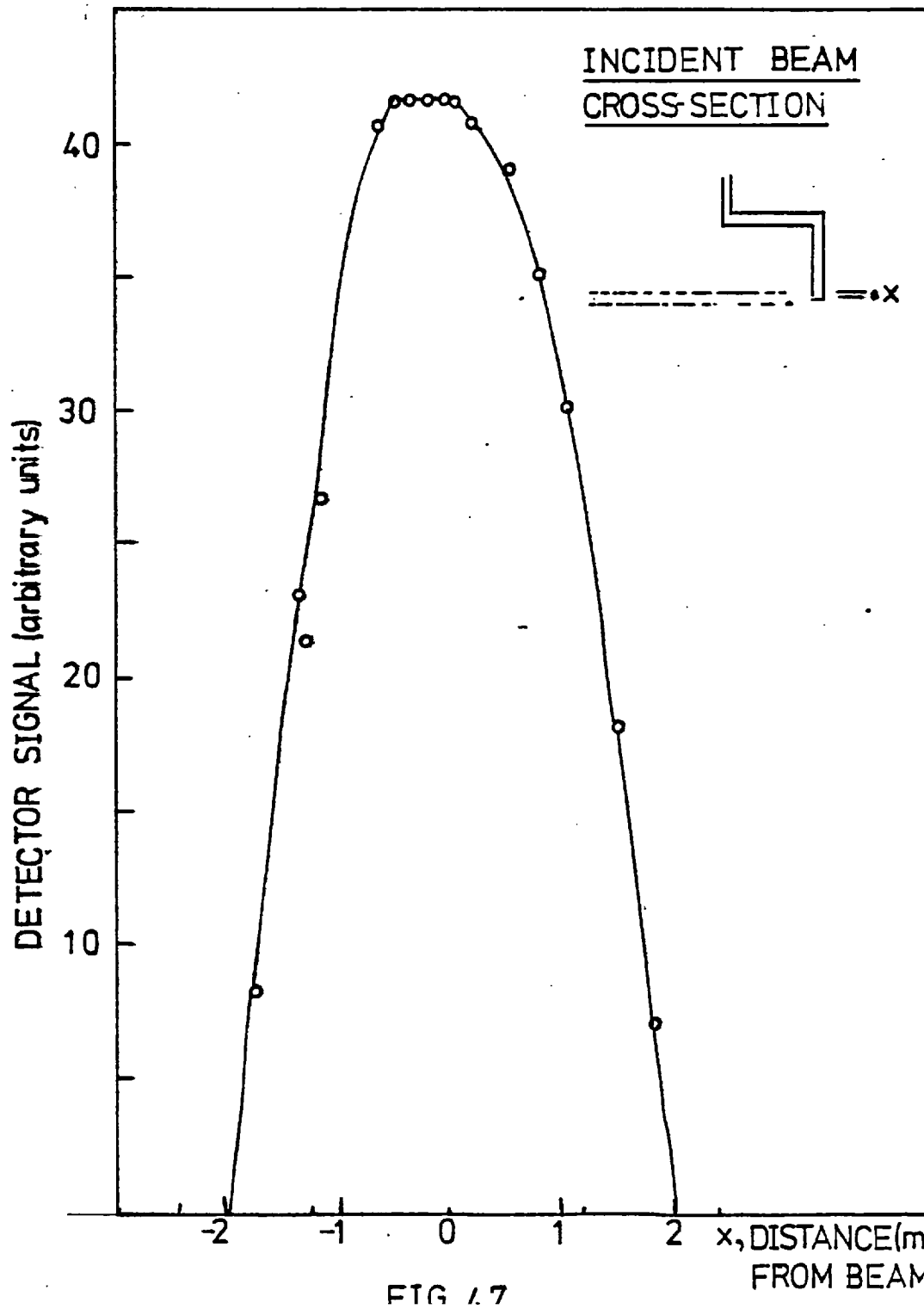

INCIDENT BEAM CROSS-SECTION
x
DETECTOR SIGNAL (arbitrary units)
40
30
20
10
-2
-1
0
1
2
x, DISTANCE (mm) FROM BEAM AXIS

FIG 4.7

position, which was dependent on the residual tilt of the crystal with respect to the beam, there was little difficulty in subsequent experiments. Next, the intensity of the scattered distribution was found as a function of angle in the horizontal plane containing the specular peak. As the crystal was almost always tilted slightly out of the vertical (one or two degrees) peaks found in-plane were maximised by moving the detector vertically. In most of the plots shown in this thesis the angles correspond to movement in a horizontal plane but the out-of-plane positions of peak maxima are given where necessary.

In order to produce accurate plots of the angular distribution of scattered gas it was necessary to subtract a background signal, obtained by placing the detector behind the target with the beam on. This background signal was recorded several times during a run, as was the reservoir gas pressure and corrections were then made to all recorded scattered signals. It was assumed that changes in background and incident beam signals varied linearly with time during the course of a run.

CHAPTER FIVE

MOLECULAR BEAM GENERATION

5.1. Introduction

Earlier work conducted in this laboratory on gas scattering utilised oven source molecular beams (Chappell 1971, Walters 1973). In such sources the reservoir pressure is such that the mean free path of the gas is greater than the diameter of the exit orifice. Molecules effuse from the orifice with a cosine distribution and have a spread in energy described by a Maxwellian relationship. A beam is obtained by collimation of this stream of particles. As the orifice is not a point source the final beam cross-section is not uniform, exhibiting a central area of high intensity and a region of lower intensity surrounding this.

As it was envisaged that this work would, at some stage, be concerned with the study of diffractive phenomena it was decided to use a more nearly mono-energetic beam as provided by a nozzle source. Kantrowitz and Grey (1951) first proposed that the oven source be replaced by a supersonic jet. A beam generated from such a source has the advantage that much of its internal energy and random motions are converted into directed mass motion. This results in a narrowing of the energy spread of the beam, which can be related to the temperature drop experienced by the gas during the adiabatic expansion to supersonic velocity. Earlier attempts by Kristiakowsky and Slichter

(1951) to put this proposal into use were unsuccessful because, with a high pressure behind the nozzle, the total flow of gas through the nozzle was large and the pumping capacity in the exhaust chamber (see Fig. 4.5) was inadequate. Becker and Bier (1954) managed to overcome this problem and the use of nozzle sources has now become widespread. The production, development and general use of nozzle type molecular beams has been reviewed by Anderson (1965, 1974).

The design of most nozzle generated beams incorporates a specially shaped first collimator, known as a skimmer. This is necessary when high intensity beams are used as it eliminates the effects of shock waves produced when the gas flow strikes the collimator. In the present work the stagnation detector used was sufficiently sensitive to detect scattered beams using an incident beam flux of 10^{13}-10^{14} molecules/sec. which is considerably less than the flux used in other nozzle beam applications. The work of Moran (1970) had shown that beams of this intensity could be generated without using the specially shaped skimmers.

The precise energy distribution of the beam used in the present work was not known as the experimental system had no facilities for energy analysis. From the experimental results (see Chapter Seven) it can be seen that the first order diffraction peaks are broader than the (00) peak, a result which does indicate that there is an energy spread in the incident beam.

Outline of Nozzle Source Arrangement

The design of the nozzle source used in this work follows closely that of Moran (1970). The experimental arrangement is shown in Fig. (4.5). The sizes and positioning of the beam collimators have been described earlier (Chapter Four). One important feature of the design is that the distance from the nozzle exit to the first collimator is much larger (approximately one cm.) than that used in most applications. At this distance intermolecular collisions within the beam are unimportant and there is no need to use a specially shaped skimmer. The pressure of gas stored behind the nozzle was normally 500 torr.

5.2. An outline of nozzle beam theory

The theory of the action of nozzle beams is a difficult problem and has been discussed at length in two reviews by Anderson (1965, 1974).

(i) Beam Energy

A basic understanding of the properties of a nozzle beam can be obtained by assuming that the reservoir gas expands isoentropically through the nozzle. Texts by Shapiro (1953) and Thompson (1972) give good accounts of the methods of continuum mechanics used in such models. The expanding gas experiences an increase in forward velocity that comes about from a reduction in the local

enthalpy of the gas. The lowering in temperature, from T_o to T_f, accompanying the expansion is given by

$$c_p T_f + \frac{mu^2}{2} = c_p T_o \qquad \text{where u is the forward velocity of gas.} \qquad (5.1)$$

Expansion in nozzle beams is usually described in terms of the Mach number M, which is equal to u/a, where a is the local sonic velocity. The velocity of sound is equal to

$$\sqrt{\frac{\gamma k T_o}{m}} \qquad k \text{ is the Boltzmann Constant.} \qquad (5.2)$$

In terms of the Mach number M equation (5.1) becomes

$$\frac{T_f}{T_o} = \left[1 + \frac{\gamma - 1}{2} M^2\right]^{-1} \qquad (5.3)$$

γ is the ratio of the specific heats of the gas.

Using a continuum model Owen and Thornhill (1948) showed by numerical methods how the Mach number in a free jet developed as a function of the ratio of distance downstream of a nozzle to nozzle diameter. They found that the Mach number increased monotonically with this ratio implying that $T_f \to 0$ as the gas travels from the nozzle.

In the expansion of a free jet into a low pressure region however the gas density decreases rapidly with increasing distance from the nozzle and the continuum solutions break down. In actual nozzle beams this appears

to occur and the beam properties depend on the gas behaviour in the so-called transition flow region - intermediate between the continuum flow and free molecular flow. Theoretical methods for dealing with the transition flow region are less well-developed than the methods used to describe the other regions.

Fenn and Deckers,(1963) and later Anderson and Fenn (1965) showed experimentally that, in contrast to the Owen and Thornhill calculations, a definite maximum or terminal Mach number is reached. The collision rate then becomes lower, leading ultimately to free molecular flow and expansion ceases. The terminal Mach number was found to be

$$M_T \approx 1.17\left(\frac{\lambda_o}{D_A}\right)^{-0.4} \qquad (5.4)$$

where λ_o is the mean free path of gas in the source and D_A is the nozzle diameter.

Anderson and Fenn (1965) determined the axial velocity distribution for a nozzle source and found it to be Maxwellian. Similarly they found that the off-axis distributions were approximately Maxwellian but with excessive tails. Other experiments by Abuaf et al (1966), Miller and Andres (1968), Scott and Phipps (1966) and others have confirmed these observations.

Theoretical descriptions of the transition flow region have led a number of workers, Anderson et al (1964),

Anderson and Fenn (1965), Hamel and Willis (1966), Birel (1970) and Brook and Oman (1964) to similar conclusions i.e. that the overall velocity distributions are non-isotropic and that the axial velocity distribution becomes frozen. For comparison it should be noted that in continuum flow the distribution of velocities about the mean velocity in parallel and perpendicular directions are identical, the overall distribution being isotropic and Maxwellian. The width of the distribution decreases with increasing distance from the source and no freezing of the parallel distribution occurs.

Fleundy and Lawley (1973) stated that in isoentropic expansion the width of the velocity distribution following expansion is

$$\frac{\Delta v}{v} \sim \left(\frac{2}{\gamma}\right)^{\frac{1}{2}}/M \ . \qquad (5.5)$$

In an effusive source freezing of the axial velocity distribution and narrowing of the distribution perpendicular to the direction of flow again occurs and arises because of geometrical effects.

The beam energy is an important parameter in molecular beam scattering and especially so in studies where diffraction is observed. Ideally velocity analysis of the incident beam should be performed but as this facility was not available only qualitative estimates of both magnitude and energy distribution can be made. In an ideal expansion the forward energy available would be

$$E = \int_{0}^{T_{nozzle}} c_p dT . \qquad (5.6)$$

In a case where a residual temperature remains

$$E = \int_{T_f}^{T_{nozzle}} c_p dT \qquad (5.7)$$

where T_f will be related to the terminal Mach number M_T by relation (5.3).

In the ideal case, for helium, the energy of an incident atom will be

$$E = 5/2\ k.T_{nozzle} \qquad (5.8)$$

which, at a reservoir temperature of 300K, leads to a value of

$$\lambda_{inc} \sim 0.57\text{Å} . \qquad (5.9)$$

This value, when used to estimate positions of peaks on the scattering distributions of diffractive systems, fits extremely well and leads to the conclusion that the expansion involves almost complete conversion of local gas enthalpy to forward motion, implying in turn that the velocity distribution is narrow. However, as the diffraction peaks themselves are wider than the (00) beam there must still be an appreciable velocity spread. Without further experimental methods no detailed discussion can be made. It should be noted that the incident energy of an atom in a nozzle-generated beam differs only slightly from that in an effusion-source generated beam

$$E_{nozzle} = \frac{5}{2} kT \qquad (5.10a)$$

monatomic case

$$E_{effusion} = 2kT . \qquad (5.10b)$$

(ii) Beam Flux

The mass flow through the nozzle source can again be estimated by assuming isoentropic flow and by using the methods of continuum mechanics.

Mass Flow per unit area

$$= \sqrt{\left(\frac{\gamma M}{R}\right) \cdot \left(\frac{2}{\gamma+1}\right)^{\left(\frac{\gamma+1}{\gamma-1}\right)}} \cdot \frac{P_o}{\sqrt{T_o}} \qquad \text{(Shapiro, 1953)} \qquad (5.11)$$

where p_o is the gas pressure in the nozzle

T_o is the gas temperature in the nozzle

M is the molecular mass

R is the gas constant

γ is the ratio of specific heats.

For a given axial flux at the nozzle, F_N, the flux at a point downstream can be estimated from the relation (Anderson (1974)).

$$f = \frac{1.95\ F_N}{\pi x^2} \qquad (5.12)$$

x is the distance of the nozzle exit.

The above relations were used prior to the construction of the instrument in order to (a) design a system that would give a beam flux at the crystal of approximately 10^{14} molecule s^{-1} and (b) ensure that adequate pumping capacity was incorporated into the nozzle exhaust chamber.

CHAPTER SIX

SURFACE CHARACTERIZATION

6.1 Introduction

In recent years many techniques have been developed in order to study the surfaces of materials. In this work two techniques, low energy electron diffraction and Auger electron diffraction spectroscopy, were used to characterize the surfaces under investigation prior to the molecular beam experiment. Few other molecular beam investigations have been carried out on well-characterized surfaces.

6.2 Basic Principles of LEED

The diffraction conditions for elastic scattering can be deduced from a kinematic analysis (Kittel, 1967). They are:-

$$\underline{K}_f = \underline{K}_i + \underline{G} \qquad \text{Conservation of Parallel Momentum} \qquad (6.1)$$

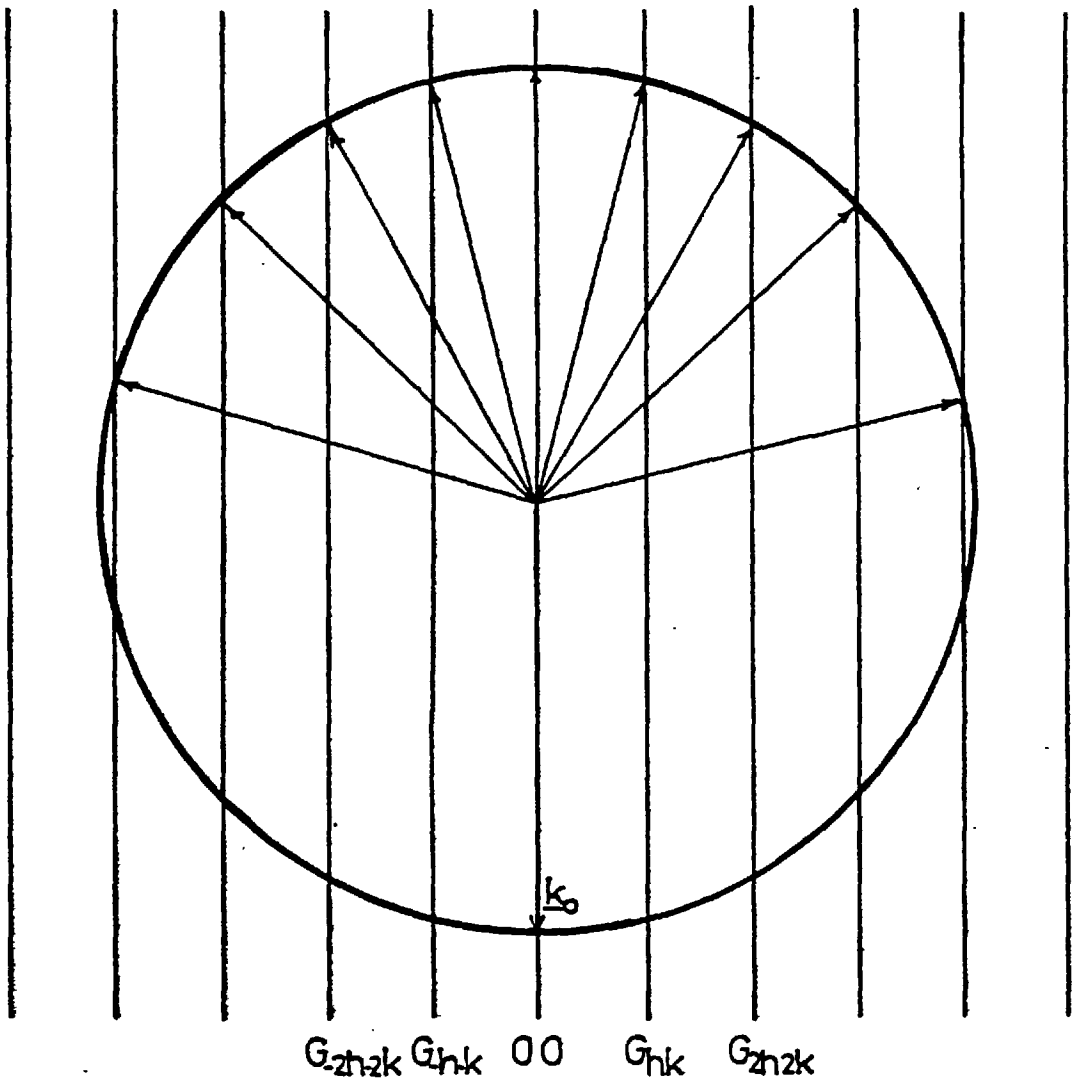
and $$k_i^2 = k_f^2 \qquad \text{Conservation of Energy} \qquad (6.2)$$

where $\underline{k}_i$, $\underline{k}_f$ are the incident and scattered wavevectors

$\underline{K}_f$, $\underline{K}_i$ are the surface components of the wavevectors

and $\underline{G}$ is a surface reciprocal lattice vector.

The diffraction process can be described by a simple Ewald sphere diagram as shown in Fig. (6.1). In this figure the normal incidence condition is drawn as this



EWALD CONSTRUCTION AT
NORMAL INCIDENCE CONDITION
FIG. 6.1

was the configuration used during the experiments. For a two-dimensional scattering process the scattering conditions are determined by the reciprocal lattice rods G_{hK}. The construction shows that for all energies, above a certain threshold, any particular rod will be crossed by the Ewald sphere implying that a diffraction spot will be obtained at all energies. From the Ewald sphere diagram it is easy to derive the two-dimensional Bragg Law.

$$d_{hk} \sin\theta_{hk} = n\lambda . \qquad (6.3)$$

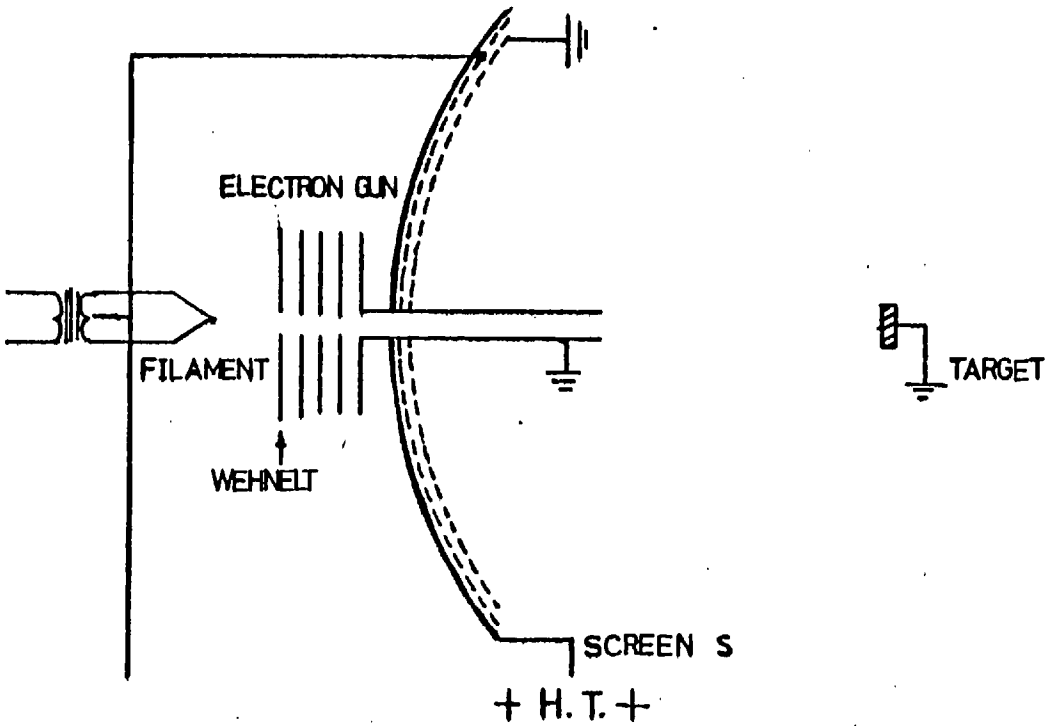
Mere observation of a diffraction pattern does not yield a great deal of structural information; in particular it does not depict the positions of adsorbed atoms with respect to substrate atoms. More advanced investigations observe the variation in diffracted beam intensities with beam energy and this can result in structural information when experimental results are compared with calculations based on one of the more sophisticated LEED theories now available. The recent publications of Pendry (1975), Duke (1975) and Tong (1975) provide detailed accounts of the progress of this work. It should be stressed that there is no simple way in which intensity measurements can be utilised to give detailed structural information. Of particular relevance to the present study is the work of Buchholz et al (1975) who studied the p(2x1)O-W(110) system and performed

calculations to predict the positions of adsorbed oxygen with respect to the tungsten lattice.

One interesting aspect of atom scattering is that, as zero penetration can be assumed for thermal energy beams, the phenomenum is a true two-dimensional scattering problem and some comparison with LEED should be possible.

6.3 The LEED System

The LEED patterns were obtained on a Vacuum Generators 2-grid optics system using an LEG1 electron gun. The set-up is shown schematically in Fig. (6.2). A nearly monoenergetic beam of electrons is directed at normal incidence onto the target. A small percentage of these electrons are back-scattered and pass through the two grids to strike the fluorescent screen S to which a high positive potential is applied. The grids act as an energy filter. The outer grid is earthed, in order to maintain a uniform field between it and the earthed target. A potential is applied to the inner grid in order to ensure than only elastically scattered (or nearly elastically scattered) electrons strike the screen and form a diffraction pattern. With a single crystal material cut along one of its principal symmetry directions a simple spot diffraction pattern is obtained. The energy resolution achieved in the simple 2-grid apparatus is poor due to field penetration, but despite this the LEED patterns obtained in the course of this work were quite well defined.



SCHEMATIC DIAGRAM
OE LEED OPTICS

FIG. 6.2

6.4 The Auger Process : Basic Principles

Auger electrons arise as a consequence of radiationless rearrangement of the electrons in the excited atoms in which a core hole has been created. In the present work excitation was brought about by electron bombardment but x-rays or ion bombardment can also be used: Fig. (6.3) shows a typical secondary electron distribution from a target bombarded with electrons of energy E_p (in the present work 3keV).

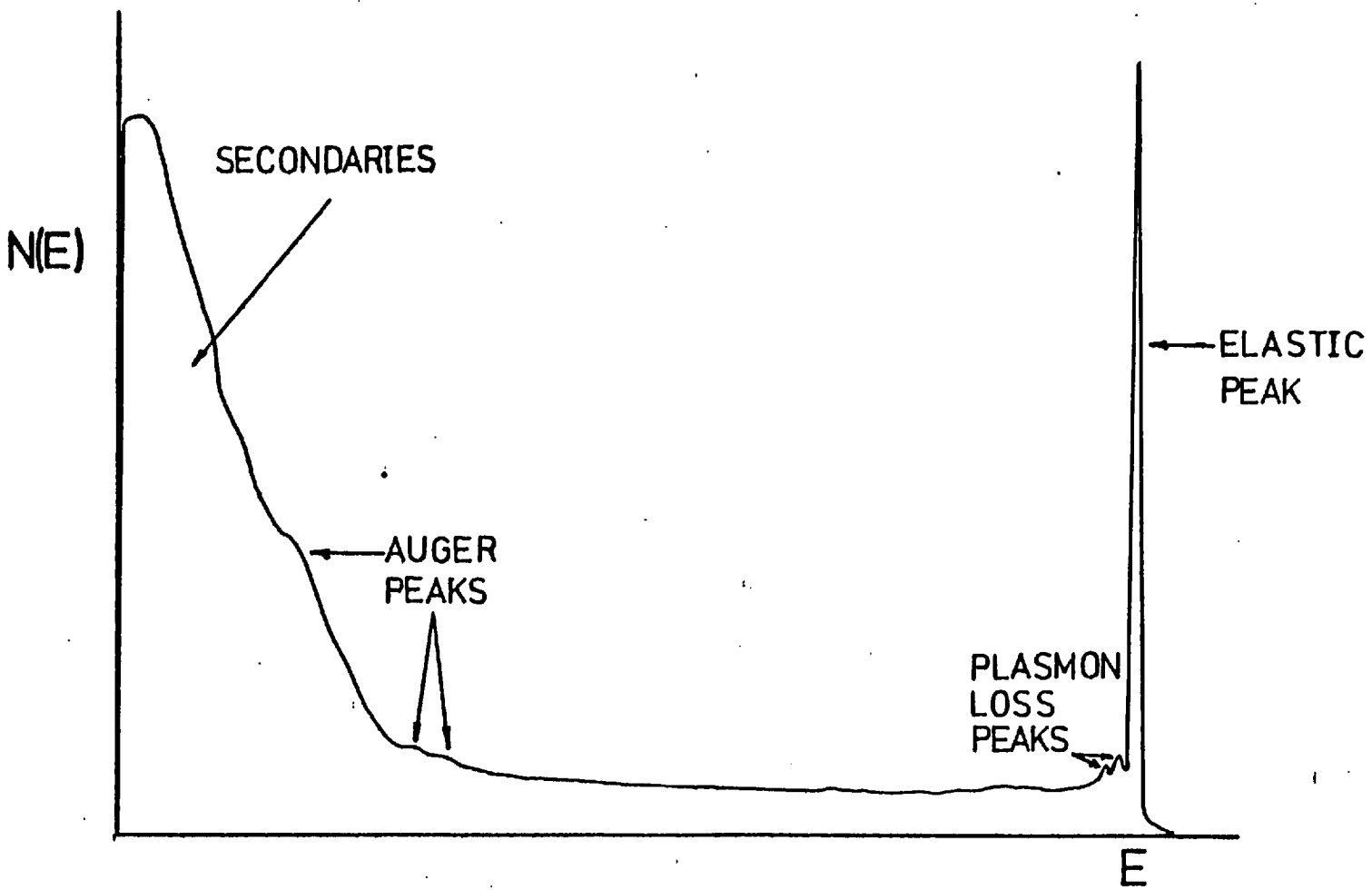
The type of rearrangement process involved in the Auger process is shown in Fig. (6.4). It can be seen that the process involves three energy levels, the energy of the ejected Auger electron being independent of the primary beam energy, excepting that this must be high enough to bring about the initial ionization.

The kinetic energy of the emitted Auger electron can be established by considering the initial and final states of a single atom: i.e.

$$E_{KIN} = E_i - E_f. \tag{6.4}$$

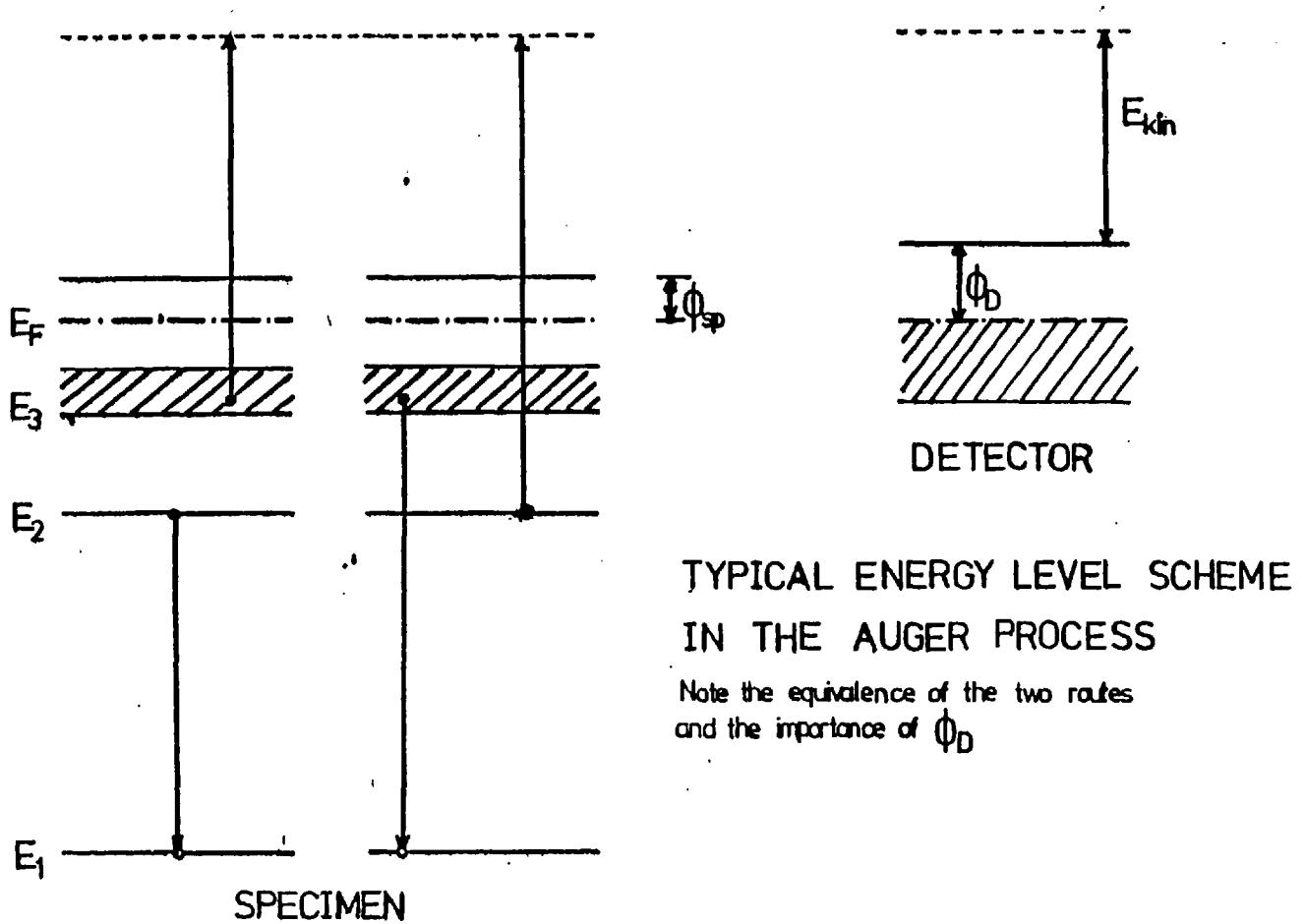
The initial state energy is given by the ionization potential or binding energy of the corresponding core electron of an atom E_K, E_L, etc. The final state, is given by the energy required to create two holes in the electron configuration i.e. typically

$$E_f = E_{L2} + E_{L3(L2)} \tag{6.5}$$



ENERGY DISTRIBUTION OF SCATTERED ELECTRONS

FIG. 6.3



TYPICAL ENERGY LEVEL SCHEME IN THE AUGER PROCESS

Note the equivalence of the two routes and the importance of ϕ_D

○ unoccupied
● occupied

FIG. 6.4

where $E_{L3(L2)}$ is the binding energy of an electron in the L3 shell in an atom already ionized in the L2 shell. (All binding energies are referred to the vacuum level). Thus one has for the kinetic energy, typically

$$E_{KIN} = E_K - E_{L2} - E_{L3(L2)} \quad . \tag{6.6}$$

To a first approximation this may be written

$$E_{KIN} = E_K - E_{L2} - L_{L3} \quad . \tag{6.7}$$

Fig. (6.4) shows, in fact, a more general case involving valence electrons. A number of discussions can be found in which more elaborate methods are used in order to calculate Auger-electron energies taking into account modification of binding energies due to the initial core hole, that of Chung and Jenkins (1970) being particularly useful. Coad and Riviere (1971) discussed in particular the case of Auger transitions involving valence electrons.

In the case of solid targets any attempt to measure the kinetic energy of an emitted Auger electron must taken into account the work function of the detector (and not the sample itself). As is shown in Fig. (6.4) the measured kinetic energy is

$$E_{MEAS} = E_{AUGER} - \phi_D \tag{6.8}$$

6.5 The Auger Electron Spectrometer

The spectrometer used was a Vacuum Generators Hemi-Cylindrical Mirror Analyser (HCMA). It has an integral electron gun, which could be operated at beam energies up to 3KeV. The incident angle was approximately 20 degrees. The spectrometer acts as a band pass device. Electrons of a given energy pass through the filter to strike a phosphor and produce scintillations that are detected by a photomultiplier which is bolted externally on the vacuum system. For a spectrometer of this type the current from the photomultiplier may be written

$$I(E) = CEN(E) \quad \text{(where C is a constant for the device).} \tag{6.9}$$

Differentiation gives

$$\frac{dI(E)}{dE} = CN(E) + CE\,\frac{dN(E)}{dE}\,. \tag{6.10}$$

It can be seen from the secondary electron spectrum given earlier, Fig. (6.3), that Auger electrons produce only small fluctuations in the N(E) distribution and consequently they are more clearly identified if the differential of the distribution is taken. This can be done electronically by applying a modulation voltage to the energy filter and detecting the first harmonic component with a lock-in amplifier. This

enables a plot proportional to $E \frac{dN(E)}{dE}$ to be obtained. It can be seen from equation (6.10) that differentiation of the photomultiplier output actually gives $CN(E) + CE \frac{dN(E)}{dE}$ which means that at low energies the spectrum is distorted by the CN(E) contribution.

The modulation voltage was applied at high frequency (2500Hz) with a peak-to-peak voltage of 8 volts. In general, in this work Auger spectra were used as a 'finger print' method of identifying surface species. The primary purpose of using the technique was to monitor the presence of oxygen and carbon at the surface.

CHAPTER SEVEN

RESULTS

7.1 Preparation of Ordered Surface Layers

Gas scattering experiments were carried out from three types of surfaces:-

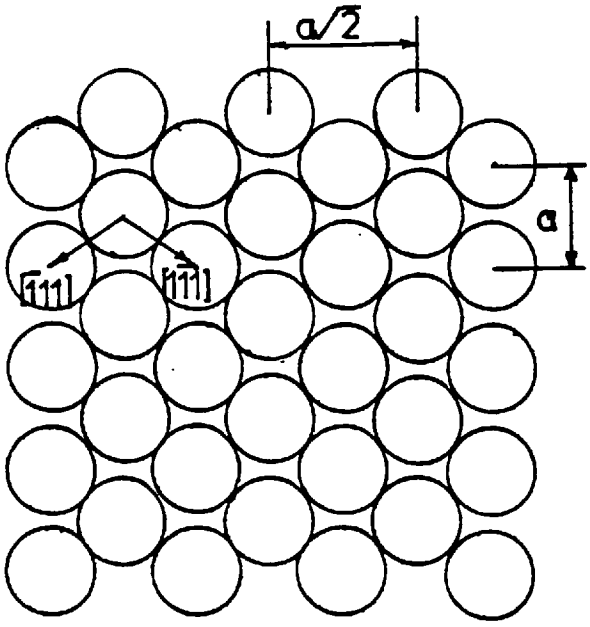
(a) The clean W(110) face

(b) The carbided W(110) face

(c) A variety of oxygen overlayers on W(110).

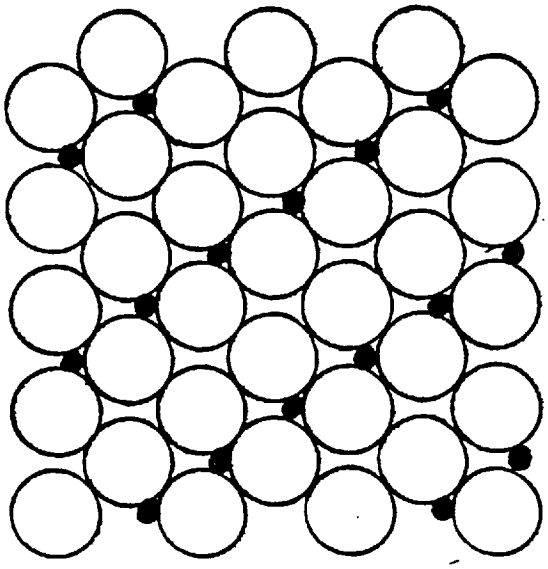
The two-dimensional structures of the clean W(110) surface and two of the various oxygen overlayers are shown in Fig. (7.1). The structure of the carbided surface will be discussed later.

The preparation of atomically clean tungsten surfaces has been discussed by many workers [Joyner et al (1973), Bas and Banninger (1974)]. One interesting aspect in the cleaning of tungsten is the behaviour of carbon impurities, which apparently diffuse from the bulk to the surface when the sample is heated, or are formed in situ by decomposition of gas phase hydrocarbons. In the two studies mentioned above carbon was removed by treatment in oxygen, and Auger electron spectroscopy was used to monitor the condition of the surface during this process. It was found that heating, for a few minutes, at 2000K in oxygen at a pressure of 5×10^{-7} torr would remove surface carbon. Prolonged heating of up to 100 hrs was recommended to remove all carbon from the bulk. Similar

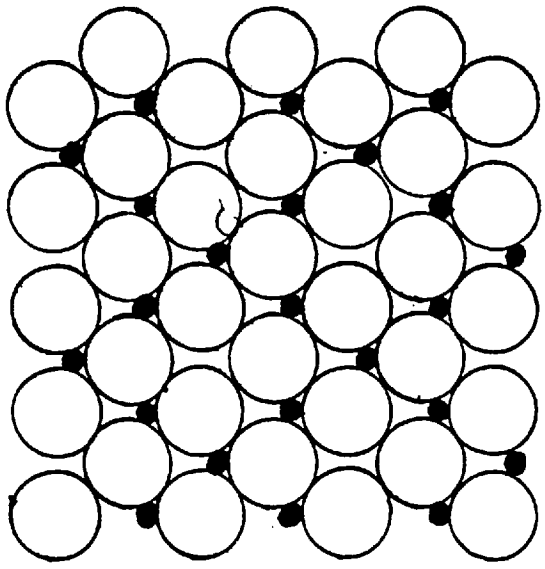


(a) W(110) SURFACE

a = 3,16 Å



(b) p(2×1)O-W(110)



(c) p(2×2)O-W(110)

FIG. 7.1

results were obtained in the present work although very prolonged heating to remove the last traces of carbon was not attempted. As Auger electron spectroscopy and LEED were available to monitor the surface composition and structure it was felt that short periods of heating were justified, and desirable in view of the frailty of the crystal holder. The two studies previously mentioned were performed on polycrystalline ribbons and it is assumed that they did not have the problems associated with mounting large single crystals. The oxygen layer, formed after the carbon has been oxidised, was removed by heating to temperatures of 2500K for 2-3 minutes.

The Auger spectra associated with the various stages of the cleaning procedure are shown in Figs. (7.2), (7.3) and (7.4). The two small peaks which appear on the low energy side of the main carbon Auger peak are thought to indicate the presence of a surface carbide. Haas et al (1972a) showed that in the Auger spectra of carbon on molybdenum the presence of these two low energy peaks was indicative of a surface carbide while for graphitic overlayers these peaks were not resolved. Bas and Bänninger (1974) observed the double peak feature for carbon on tungsten and took its presence to imply that the surface carbide W_2C had been formed. They pointed out that hydrocarbon overlayers did not give rise to this double peak structure in Auger spectra.

In attempting to interpret Auger spectra where adsorption from the gas phase has occurred it should be remembered that the primary electron beam may promote decomposition and desorption phenomena. Haas et al (1972a) had noted that

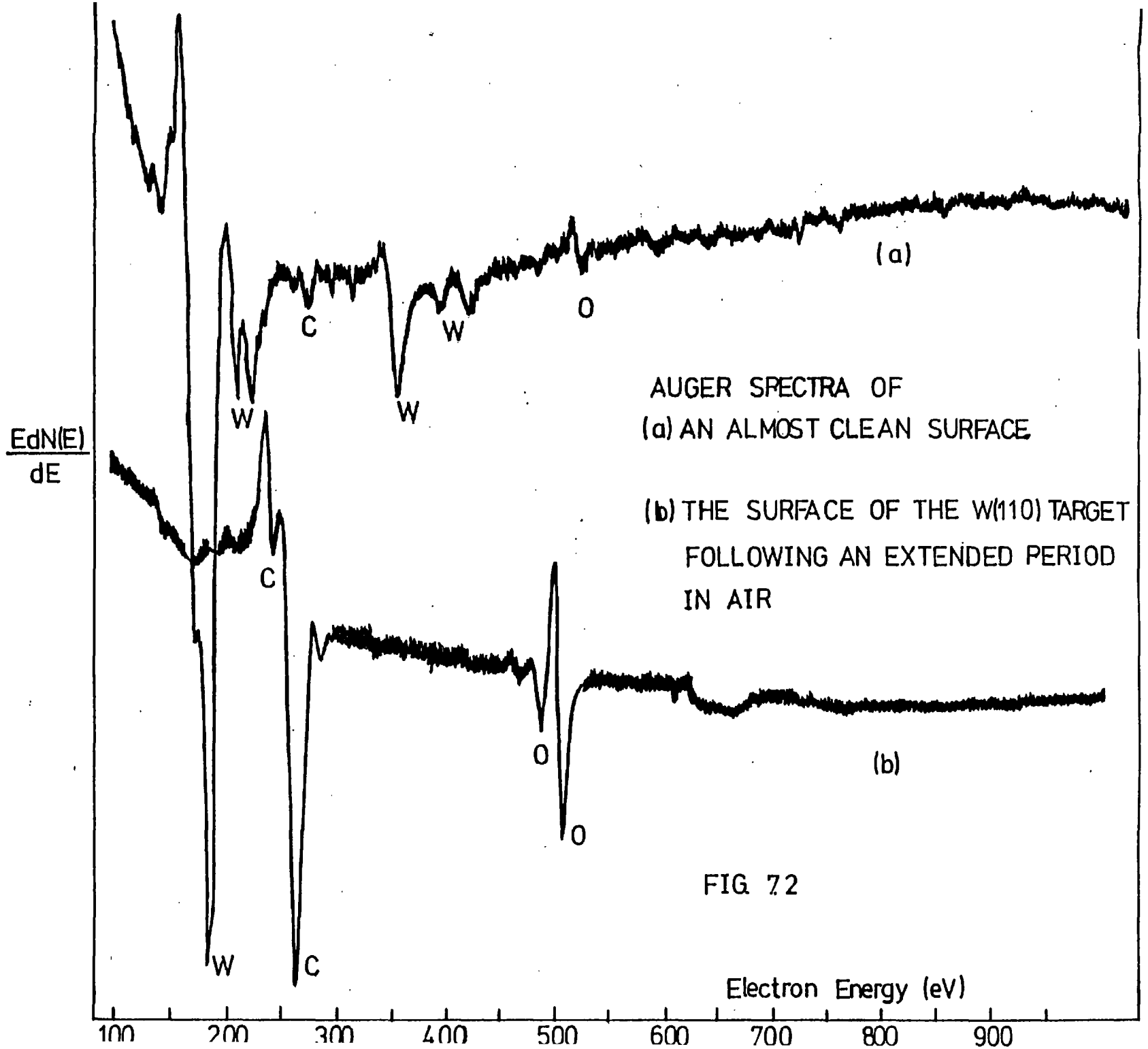
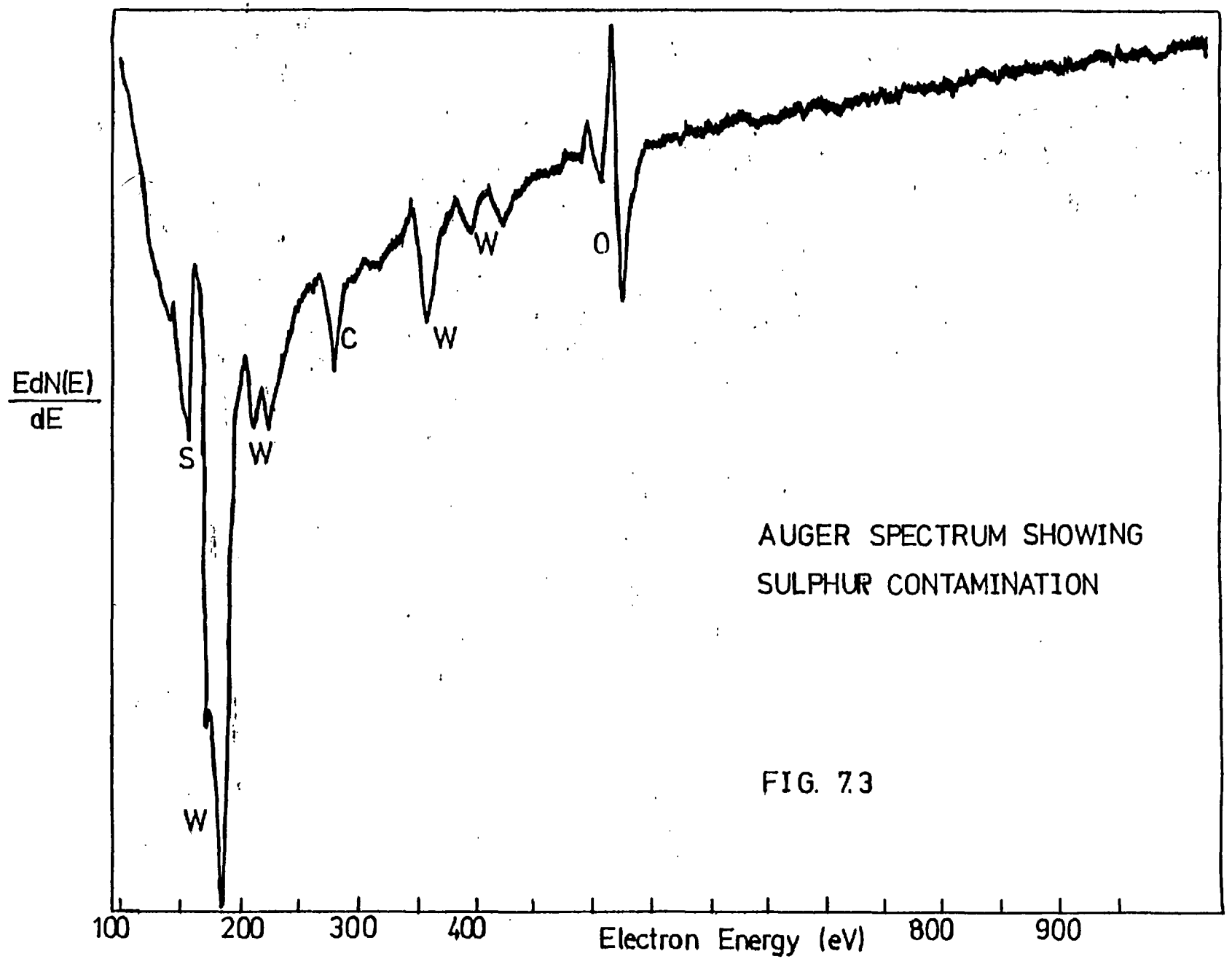
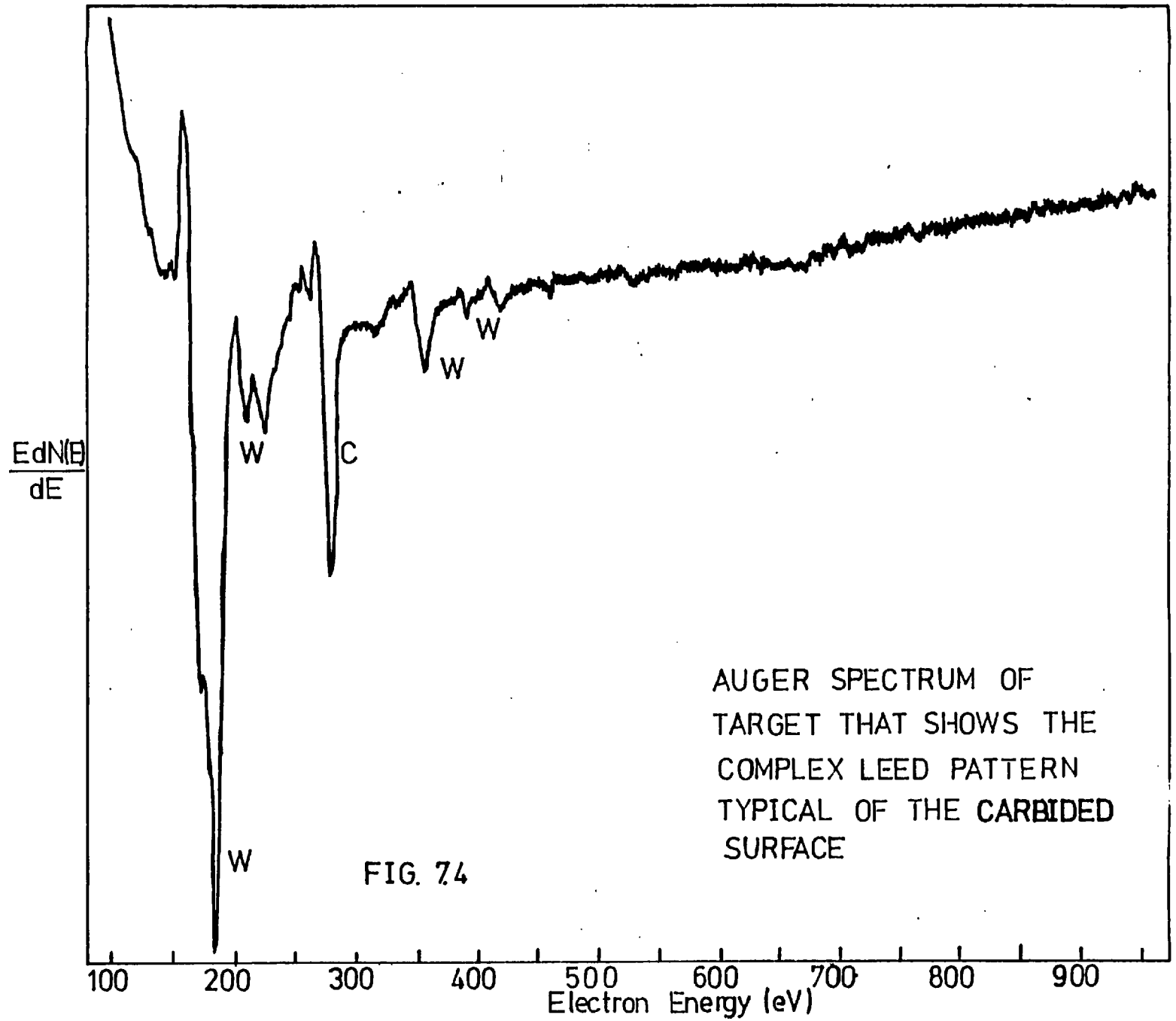

EdN(E)
dE
W
C
W
W
O
(a)
AUGER SPECTRA OF
(a) AN ALMOST CLEAN SURFACE
(b) THE SURFACE OF THE W(110) TARGET
FOLLOWING AN EXTENDED PERIOD
IN AIR
C
O
O
(b)
W
C
Electron Energy (eV)
100
200
300
400
500
600
700
800
900

FIG. 7.2



AUGER SPECTRUM SHOWING
SULPHUR CONTAMINATION

FIG. 7.3



AUGER SPECTRUM OF TARGET THAT SHOWS THE COMPLEX LEED PATTERN TYPICAL OF THE CARBIDED SURFACE

FIG. 7.4

CO adsorption on Mo targets produced an Auger spectrum typical of surface carbide initially,but after prolonged exposure to the electron beam an Auger spectrum corresponding to a graphitic surface was obtained. The spectra observed in the present work show quite clearly that the surface carbon layer was in the form of a carbide, and as will be proposed later this was probably W_2C.

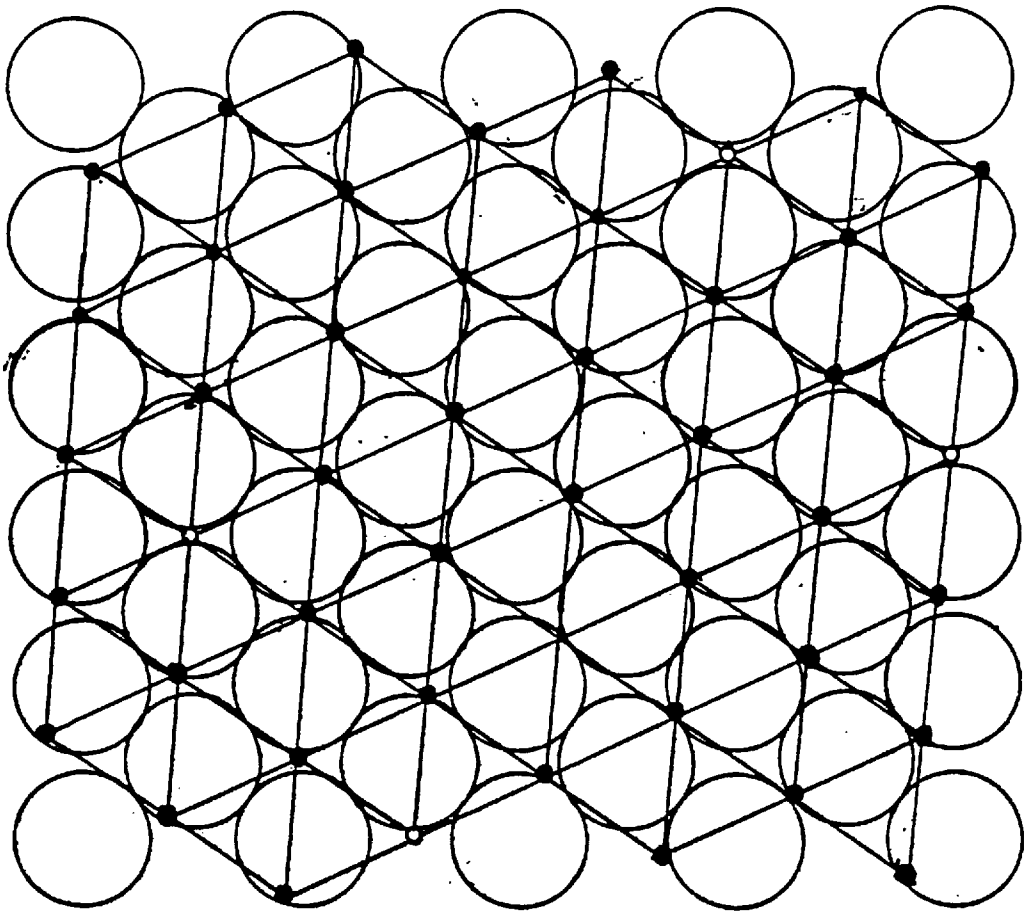
Auger spectroscopy also indicated that sulphur was a contaminant in the target. Previous work on tungsten does not appear to have investigated the extent of sulphur contamination. In fact Bas and Bänninger appear to have overlooked the sulphur Auger peak when discussing the cleaning of tungsten. After heat treatment at 1600K in a pressure of 10^{-7} torr of oxygen the Auger spectrum given in their paper shows, besides a large oxygen peak, a sulphur peak at about 150eV. This was not present on the carbon contaminated surface prior to the heat treatment. The problem of sulphur contamination of palladium and molybdenum surfaces has been discussed by Szmerska and Lipska (1976, 1977) and by Bernasek and Staudt (1976). Exposure of the surfaces to hydrogen apparently brought about increased sulphur concentration at the surface. Bernasek and Staudt observed this on Mo while attempting to reduce a surface oxide by heating the sample in hydrogen. This method of removing oxygen from tungsten was previously used by Joyner et al (1973). In the present work evaporation of oxygen and oxide was found to be more successful than heating in hydrogen,and in view of the results of the studies mentioned above this may have been a more appropriate method.

(i) Ordered Carbon Overlayers

The diffusion of carbon to the surface of a W(110) face has been found to give rise to two surface structures dependent upon the amount of carbon present. (Weinberg and Merrill 1972b). One of these is a simple (1x1) structure and the other has a (3x5) unit cell rotated 35^{o} with respect to the tungsten unit cell. A schematic diagram representing this (3x5) structure and its reciprocal lattice is shown in Fig. (7.5). This structure was originally interpreted in terms of a very dilute carbon layer with carbon atoms at the corners of the unit cell (Stern 1964) but a more realistic explanation in terms of a coincidence lattice has been put forward by Bauer (1966). This structure will be discussed more fully later. In the present work it was possible to produce this (3x5) carbon overlayer by heating for short periods, in vacuum, at 1500K. (Occasionally the structure would appear without heating). The (3x5) structure can be obtained in two domains as shown in Fig. (7.6).

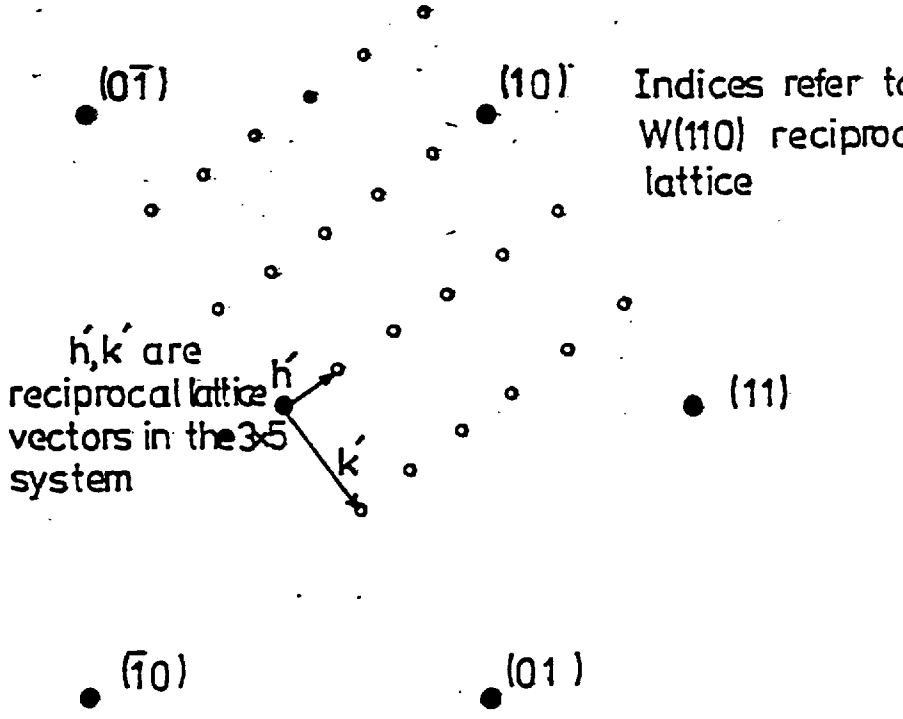
(ii) Ordered Oxygen Overlayers

The adsorption of oxygen on W(110) gives rise to at least six different phases as shown by distinctive LEED patterns (Avery (1974), Germer and May (1966) and Bauer and Engel (1977, 1978). With increasing oxygen exposure a p(2x1) structure is observed at ½ monolayer coverage, a p(2x2) structure at ¾ monolayer coverage and a (1x1) structure at monolayer coverage. Following monolayer coverage extensive heating at temperatures between 1200 and 1500K gives rise to a complex LEED pattern.



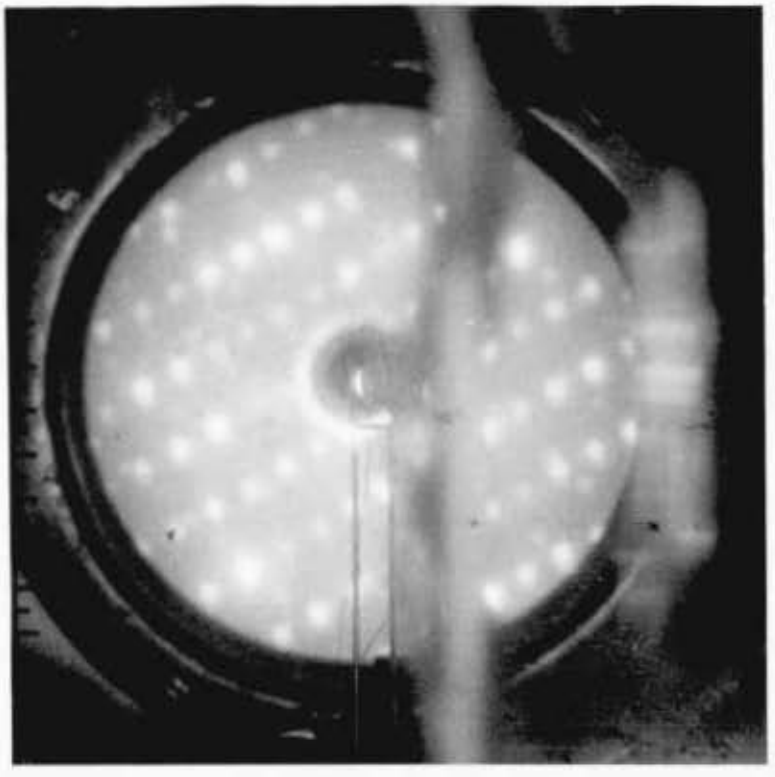
° Open circles indicate positions of coincidence that give rise to a 3×5 structure

(a)
MODEL OF A HEXAGONAL OVERLAYER ON A b.c.c. (110) FACE



(b)
RECIPROCAL LATTICE OF A SINGLE ORIENTATION OF THE (3×5) CARBIDE SUPERIMPOSED ON THE RECIPROCAL LATTICE OF W(110)
(from Weinberg and Merrill 1972a)

FIG 7.5



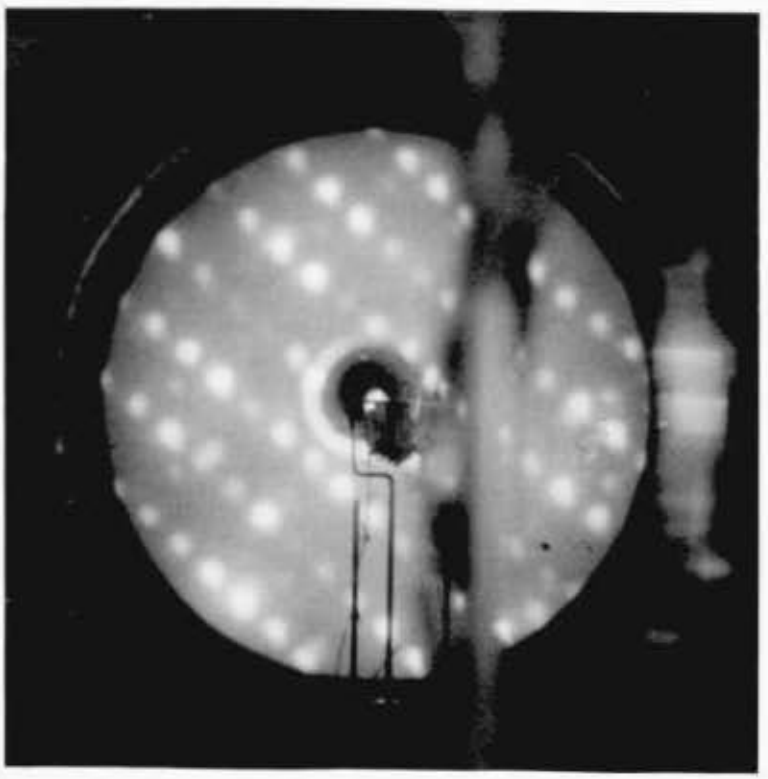
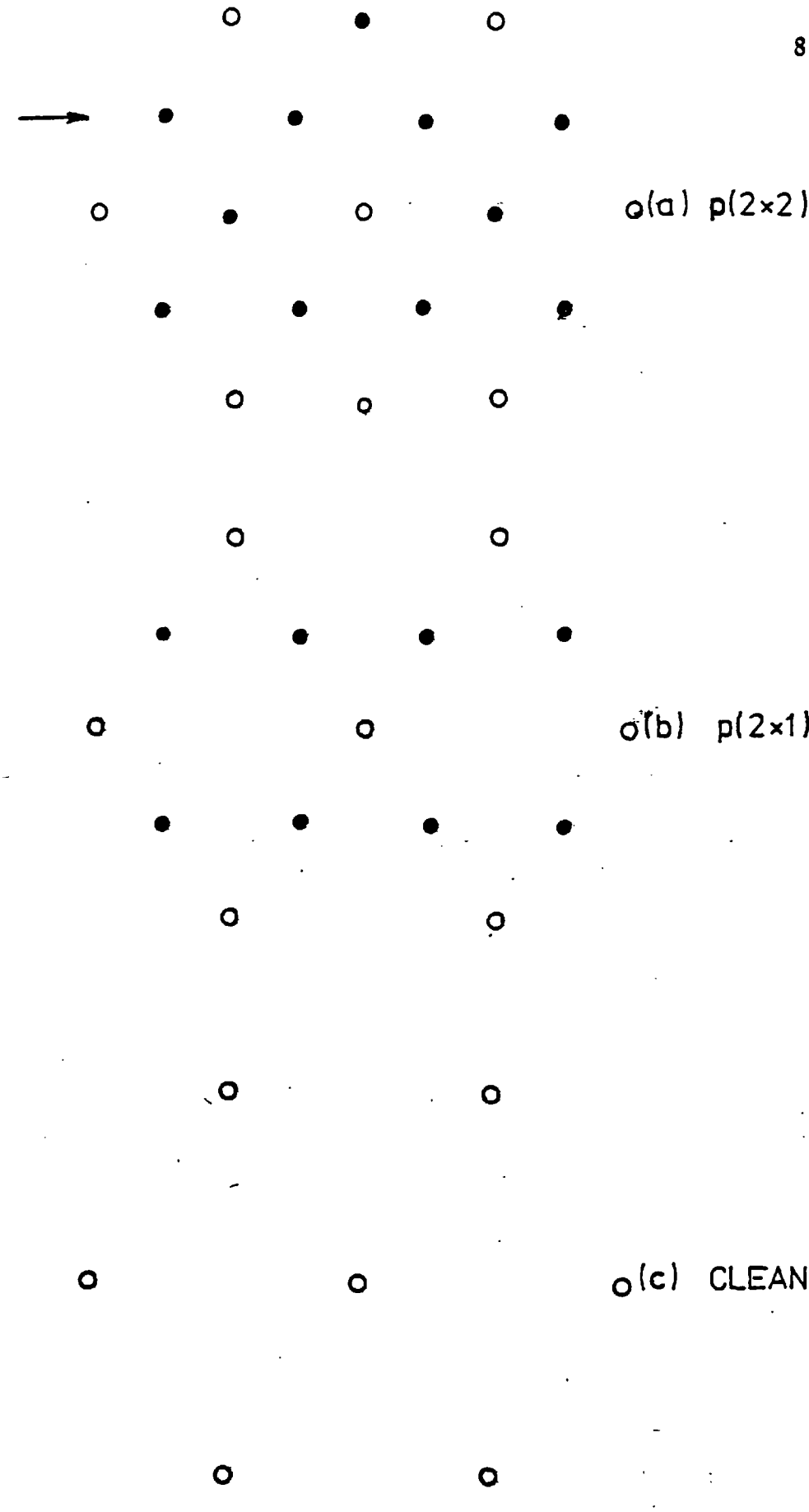


FIG. 7.6

Further heating produces a reversal of the sequence resulting in the p(2x2) structure being reformed at 1800K, the p(2x1) structure at 1860K and finally a clean surface at 2200K. Gas scattering experiments were, in general, confined to the simpler surface structures observed at low coverages ($\theta \leq 1$). The LEED patterns corresponding to the complex phases were observed especially during crystal cleaning cycles. The simple structures found are assumed to be due to unreconstructed surfaces, the oxygen sitting in its atomic state on top of the W(110) face. This view is supported by the studies of Bauer (1966) using LEED, Mazumdar and Wassmuth (1972) using thermal desorption techniques, and by Buchholz et al (1975) who observed LEED beam intensities and used this data to deduce the position of oxygen in the surface unit cell. Reconstructed surfaces had been proposed by Germer and May (1966). Reciprocal lattices for the clean W(110), p(2x1) overlayer and p(2x2) overlayer are shown in Fig. (7.7).

7.2. Scattering on Clean and Contaminated Surfaces

A scattering distribution for helium on clean W(110) is shown in Fig. (7.8). It can be seen that a single peak centred at the specular angle is obtained. This peak has a full width at half maximum (FWHM) of 3^{o} and an I/Io value of 0.3. The shape and magnitude of this peak was critically dependent on the condition of the surface. The distribution shown in Fig. (7.8) was obtained immediately after flashing the crystal to 2000K to remove adsorbed gases. The angular distribution was recorded after first



RECIPROCAL LATTICE STRUCTURES
OF CLEAN AND OXYGEN COVERED W(110)

FIG. 7.7

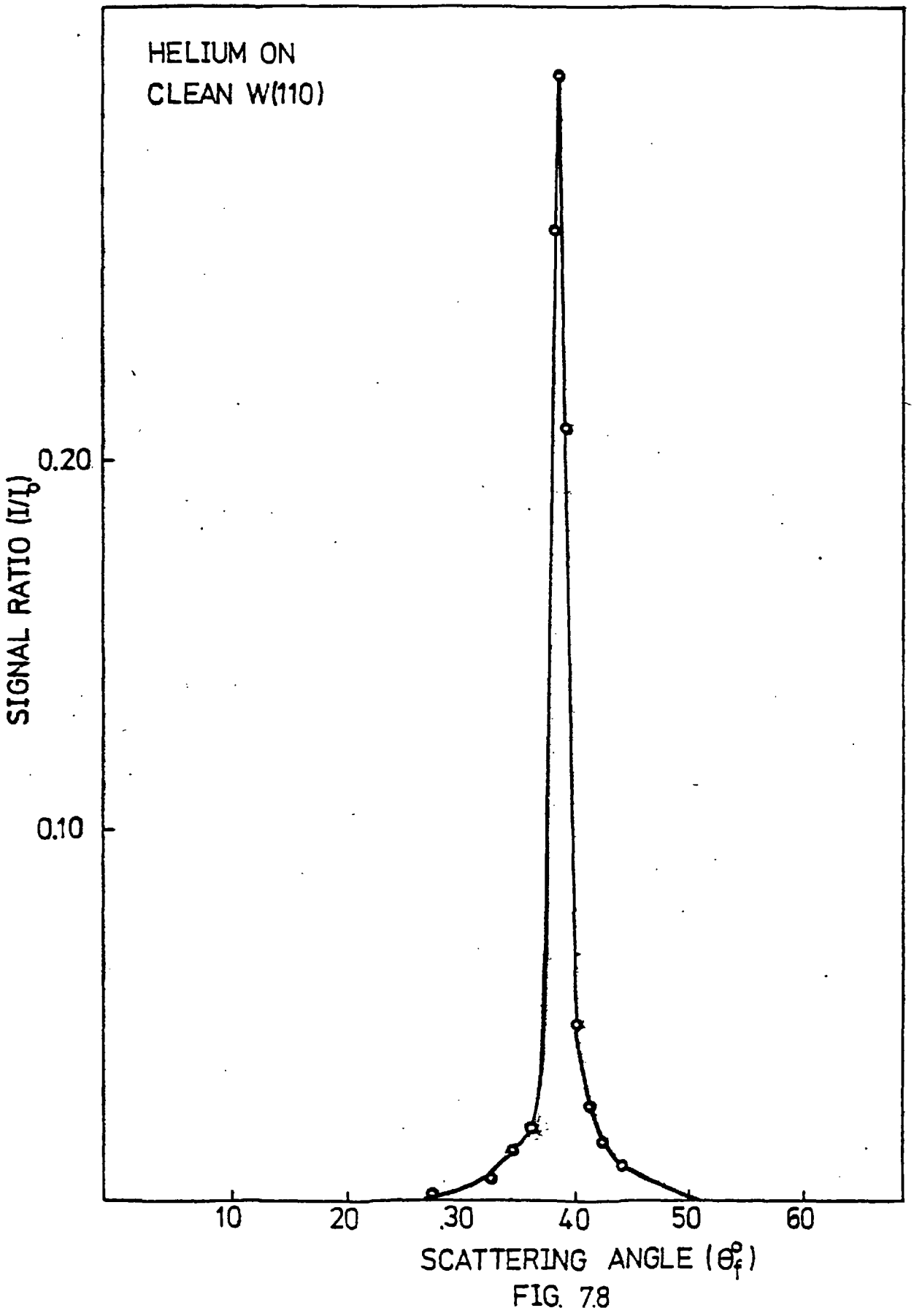

HELIUM ON
CLEAN W(110)
SIGNAL RATIO (I/I$_0$)
0.20
0.10
10
20
30
40
50
60
SCATTERING ANGLE (θ_f^o)

FIG. 7.8

locating the precise position (both horizontal and vertical) of the detector at which the maximum scattered signal was obtained. The angular distribution was then recorded at that particular vertical position of the detector. Location of the maximum of the scattered signal was always necessary after heating the crystal to high temperatures in order to safeguard against slight movement of the target holder.

7.3. Scattering from the Carbide Surface

A typical in-plane angular scattering distribution obtained from a surface showing the low energy electron diffraction pattern corresponding to a R35^{o} (3x5)C-W(110) structure is shown in Fig. (7.9). It is seen to be a multipeaked distribution. All the peaks appear to be quite sharp and there is no dominant peak. This makes indexing difficult. As the (00) beam should show least broadening due to the distribution of wavelengths in the incident beam the narrowest peak was assigned as (00). This then enables the incident angle to be calculated and further indexing of the distribution to be made.

The position of the specular beam was also determined from the position of the surface tangent. This could easily be found since the scattered signal becomes zero at this angle. It is seen in Fig. (7.9) that indexing on the basis of the unit cell for the carbide layer shown in Fig. (7.5) does not conclusively confirm the nature of the diffraction.

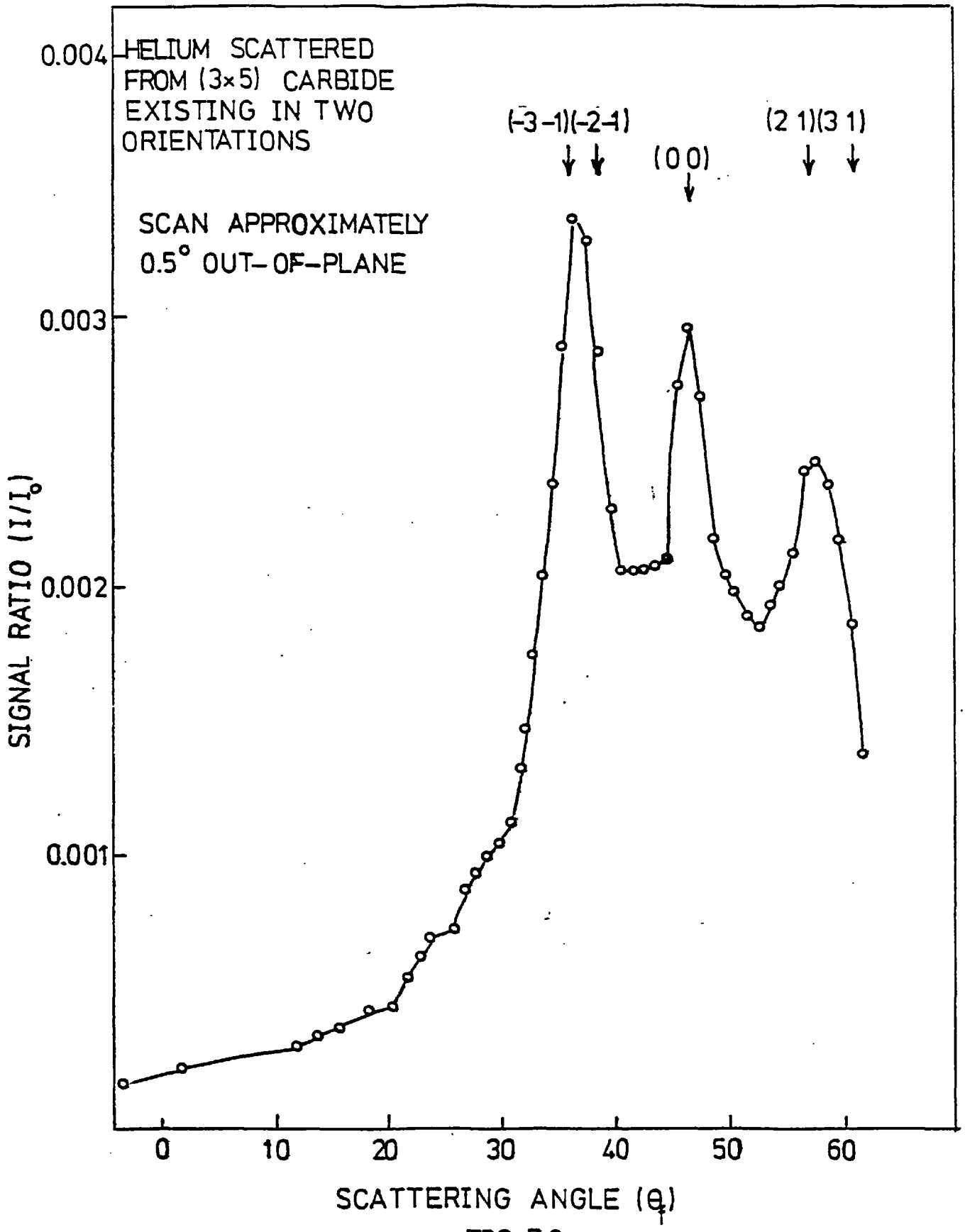

HELIUM SCATTERED
FROM (3×5) CARBIDE
EXISTING IN TWO
ORIENTATIONS
SCAN APPROXIMATELY
0.5° OUT-OF-PLANE
(-3 -1)(-2 -1)
(0 0)
(2 1)(3 1)
0.004
0.003
0.002
0.001
SIGNAL RATIO (I/I0)
0
10
20
30
40
50
60
SCATTERING ANGLE (θf)

FIG. 7.9

Fig. (7.10) shows the result of a scan vertically through the lowest angle peak of Fig. (7.9). This was obtained by changing the vertical position of the detector but not its horizontal angle. It is seen that the peak observed in the angular scan is split into a doublet. Detailed observations in vertical scans is possible because, as stated earlier, there is fine control on the vertical motion of the detector, allowing movement corresponding to variations in scattered angles of the order of $1/9^{o}$ to be made.

Scattering distributions for deuterium and neon beams were also obtained on the carbided surface. The angular distribution for deuterium, shown in Fig. (7.11), is similar to that for helium except that the peaks appear as spikes on a broad background. The intensity ratios, I/Io, of the peaks are also somewhat lower for deuterium than for helium. These differences may arise because of energy exchange with the rotational modes of deuterium. A scattering distribution for neon is shown in Fig. (7.12). There is no apparent fine structure in the peak indicative of a diffraction process. The single peak is much broader than the specular peak obtained for helium on a clean surface indicating that there are considerably more inelastic events. The maximum signal is over one hundred times smaller than that observed with helium on the clean surface.

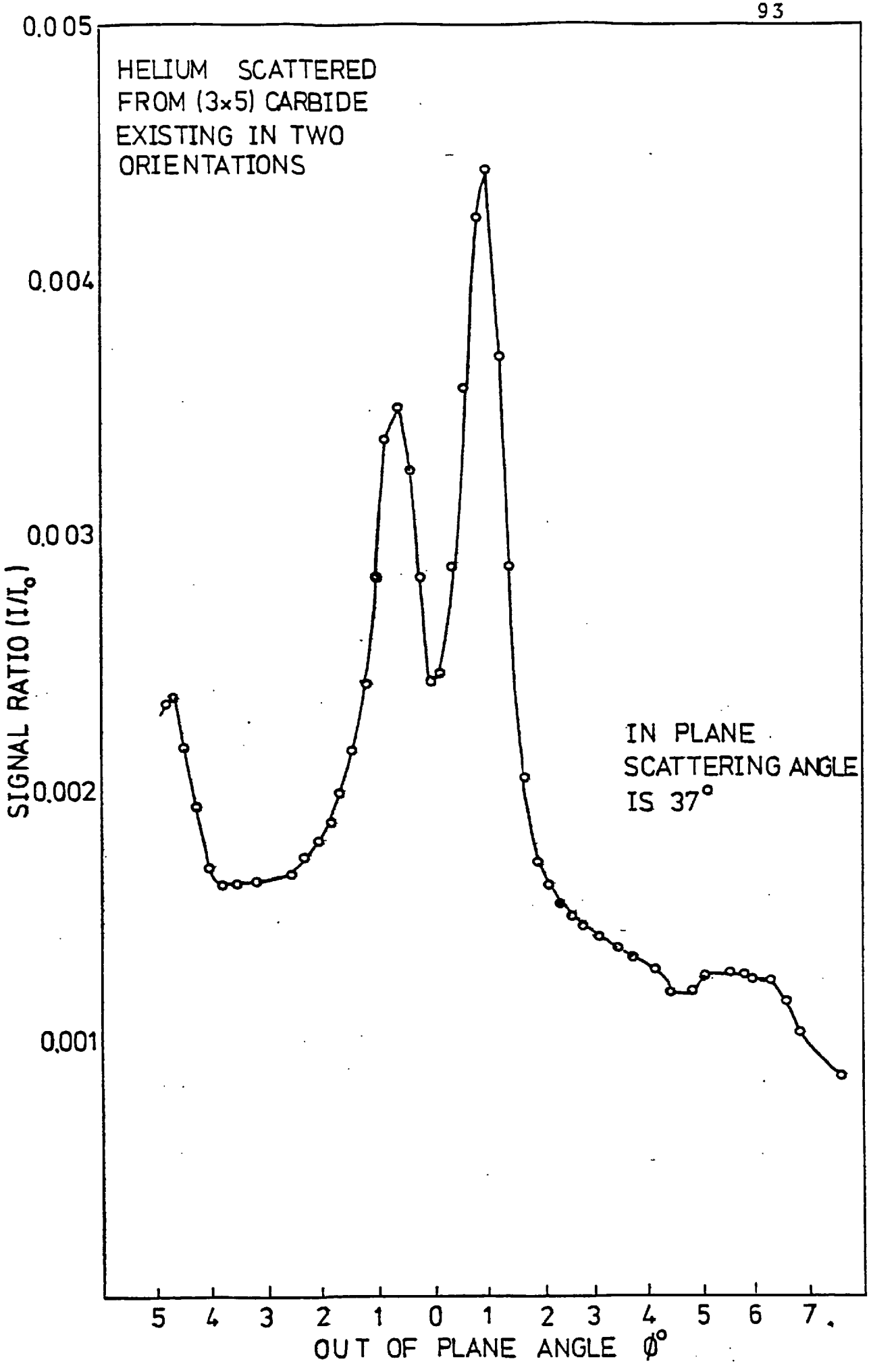

HELIUM SCATTERED
FROM (3×5) CARBIDE
EXISTING IN TWO
ORIENTATIONS
IN PLANE
SCATTERING ANGLE
IS 37°
0.005
0.004
0.003
0.002
0.001
SIGNAL RATIO (I/I0)
5 4 3 2 1 0 1 2 3 4 5 6 7
OUT OF PLANE ANGLE Ø°

FIG. 7.10

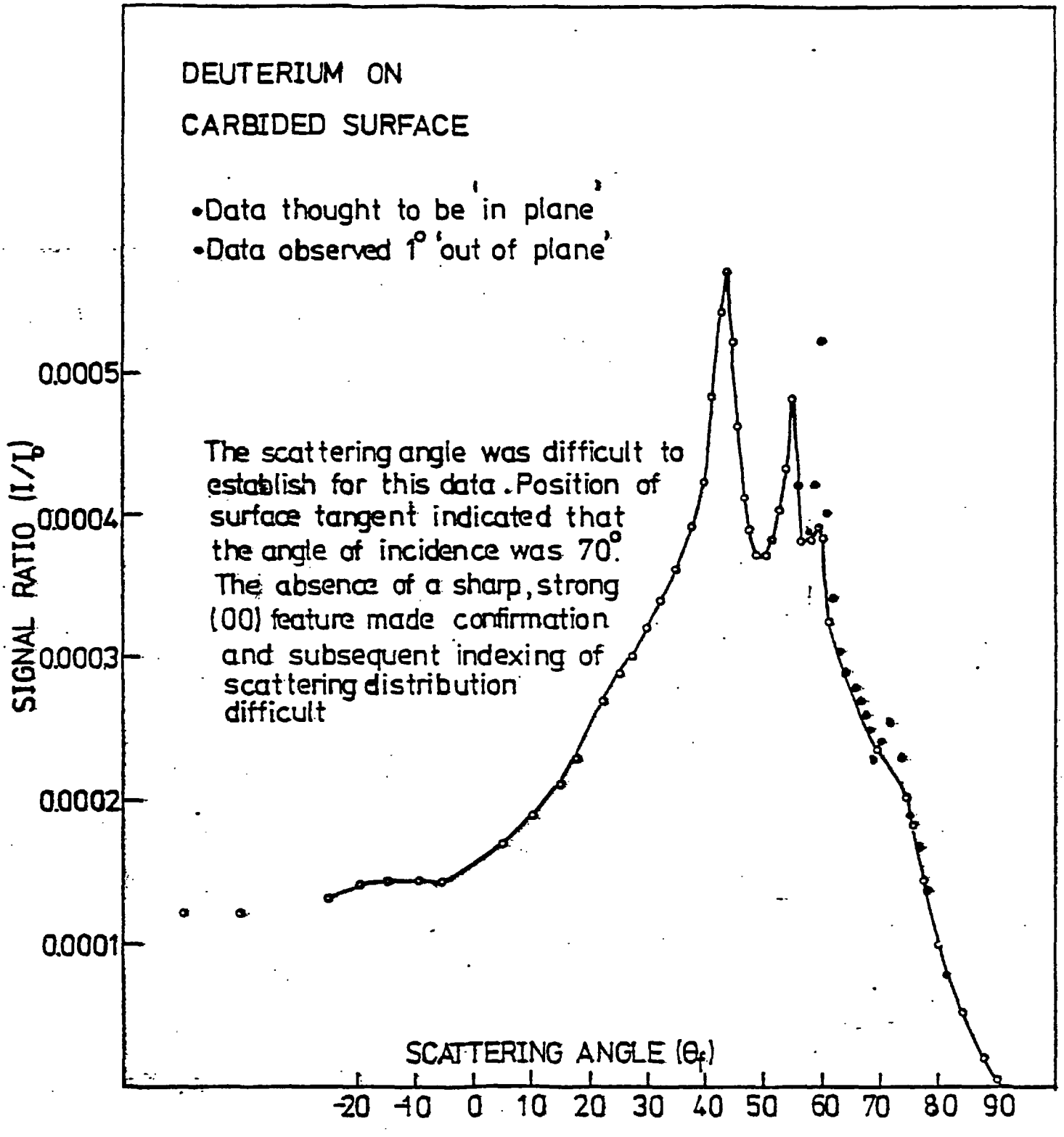

DEUTERIUM ON
CARBIDED SURFACE
•Data thought to be 'in plane'
•Data observed 1° 'out of plane'
The scattering angle was difficult to establish for this data. Position of surface tangent indicated that the angle of incidence was 70°. The absence of a sharp, strong (00) feature made confirmation and subsequent indexing of scattering distribution difficult
SIGNAL RATIO (I/I0)
0.0005
0.0004
0.0003
0.0002
0.0001
SCATTERING ANGLE (θf)
-20 -10 0 10 20 30 40 50 60 70 80 90

FIG. 7.11

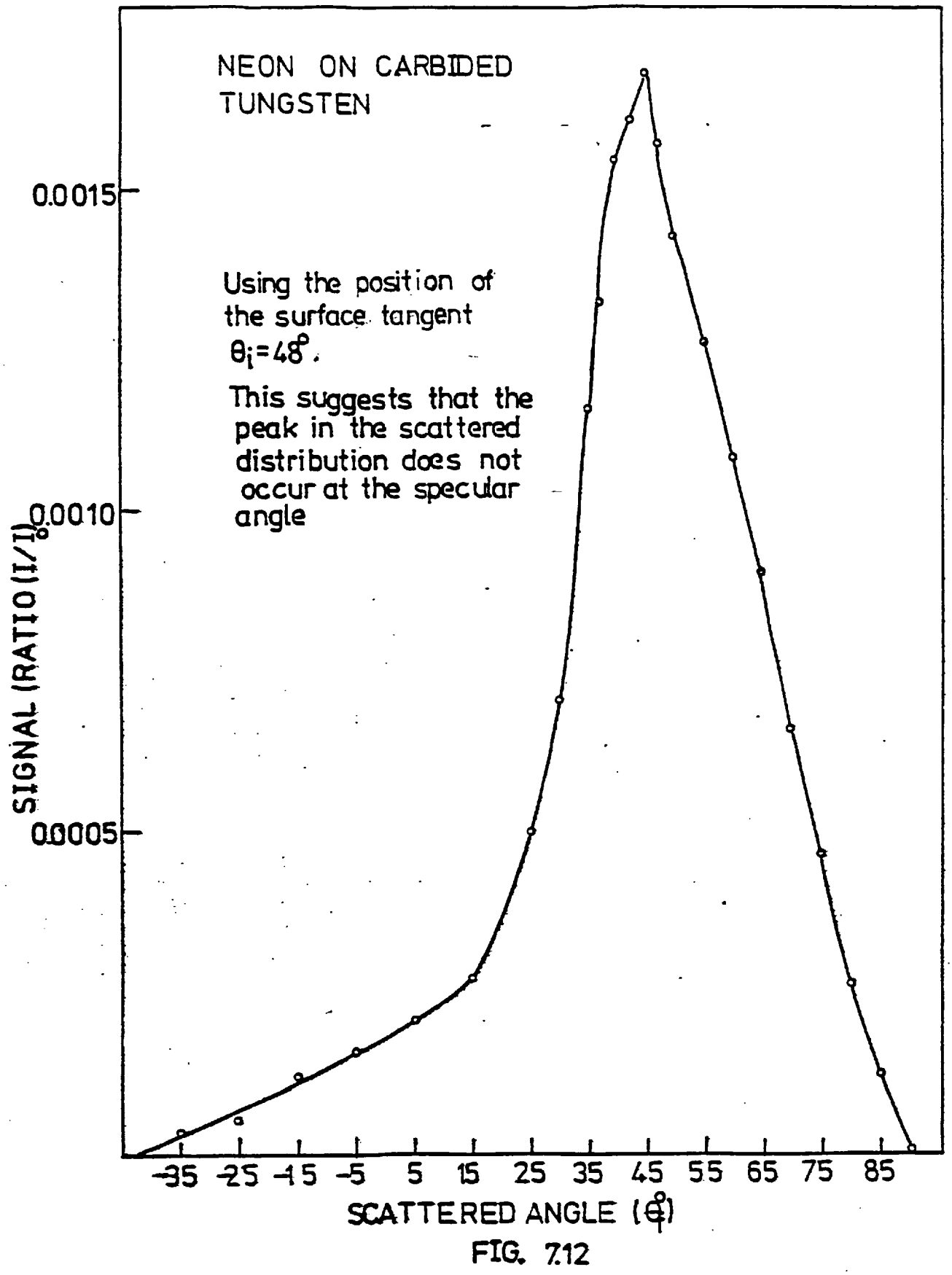

NEON ON CARBIDED TUNGSTEN
Using the position of the surface tangent $\theta_i = 48^\circ$.
This suggests that the peak in the scattered distribution does not occur at the specular angle
0.0015
0.0010
0.0005
SIGNAL (RATIO (I/I$_0$))
-35 -25 -15 -5 5 15 25 35 45 55 65 75 85
SCATTERED ANGLE (ϕ°)

FIG. 7.12

7.4. Helium Scattering from Adsorbed Oxygen Layers

Helium has been scattered from the oxygen p(2x1), p(2x2), and (1x1) structures referred to previously and the results are shown in Figs. (7.13, 7.14, 7.15). The reciprocal lattice diagrams indicate that for in-plane scattering only the p(2x2) structure will show half-order features and that the p(2x1) and (1x1) distributions will have the same peaks. This, in fact, is what is observed. The diffraction peaks are easily identified and their positions are in good agreement with predicted values (as shown in Fig. (7.14) and Table I). The incident wavelength was taken to be 0.565Å and the tungsten lattice parameter to be 3.17Å. Relative intensities of the diffraction peaks cannot be established from these in-plane angular distributions as the incident conditions used contain a slight tilt which required the maximum for each peak to be obtained using a slight vertical movement of the detector. Although the movement required to maximise a peak height was only slight, peak magnitudes may differ from the in-plane height by a factor of about two.

The oxygen covered surfaces were more easily controlled than the carbided surface and consequently more detailed experiments were conducted in which the following were investigated:-

(i) Variation of angle of incidence

(ii) Effect of temperature on diffracted beam intensities

(iii) Ability of the instrument to obtain out-of-plane scattering distributions.

TABLE I

FIGURE	DIFFRACTION PEAK POSITIONS											
	(-2 -2)		$(-\frac{3}{2}\ -\frac{3}{2})$		(-1 -1)		$(-\frac{1}{2}\ -\frac{1}{2})$		$(\frac{1}{2}\ \frac{1}{2})$		(1 1)	
	Predicted Pos.	Expmtl. Pos.	Predicted Pos.	Expmtl. Pos.	Predicted Pos.	Expmtl. Pos.	Predicted Pos.	Expmtl. Pos.	Predicted Pos.	Expmtl. Pos.	Predicted Pos.	Expmtl. Pos.
7.13	14^o	14^o	21^o	NR	29^o	31^o	38^o	38^o	60^o	60^o	85^o	NR
7.14	11^o	11^o	NE		25^o	24^o	NE		NE		69^o	68^o
7.15	-6^o	-6^o	NE		8^o	8^o	NE		NE		40^o	40^o
7.16	not scan		NE		14^o	13^o	NE		NE		49^o	48^o
7.17	4^o	5^o	NE		19^o	18^o	NE		NE		56^o	54^o
7.19	0^o	0^o	6^o	NR	13^o	NR	21^o	20^o	38^o	38^o	48^o	48^o
7.20	2^o	3^o	9^o	NR	16^o	18^o	24^o	24^o	41^o	40^o	52^o	50^o

NE = Peak Not Expected
NR = Peak Not Resolved

In subsequent figs. Predicted Positions are indicated by arrows.

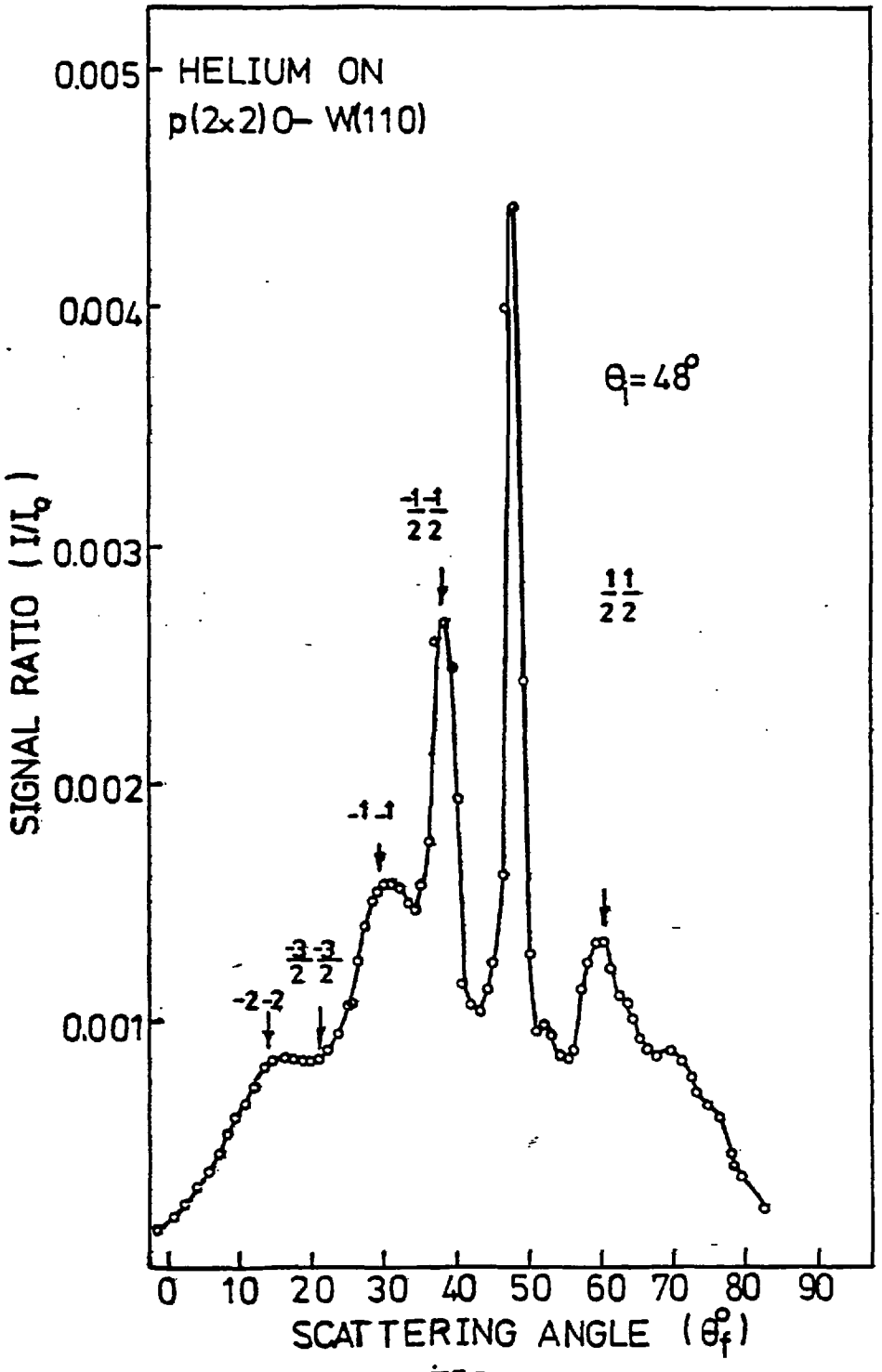

HELIUM ON
p(2x2)O- W(110)
θi = 48°
SIGNAL RATIO (I/I0)
0.005
0.004
0.003
0.002
0.001
0 10 20 30 40 50 60 70 80 90
SCATTERING ANGLE (θf°)
-2 -2
-3/2 -3/2
-1 -1
-1/2 -1/2
1/2 1/2

FIG. 7.13

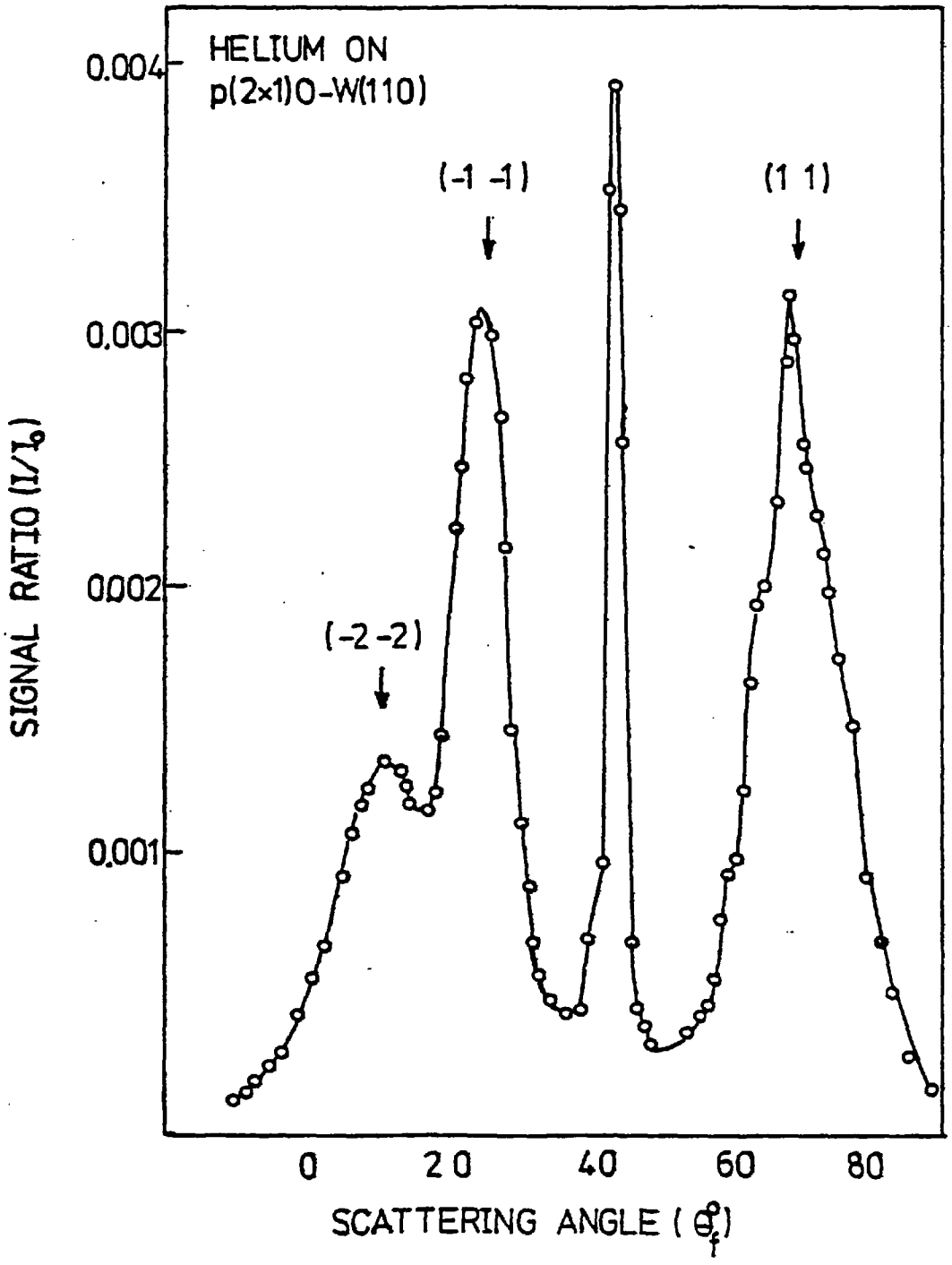
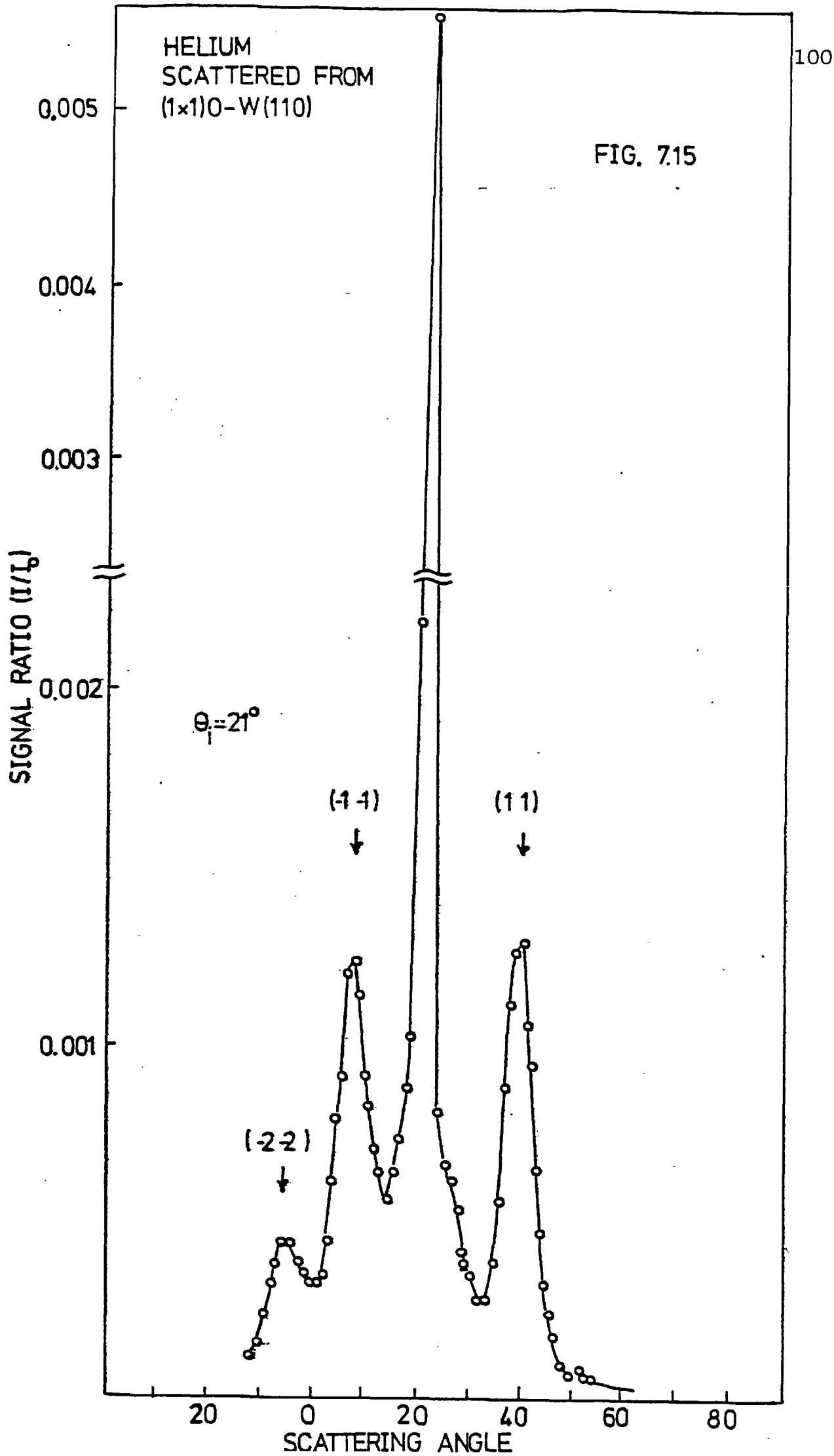

HELIUM ON
p(2×1)O-W(110)
(-1 -1)
(1 1)
(-2 -2)
0.004
0.003
0.002
0.001
SIGNAL RATIO (I/I₀)
0
20
40
60
80
SCATTERING ANGLE (θf)

FIG. 7.14


HELIUM
SCATTERED FROM
(1×1)O-W(110)
FIG. 7.15
100
0.005
0.004
0.003
0.002
0.001
SIGNAL RATIO (I/I0)
θi=21°
(-1 -1)
(1 1)
(-2 -2)
20
0
20
40
60
80
SCATTERING ANGLE

Some of the angular scans are incomplete, in so far as only the important features were observed. The results of these experiments are outlined below.

Oxygen was admitted to the work chamber via the beam system. After the surface had been saturated with oxygen the target was left overnight in a vacuum of about 10^{-10} torr. Prior to any cleaning, in-plane helium scattering distributions, Figs. (7.16, 7.17), were obtained. These distributions indicate quite clearly that the surface is still able to diffract an incident beam of helium but the peak intensities are lower than those of a newly formed (1x1) oxygen overlayer. The temperature of the crystal was then raised to about 900K for 5 minutes by radiant heating from the tungsten filament placed immediately behind it (no H.T. was applied). The diffraction peaks (Fig. 7.18) show increased intensity and also some additional structure that may arise from inelastic scattering. The LEED pattern following this scan showed (1x1) symmetry.

After heating the crystal to much higher temperatures for about 30 secs, using electron bombardment heating, the distribution shown in Fig. (7.19) was obtained. The appearance of ½ order diffraction peaks shows that the p(2x2) structure has been formed following desorption of some oxygen. The poor peak resolution would seem to indicate that the surface layer was imperfect; a fact confirmed by poor LEED patterns in which only the main (110) spots were clearly observed, the fractional order spots being blurred and streaked.

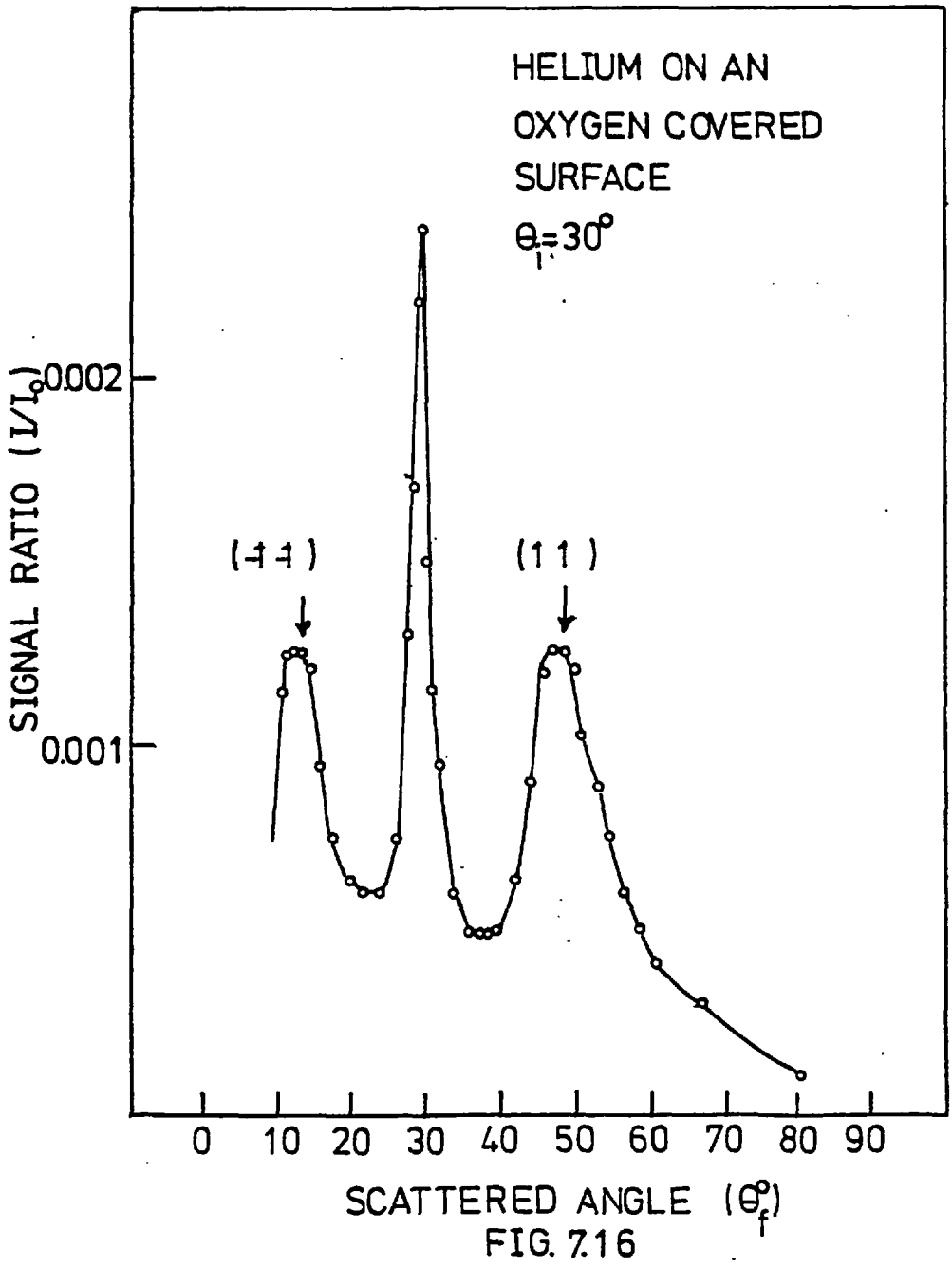

HELIUM ON AN
OXYGEN COVERED
SURFACE
$\theta_i = 30^\circ$
(-1 -1)
(1 1)
SIGNAL RATIO (I/I_o)
0.002
0.001
0
10
20
30
40
50
60
70
80
90
SCATTERED ANGLE (θ_f°)

FIG. 7.16

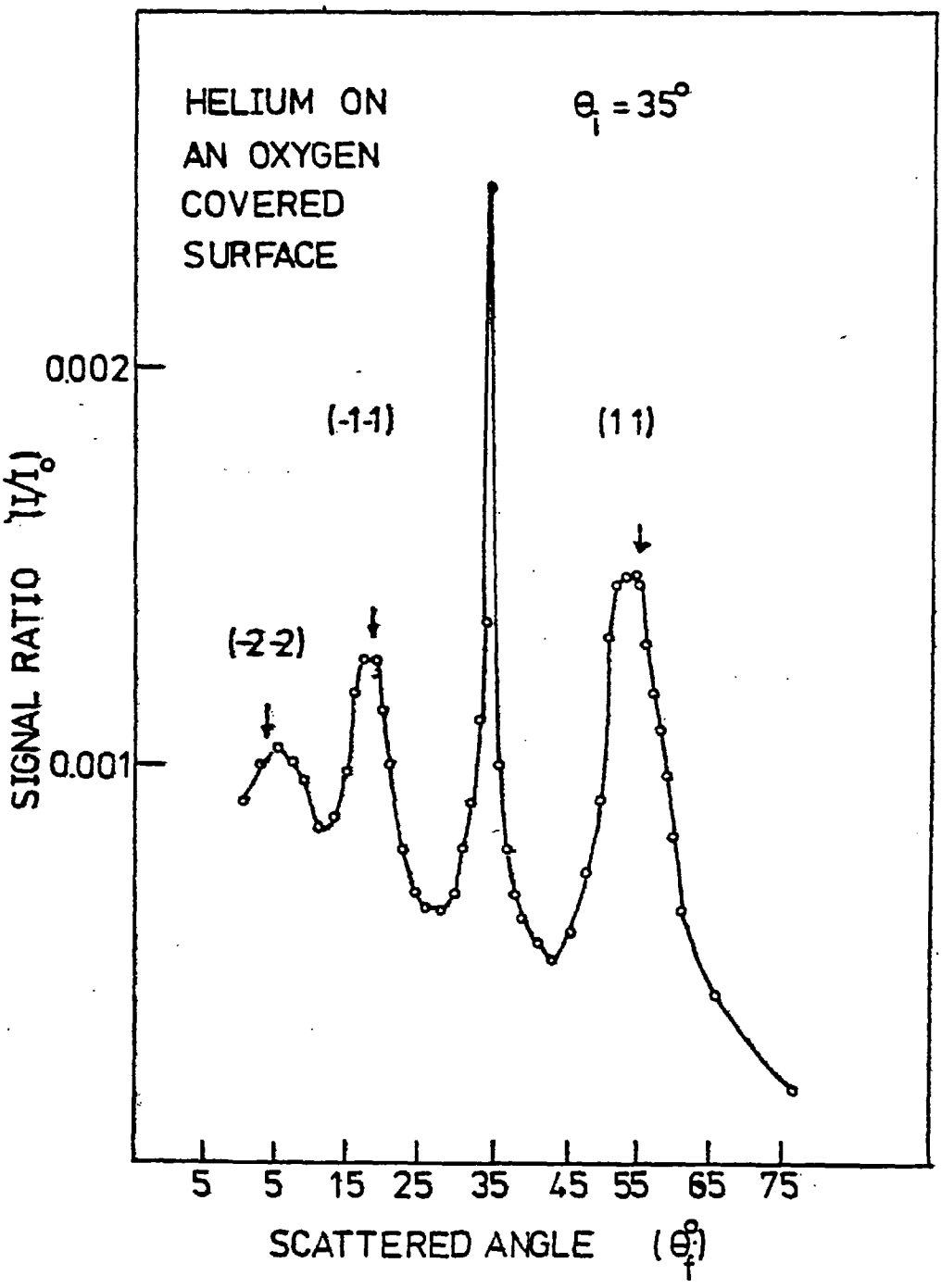

HELIUM ON
AN OXYGEN
COVERED
SURFACE
$\theta_i = 35°$
0.002
0.001
(-1-1)
(1 1)
(-2-2)
SIGNAL RATIO (I/I_0)
5 5 15 25 35 45 55 65 75
SCATTERED ANGLE (θ_f^0)

FIG. 7.17

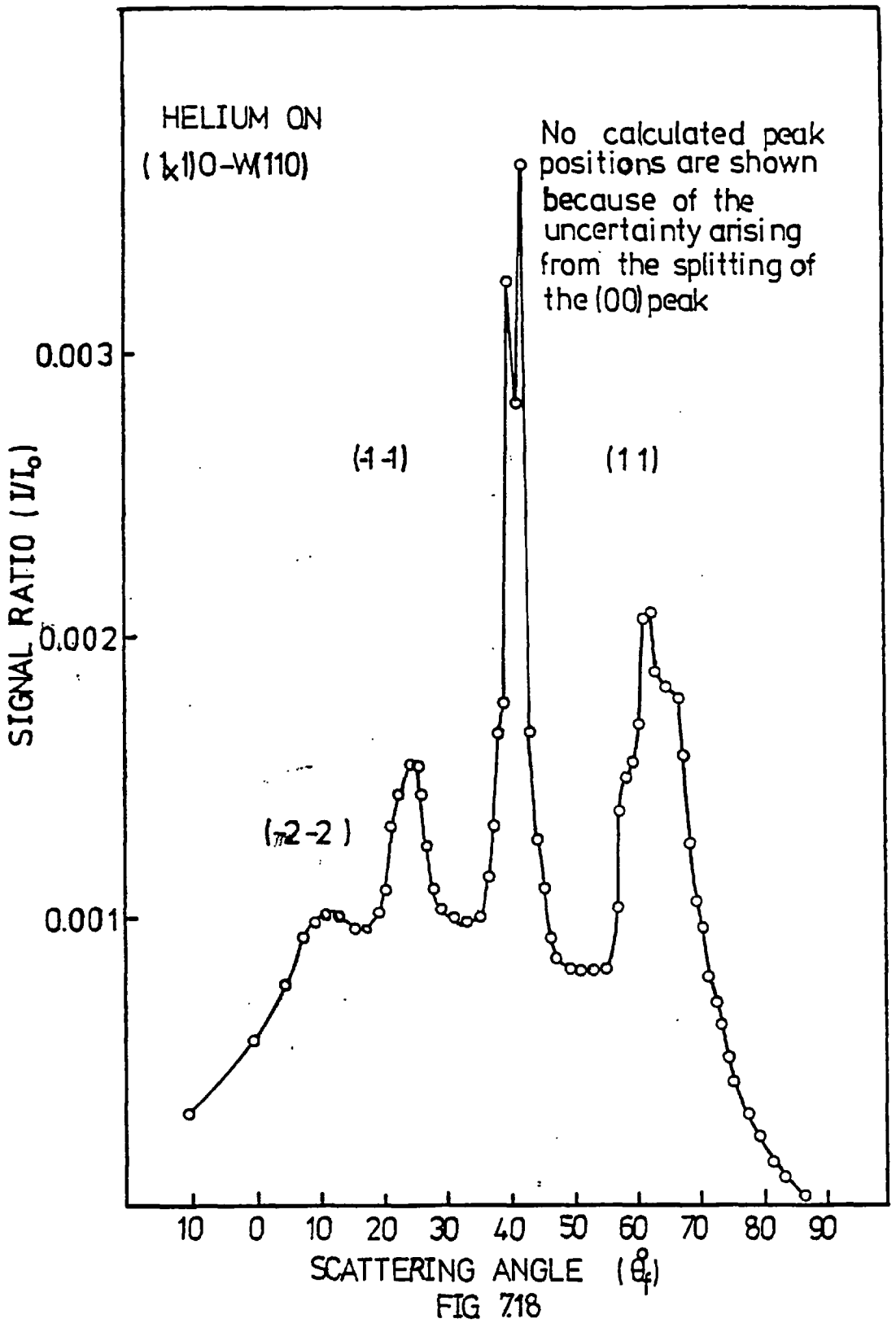

HELIUM ON
(1x1)O-W(110)
No calculated peak positions are shown because of the uncertainty arising from the splitting of the (00) peak
(-1 -1)
(1 1)
(-2 -2)
0.003
0.002
0.001
SIGNAL RATIO (I/I$_0$)
10 0 10 20 30 40 50 60 70 80 90
SCATTERING ANGLE (θ_f)

FIG 7.18

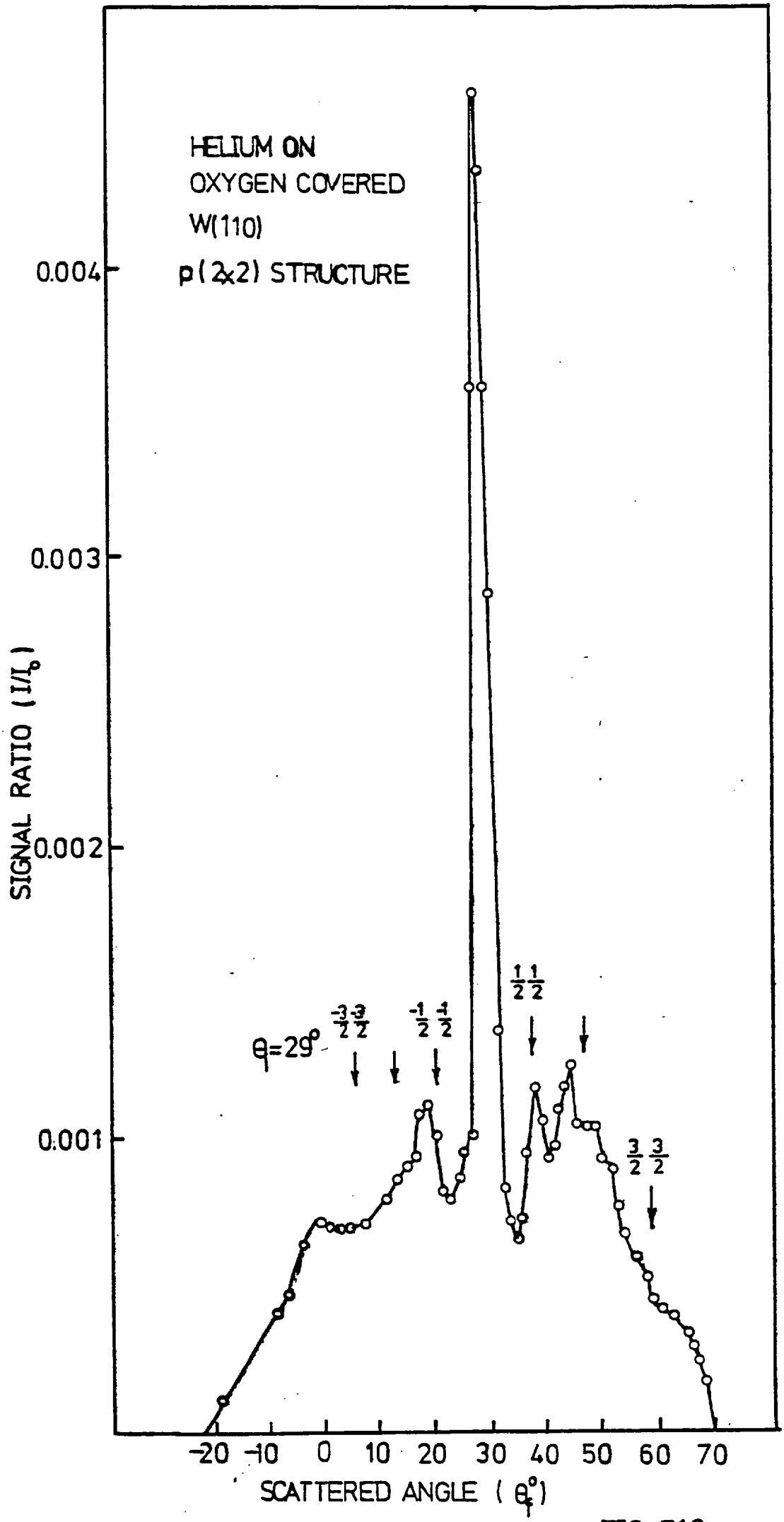

HELIUM ON
OXYGEN COVERED
W(110)
p(2x2) STRUCTURE
0.004
0.003
0.002
0.001
SIGNAL RATIO (I/I$_0$)
θ=29°
-3/2 -3/2
-1/2 -1/2
1/2 1/2
3/2 3/2
-20 -10 0 10 20 30 40 50 60 70
SCATTERED ANGLE (θ$_f^0$)

FIG. 7.19

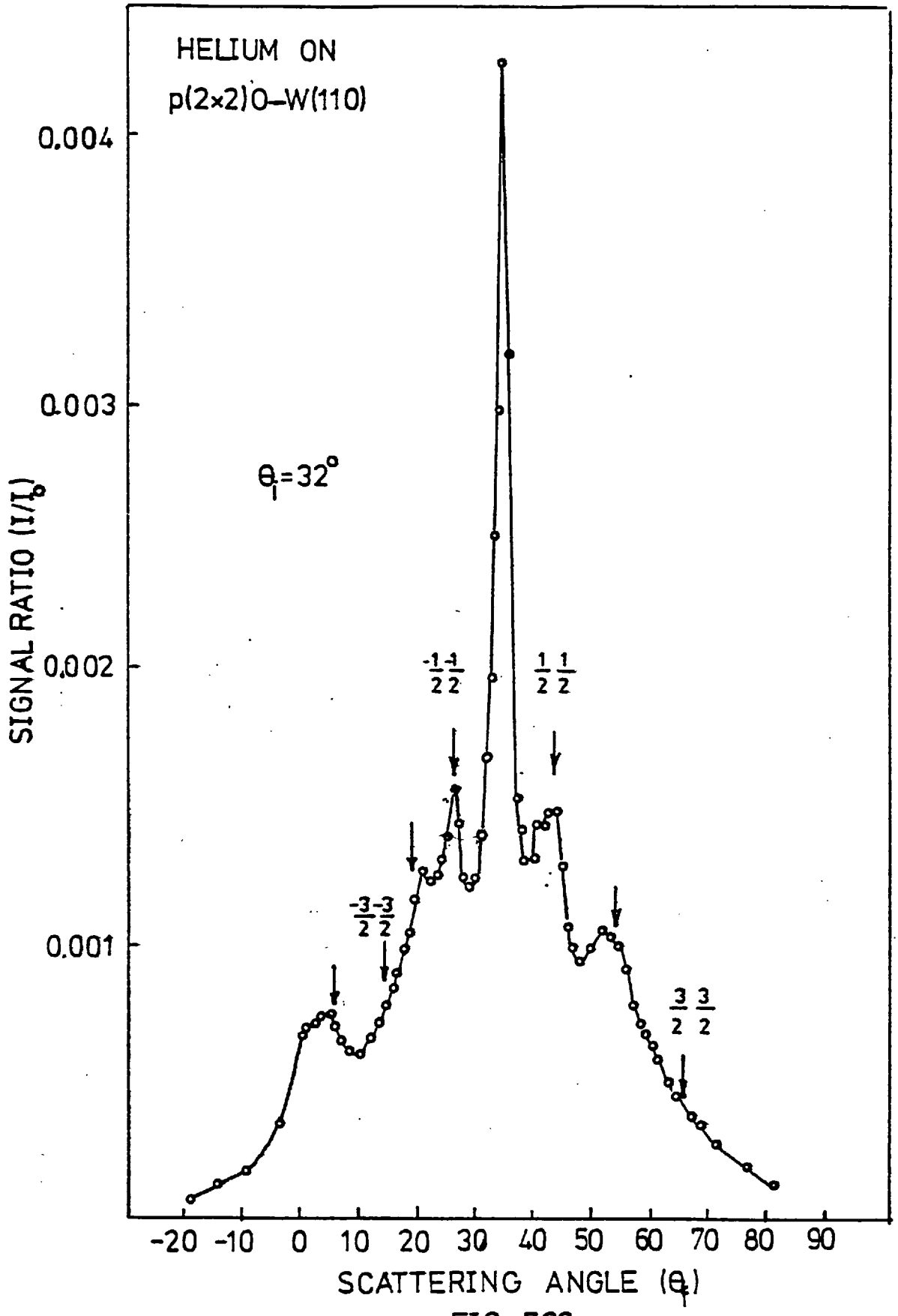

HELIUM ON
p(2×2)O–W(110)
0.004
0.003
0.002
0.001
SIGNAL RATIO (I/I0)
θi=32°
-1/2 -1/2
1/2 1/2
-3/2 -3/2
3/2 3/2
-20 -10 0 10 20 30 40 50 60 70 80 90
SCATTERING ANGLE (θf)

FIG. 7.20

A somewhat better distribution Fig. (7.20) was obtained after a further short heating cycle, although there was also a change in the angle of incidence which might have had some effect. Vertical scans through the major features in Fig. (7.20) indicated that a second set of diffraction features occur out-of-plane and these are shown in Fig. (7.21).

After further heating the diffraction features sharpened for both the in-plane and out-of-plane scans, as shown in Fig. (7.22). A LEED pattern observed after this experiment clearly indicated the presence of half order spots. (The higher angle of incidence resolves the diffraction features).

Some discrepancy between LEED results and atom scattering results did occur so that half order features obtained in the atom scattering distributions were not always observed in LEED patterns following the beam experiments. The half order features were generally of low intensity and the discrepancy is probably a reflection of the greater sensitivity of the molecular beam technique, where flux is measured directly, as opposed to LEED patterns where one relies on contrast effects on the fluorescent screen and the response of the eye.

7.5 Deuterium Scattering from Ordered Oxygen Layers

As only a limited amount of deuterium was available a detailed study of its scattering behaviour could not be attempted. Fig. (7.23) shows the result of a scattering experiment conducted on a p(2x1) oxygen overlayer. The distribution shows quite clearly that diffractive

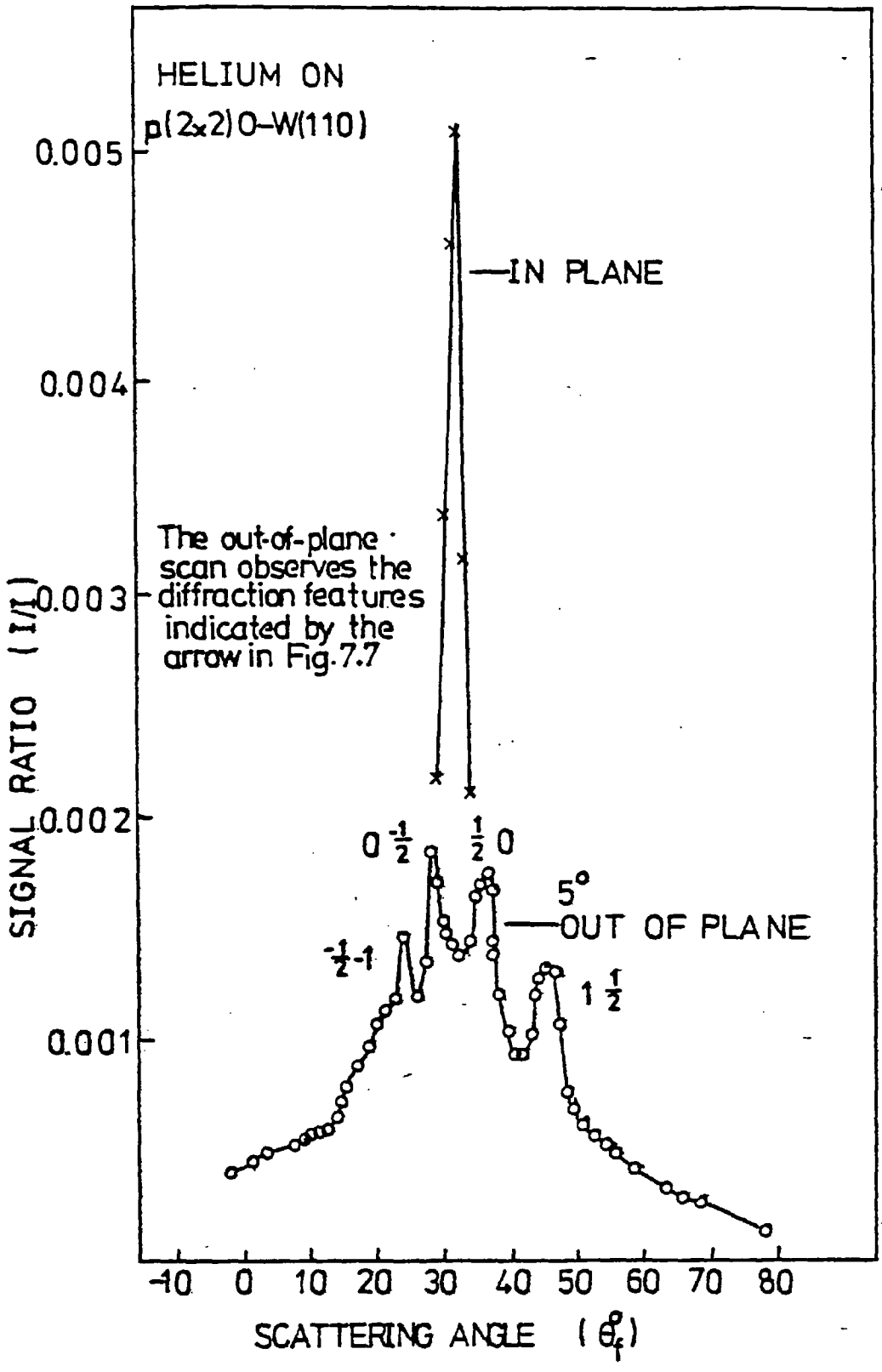

HELIUM ON
p(2x2)O-W(110)
0.005
0.004
0.003
0.002
0.001
SIGNAL RATIO (I/I)
—IN PLANE
The out-of-plane scan observes the diffraction features indicated by the arrow in Fig. 7.7
0 -1/2
1/2 0
5°
—OUT OF PLANE
-1/2 -1
1 1/2
-10 0 10 20 30 40 50 60 70 80
SCATTERING ANGLE (θf°)

FIG. 7.21

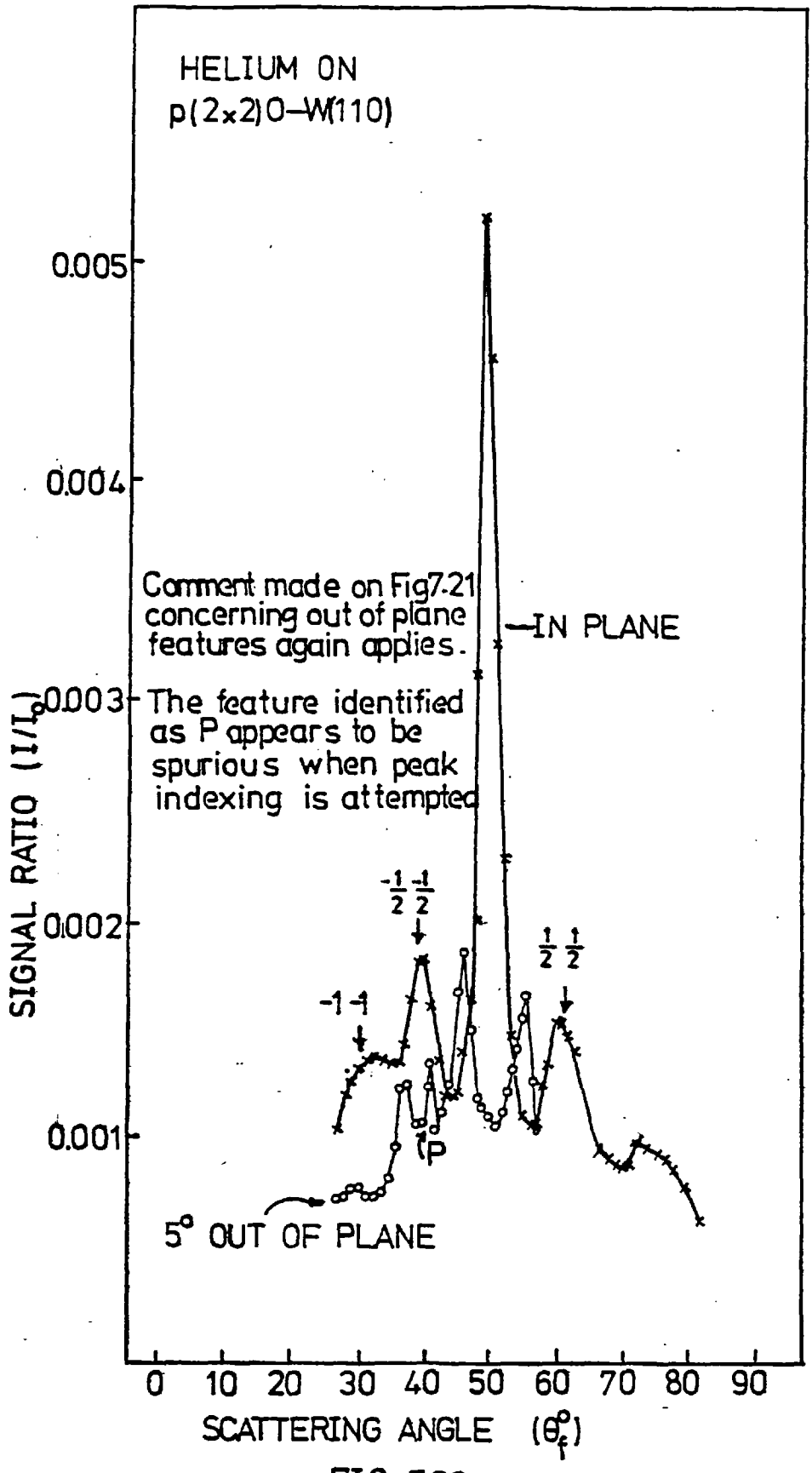

HELIUM ON
p(2x2)O–W(110)
0.005
0.004
0.003
0.002
0.001
SIGNAL RATIO (I/I0)
Comment made on Fig7.21 concerning out of plane features again applies.
The feature identified as P appears to be spurious when peak indexing is attempted
IN PLANE
-1/2 -1/2
1/2 1/2
-1 -1
P
5° OUT OF PLANE
0 10 20 30 40 50 60 70 80 90
SCATTERING ANGLE (θf°)

FIG. 7.22

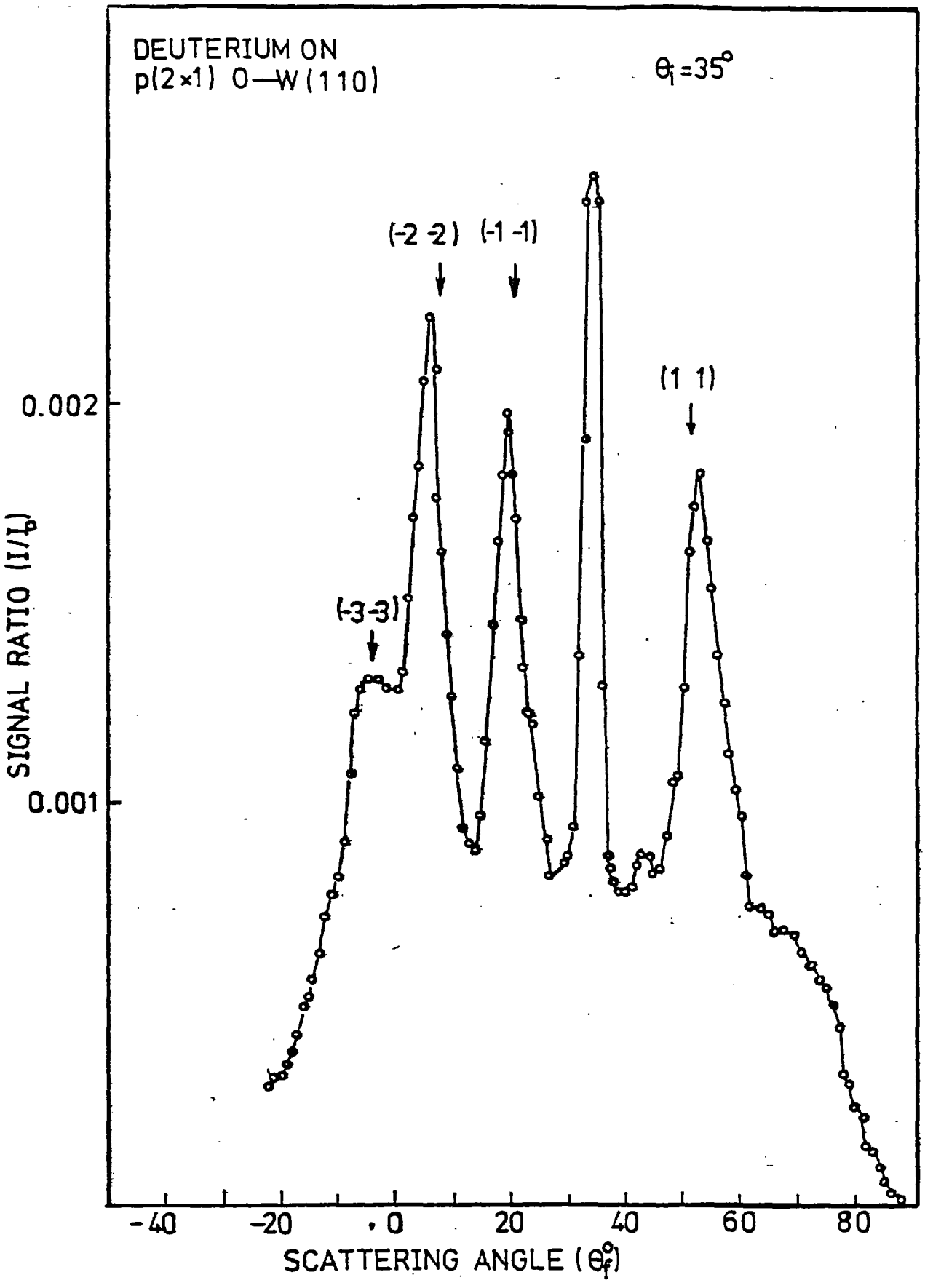

DEUTERIUM ON
p(2×1) O—W(110)
θi=35°
(-2 -2)
(-1 -1)
(1 1)
(-3-3)
0.002
0.001
SIGNAL RATIO (I/I0)
-40
-20
0
20
40
60
80
SCATTERING ANGLE (θf°)

FIG. 7.23a

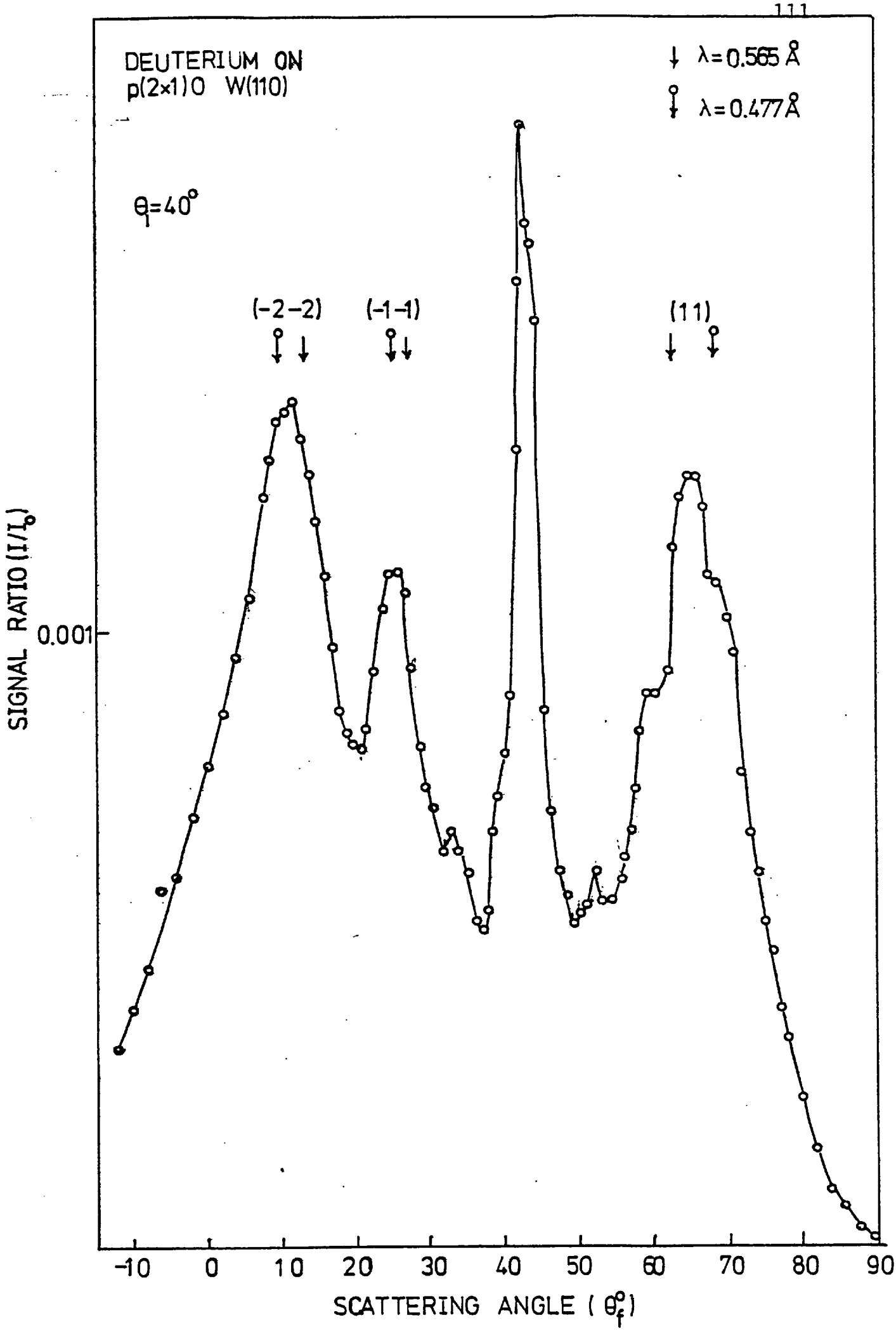

DEUTERIUM ON
p(2×1)O W(110)
λ=0.565 Å
λ=0.477 Å
θi=40°
(-2-2)
(-1-1)
(11)
SIGNAL RATIO (I/I0)
0.001
-10
0
10
20
30
40
50
60
70
80
90
SCATTERING ANGLE (θf°)

FIG. 7.23b

phenomena are observed. The arrows on the figure are an attempt to index the peaks on the basis of a wavelength $\lambda = 0.47\text{Å}$. This wavelength is however only approximate, for in the case of diatomics it is difficult to assess accurately the full extent of energy conversion from internal modes to translational motion without experimental measurements of beam energy. The distribution also shows a considerable amount of additional structure superimposed on the main diffraction peaks, notably on the (11) peak. This structure was present to a lesser extent in the case of helium beams scattered from overlayers. An explanation of this additional structure may be attributable to inelastic scattering of some kind.

Comparing the deuterium scattering (Fig. 7.23) to helium scattering (Fig. 7.14) it is seen that there is a more significant background contribution in the deuterium scattering.

7.6 Helium Scattering from High Coverage Oxygen Layers

During the preparation of the clean, carbided and oxygen covered surfaces mentioned above a number of more complex structures were observed in the LEED analysis. A scattering experiment was conducted from one of these surfaces and the result is shown in Fig. (7.24). The peak positions are again consistent with a surface structure having the W(110) lattice spacings. The most significant feature of the distribution is the splitting of the high scattered angle peak. The LEED patterns of these complex structures may be explained, as in the case of the carbide

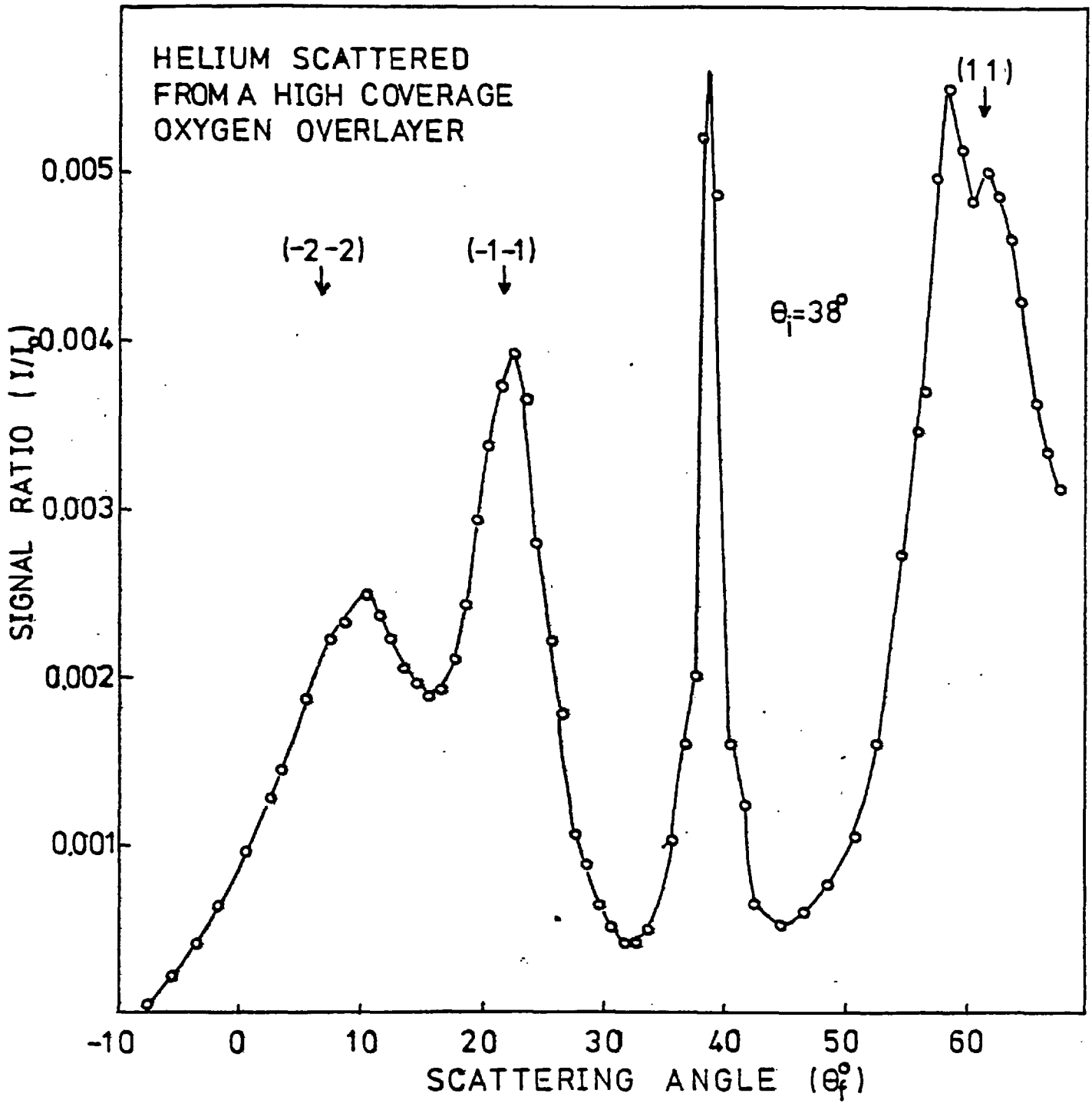

HELIUM SCATTERED
FROM A HIGH COVERAGE
OXYGEN OVERLAYER
(-2-2)
(-1-1)
(1 1)
θi=38°
0.005
0.004
0.003
0.002
0.001
SIGNAL RATIO (I/I0)
-10
0
10
20
30
40
50
60
SCATTERING ANGLE (θf°)

FIG. 7.24

surface, by coincidence lattice structures and similar problems of interpretation of the helium scattering arise.

CHAPTER EIGHT

DISCUSSION

(i) Helium on Clean Metals

The intense specular reflection and lack of diffraction observed for helium scattering from clean W(110) surface at room temperature is in agreement with the results of Weinberg and Merrill (1972a). Similar results have been obtained on other clean metals, see for example Palmer et al (1970), Mason and Williams (1972), and Sau and Merrill (1973). These studies, performed under a variety of experimental conditions, show that metals in general do not exhibit diffraction phenomena. Exceptions have been rare. Tendulkar and Stickney (1971) showed that the deeply corrugated W(112) surface yielded diffraction peaks for helium beams incident along the <110> direction but showed only specular reflection for beams incident along the <11$\bar{1}$> direction. Hayward and Walters (1974) showed that diffraction peaks were obtained from a W(100) surface following self-adsorption of the incident hydrogen beam. Recently Boato et al (1976) have indicated that the (100) face of silver shows diffraction features for both helium and molecular hydrogen beams if the surface is cooled to 80K. These results have been confirmed by Horne and Miller (1977), who cooled their target to 138K. In both instances hydrogen beams showed the more intense diffraction peaks. For both gases, however, the diffraction peak intensities are only about 1% of the specular peak intensity. These results have been interpreted as indicating an increase in

the elastic cross-section for scattering due to a reduction in the thermal motion of the surface layer. Earlier proposals offered to explain the general lack of diffraction of helium by simple metal surfaces in terms of Debye-Waller factors would therefore appear to be vindicated. Most of the previous studies on metal surfaces have been conducted at temperatures much higher than room temperature in order to ensure clean surfaces. This naturally leads to large thermal displacements of the surface atoms. Beeby (1971) calculated a value of 0.04 for the Debye-Waller factor of silver at 576K and for tungsten he obtained a Debye-Waller factor of 0.17 at 1300K. On cooling a surface the Debye-Waller factor will increase. As the cooled silver surface has been claimed to show diffraction one might expect, on the basis of the Debye-Waller factors, that tungsten would show similar behaviour at room temperature. This was not found in the course of the present experiments.

Several explanations of this disagreement are possible.

(a) The results of the two studies on silver may not have originated from clean silver. Results of the present work have indicated that gas-adsorption can produce structures capable of giving diffraction. At the low temperatures used in the studies on silver the possibility exists that gas-adsorption has occurred. Although Boato et al had no way of checking the composition of their surface, Horne and Miller used Auger spectroscopy to show that their surface was clean. However there may

be a doubt about the validity of Auger analysis on silver, especially at low temperatures, in view of the likelihood of desorption induced by the incident beam. A further comment related to adsorption effects can be made when it is noted that Hayward and Walters (1974) found that hydrogen was diffracted from the surface of tungsten W(100) following initial chemisorption. If a similar process occurs with silver then the reason for hydrogen showing somewhat more marked diffraction than helium may, in part, be explained.

(b) The low intensity of the diffraction features observed by Boato et al and Horne and Miller makes it seem possible that diffraction effects in earlier systems could have been overlooked. It cannot be stated emphatically that a diffraction feature of this magnitude was not overlooked in the present work. Horne and Miller operated at an angle of incidence of 80^{o} which resulted in a separation of 35^{o} between the observed diffraction feature and the specular beam. In the present work an incident angle of 20^{o} was used. In most other studies the incident angle was not greater than 45^{o}. At these incident angles the diffraction features would be much closer to the specular direction and might possibly be obscured unless the resolution was exceptionally good.

(c) An argument based simply on Debye-Waller factors may be incomplete. Although diffraction effects have been absent in many studies specular scattering is always a feature in helium from metal surfaces. Comsa (1974) has proposed that a clear distinction be made between two

types of elastic scattering process. These he has termed:

(1) Ordered elastic: resulting in real diffraction as have been observed in studies on ionic crystals.

(2) Disordered elastic: resulting in specular reflection as observed on metal crystals.

The first process is characterised by the coherent interference of waves scattered from discrete sites. The second process, not showing diffraction, should show no coherence properties. This second process can be explained in terms of a smooth interaction potential resulting from the superposition of long range interactions between the incident atom and several surface atoms.

Smooth potential arguments are qualitatively very attractive and have been discussed by Garibaldi et al (1975) who developed a quantum mechanical theory based on a corrugated potential surface. He noted that a small corrugation would still result in weak diffraction features but emphasised that thermal displacement of the surface could average out such corrugations. He concluded that arguments based solely on Debye-Waller factors or smooth interaction potentials were inadequate.

The use of the Debye-Waller factor in atom surface scattering is still under discussion. Comsa (1974), as has been pointed out, thought of specular reflection on metals as being a non-diffractive process and concluded

that the Debye-Waller is not a suitable parameter to describe the temperature variation of the scattering. He also suggested that the Debye-Waller factor should not be used in cases where diffraction occurs that is not produced by the coherent interference of atomic waves from individual surface oscillators. If coherent scattering occurs from a wavy but smooth potential then thermal roughening is reduced and the $\langle u^2 \rangle$ must need some modification.

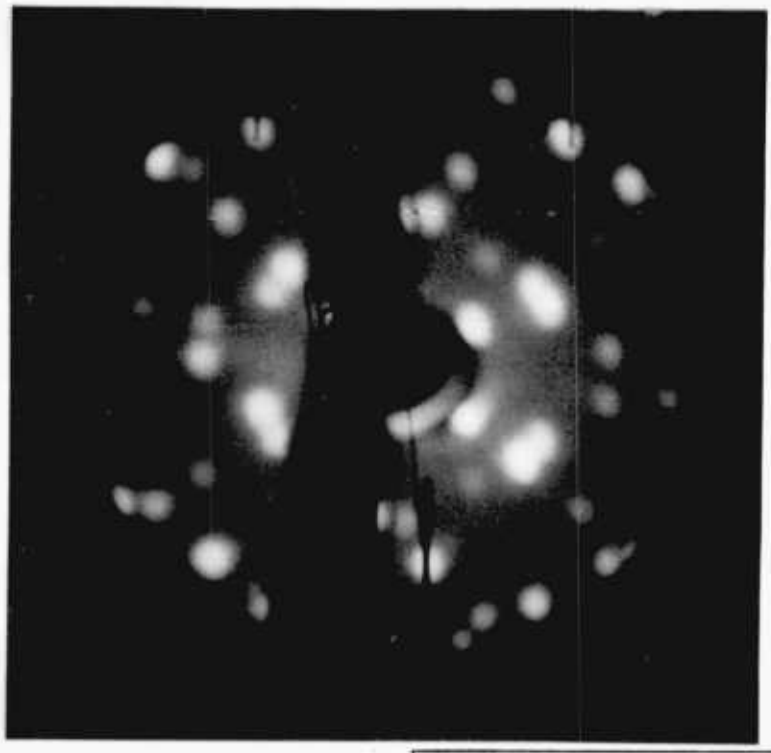
Goodman (1977) appears to support these arguments and also queries Beeby's correction to the momentum transfer on the grounds that at z_o, the position of the potential minimum where the well-depth is calculated, there is no repulsive force and $\Delta\underline{k}$ should be calculated in the region where 'effective repulsive scattering' occurs.

(ii) Helium, Deuterium and Neon on Carbided Surfaces

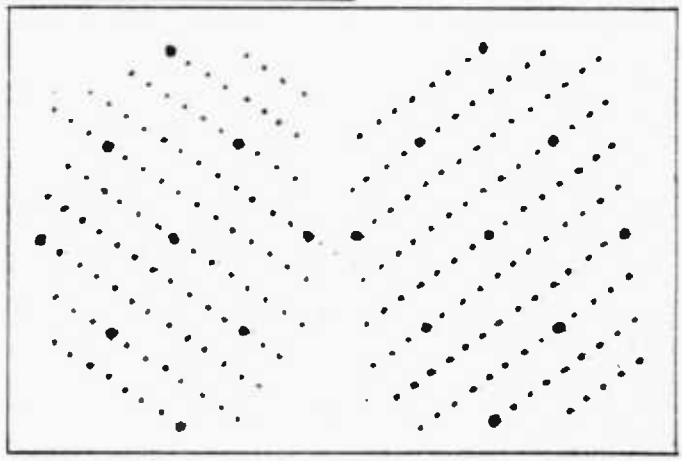
The R35° (3x5) C-W(110) surface has been studied previously by Weinberg and Merrill (1972b), who concluded that diffraction of the lighter gases occurred, this then being the first observation of diffraction from an ordered layer on a metal surface. However, the interpretation of the results of this earlier investigation is not, entirely clear for despite the use of an oven-type source, having an appreciable spread in incident wavelength, the diffraction peaks observed had in most cases half widths less than that of the incident beam. Goodman (1976) recently performed calculations to determine the

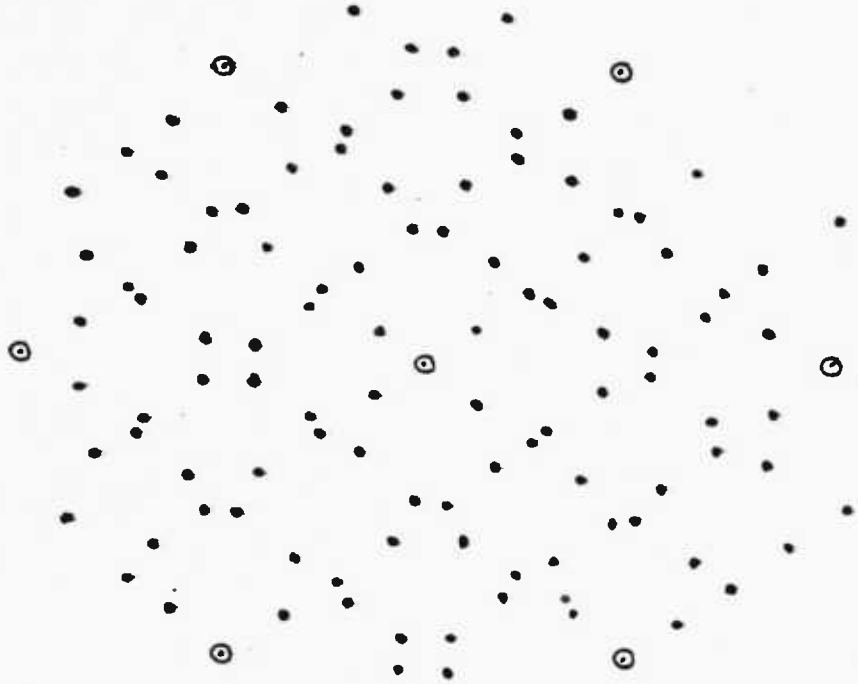
properties of Maxwellian incident beams and, although he was able to successfully account for features observed in studies on the helium on lithium fluoride system, he was unable to explain the findings of Weinberg and Merrill. One explanation that has not been discussed is the possibility of the carbide surface being incomplete and existing only as small islands in a relatively broad incident beam.

A further point is that Weinberg and Merrill discuss their results in terms of a single orientation of the carbide layer whereas in the experiments detailed earlier it was found that two distinct orientations are possible and can be identified separately. In agreement with others (Stern (1964)), it was found that a mixed orientation was more probable than either individual orientation. Stern found that single orientations were most easily observed near to the crystal edge. A LEED photograph and a reciprocal lattice corresponding to the mixed orientation are shown in Fig. (8.1). Clearly gas scattering from these mixed orientations will be complex and may not be amenable to simple analysis. Even if the discussion is limited to the single orientation discussed by Weinberg and Merrill other problems arose from a consideration of their data. In their experimental arrangement the detector has no side-ways movement and out-of-plane diffraction peaks could be obtained only after tilting the crystal thereby causing slight changes in the incident conditions. Three peaks were found in this way designated (10), (20) and (30). (See reciprocal lattice, Fig. (7.4)). The tilting of the crystal complicates



LEED PHOTOGRAPH AND RECIPROCAL LATTICE DIAGRAM FOR A CARBIDED W(110) SURFACE EXISTING IN TWO DOMAINS (insert to right shows individual reciprocal lattices, overlap gives diagram below)





enlarged spots/circles depict normal (110) pattern

FIG. 8.1

the incident conditions and makes it difficult to identify the diffraction peaks with any certainty. It is also significant that no diffraction peaks were observed in the plane of incidence in contrast to the present work.

According to calculations based on the simple Bragg Law the separation between the (10) and the (00) peaks should be 4^{o} at the angle of incidence used in Weinberg and Merrill's work. As the beam half-width was found to be about 7^{o} and the beam had an appreciable energy spread, it is surprising that peaks could be found at all. The beam half-width used in the present work was approximately 2^{o} and resolution of the diffraction peaks is expected. No confirmation of Weinberg and Merrill's results can be given although it must be said that only preliminary out-of-plane scans were attempted. The peaks that are found are sufficiently sharp and intense to cause confusion as to the identity of the (00) peak. The angle of incidence as measured to an accuracy of about $\pm 2^{o}$ (by estimation of the surface tangent) producing an uncertainty in the position of the specular peak of about $\pm 4^{o}$. It therefore becomes very difficult to give an unambiguous assignment to the specular peak when the diffraction peaks are close together. It would appear, however, that the specular peak is not the most dominant feature in the scattering patterns. Determination of the surface structure of the carbide has been under discussion for some time. Early interpretations of the $R35^{o}$(3x5)C-W(110) LEED pattern were based on the possibility of long range surface structures. A structure having a low carbon

concentration with carbon atoms at the corners of a (3x5) cell was proposed by Stern (1964). Interpretations based on long range superstructures have now been replaced by coincidence lattice models, as first put forward by Bauer (1966). He in fact discussed the carbon on W(110) system but the reciprocal lattice that he proposed had a (3x6) unit cell whereas there seems little doubt from the LEED pattern that the correct unit cell is (3x5). Fig. (7.4) represents the coincidence lattice formed for the surface carbide W_2C having hexagonal symmetry and the underlying W(110) crystal. The experimentally observed coincidence lattice is formed with only a very small distortion of the hexagonal carbide layer.

If this explanation of the LEED patterns is correct the diffraction of gas-atoms becomes very interesting. The above argument requires the incident electron to penetrate, and be scattered from, the underlying tungsten atoms as well as the carbide layer. In gas scattering it is assumed that there is no penetration below the top layer, so that it is debatable whether or not the gas diffraction is able to show the (3x5) periodicity.

Weinberg and Merrill offered no explanation of the surface structure of the carbide other than that it appeared to contain furrows showing rows of tungsten atoms between blocks of carbide having a (3x5) size. The preceding discussion implies that their simple interpretation of the surface is inadequate. From the preliminary results of the molecular scattering presented it would appear that Weinberg and Merrill may have been over-zealous in attempting to deduce surface structures from atom-scattering

data.

(iii) Helium Scattering from Oxygen Covered Surfaces

The major part of the results presented in Chapter Seven were concerned with the scattering of molecular beams from oxygen layers on W(110). At the present time there is little reported work to which these results may be compared. Hayward and Walters (1975) reported on the diffraction of H_2 beams from W(100) following initial chemisorption of the incident beam to give monolayer adsorption. Apart from that work the only reported effect of gas adsorption on scattering from metal surfaces has been a dramatic fall in the specular peak intensity. Yamamoto and Stickney (1970), for example, observed this effect with helium scattering when oxygen was adsorbed on W(110). Merrill and Smith (1971) actually used the helium specular peak intensity as a criterion for surface cleanliness in experiments on the adsorption of ethylene on Pt(111). Although they observed LEED patterns at various stages of the adsorption no attempt was made to correlate the LEED data with helium scattering, as was attempted in the present study. The results presented in Chapter Seven can be summarized as follows:

(i) The major features in the scattering distributions are consistent with diffraction of the incident beam by a surface mesh of adsorbed oxygen atoms in registry with the underlying tungsten lattice.

(ii) When helium is scattered from the clean surface the intensity of the specular peak is greater than that of any feature in the scattering distribution from the oxygen covered surface, including the (00) peak, by a factor of between 20-100.

(iii) Many of the scattering distributions show subsidiary details generally in the form of shoulders on the main diffraction peaks.

These results are of some significance since at room temperature the only clean metal surface found to diffract helium is W(112) and this is a highly corrugated surface, as shown in Fig. (3.1). Adsorption of oxygen is also likely to cause a corrugation in the surface interaction potential, especially when the oxygen atoms sit above the surface. At low coverages of oxygen, when the p(2x2) and p(2x1) LEED patterns are observed, the adsorbed oxygen atoms are some distance apart and diffraction of helium beams would be anticipated. At coverages approaching a monolayer the surface would, however, appear faintly smooth, assuming that no surface reconstruction occurs (Bauer & Engel 1978). The present results show clearly that diffraction of helium does occur both from a (1x1) layer of oxygen and also from other structures formed at higher coverages. This suggests that, even when densely packed, the oxygen atoms act as discrete scattering sites probably because of the lower electron density in the adsorbed layer..

(iv) Inelastic Effects in Helium Scattering

In Chapter Seven it was tentatively suggested that the subsidiary structure observed in many of the scattering distributions arises as a consequence of inelastic scattering processes. Without energy analysis of the scattered gas atoms this conjecture is difficult to confirm although evidence from other experimental methods indicates that there is a strong possibility of observing inelastic processes. Boato et al (1975a) and Williams (1971a,b) have interpreted structure observed in the angular distributions of helium scattered from LiF(001) surfaces in terms of energy exchange between the helium and the surface vibrational modes. From his data Williams attempted to establish a surface phonon dispersion relationship for LiF(001). Only two attempts have been made to identify vibrational modes by the energy analysis of the scattered beam (Bledsoe & Fisher (1974), and Williams & Mason (1978)). In both studies low signal strengths made it difficult to draw firm conclusions from the results.

The difficulty in interpreting inelastic interactions when the only evidence for them comes from angular scattering distributions can be seen by examining the kinematic scattering relations, modified to take into account inelastic processes.

$$\begin{aligned} \underline{K}_f &= \underline{K}_i + \underline{G} \pm \underline{Q} \\ E_f &= E_i \pm \hbar\omega(\underline{q}) \end{aligned} \qquad (8.1)$$

where $\underline{q}$ is a phonon wavevector

$\underline{Q}$ is the projection of q parallel to the surface

$\omega(\underline{q})$ is the corresponding frequency of vibration.

These relations can be depicted diagramatically (see Figs. (3.2), (8.2) & (8.3)). It is easily seen that the final scattered angle does not uniquely determine the exit energy.

Before extending the discussion to the results for the system studied some background information concerning the vibrational spectra of adsorbed layers on metals should be given. Alldredge, Allen & de Wette (1971) and Armand, Dobrzysnski and Masri (1972) have shown how the adsorption of a light atom on a heavy metal lattice results in the appearance of vibrational modes with higher frequencies than the bulk modes of the metal lattice. Adsorption also has the effect of raising the frequency of the original surface Rayleigh mode of the metal so that it becomes closer to the original bulk modes. The former effect has been confirmed experimentally, principally through the technique of high resolution energy loss spectroscopy (HRELS).

To date most of the electron loss work reported on simple gas-metal adsorption systems has been restricted to the energy analysis of the region of the scattered distribution within 2^{o} of the specular beam. In order to detect inelastic scattering due to a vibrational mode in this region the mode must have a

dynamic dipole moment component perpendicular to the surface (Ibach, 1977). A theoretical analysis has been given by Evans and Mills (1972). This means that the technique is limited in the case of adsorbed atoms to determining the vibrational frequency of the symmetric stretch mode. As the interaction excites surface waves which have only a small wave vector compared to the reciprocal lattice vector of the substrate the vibrational frequency does not show any dispersion effect.

Recently Ho et al (1978) have analysed parts of the angular distribution of electrons scattered from a hydrogen covered W(100) surface far from the specular beam and have found inelastically scattered electrons arising from vibrational modes that do not obey the dipole moment selection rule. They identify these observations with a short range impact scattering mechanism. This type of scattering has been investigated theoretically by Roundy & Mills (1972). Ho et al (1978) propose that the new vibrational modes are the asymmetric stretching mode and the out-of-plane bending mode of an H atom adsorbed in a bridge site. The finding of these additional fundamental modes allows the bonding site of the adatom on the surface to be established with some certainty.

The information obtained from HRELS experiments can be used to deduce possible atom-phonon interactions that might be observed in the present atom scattering experiments. The results of Ho et al (1978) for

dissociative adsorption of hydrogen on W(100) give a 'bending' mode excitation energy of between 60-80 meV, depending on coverage, compared to a symmetric stretch mode energy of 130-150 meV. Ibach et al (1976) have shown that the lowest symmetric stretch mode energy in the oxygen/W(100) system is about 50meV. At the present time no other evidence is available that enables an estimate of the energies of the fundamental modes for oxygen on W(110) to be made. The theoretical models of Alldredge et al (1971) and Armand et al (1972) suggest that the frequencies of these modes will be somewhat greater than those at the top of the bulk tungsten band, which have energies of about 30 meV. Thus a very crude estimate would put the energies of the fundamental modes of the adsorbate system in the range 30-50 meV.

The helium atoms generated from the nozzle source in the present work have a translational energy of approximately 65meV and any interactions with the fundamental modes of the adsorbate system will involve a significant change in total translational energy. Alternatively the incident atoms may interact with the modified surface Rayleigh mode. This would involve much lower energy transfer as the energy of this mode in pure materials ranges from zero to about 10meV as the wavevector $\underline{Q}$ increases from zero to the magnitude of a reciprocal lattice vector. Williams (1971a) identified inelastic interactions in the He/LiF(001) system with the surface Rayleigh mode; there exists, therefore, the strong possibility that the inelastic interactions observed in a gas-adsorption system are due

to the modified Rayleigh mode of the gas-metal system and not to any 'stretching' or 'bending' modes. Clearly this matter cannot be resolved without energy analysis.

(v) Analysis of Inelastic Interactions of Helium

Ewald diagrams can be used in a qualitative discussion of the scattering results presented in Chapter Seven. Fig. (8.2) shows the situation for an inelastic process involving a phonon with wavevector $|\underline{Q}| = 0$. The following features are evident:-

(a) The angular separation between elastic and inelastic scattering for a given diffraction channel is largest when $|\theta_{sc}^{elastic}|$ is high.

(b) A gain in translational energy shifts scattered angles towards the normal, while a loss in translational energy shifts the scattered angles away from the normal.

The first of these points explains why in the scattering distributions discussed in Chapter Seven subsidiary structure is most clearly observed in the high angle, (11) diffraction peak. The Ewald diagram shows that it should be possible to resolve energy gain and loss processes on either side of the (00) and (11) elastic peaks provided that $|\underline{Q}|$ is small, but that, as $|\underline{Q}|$ becomes larger, the possibility of overlap between

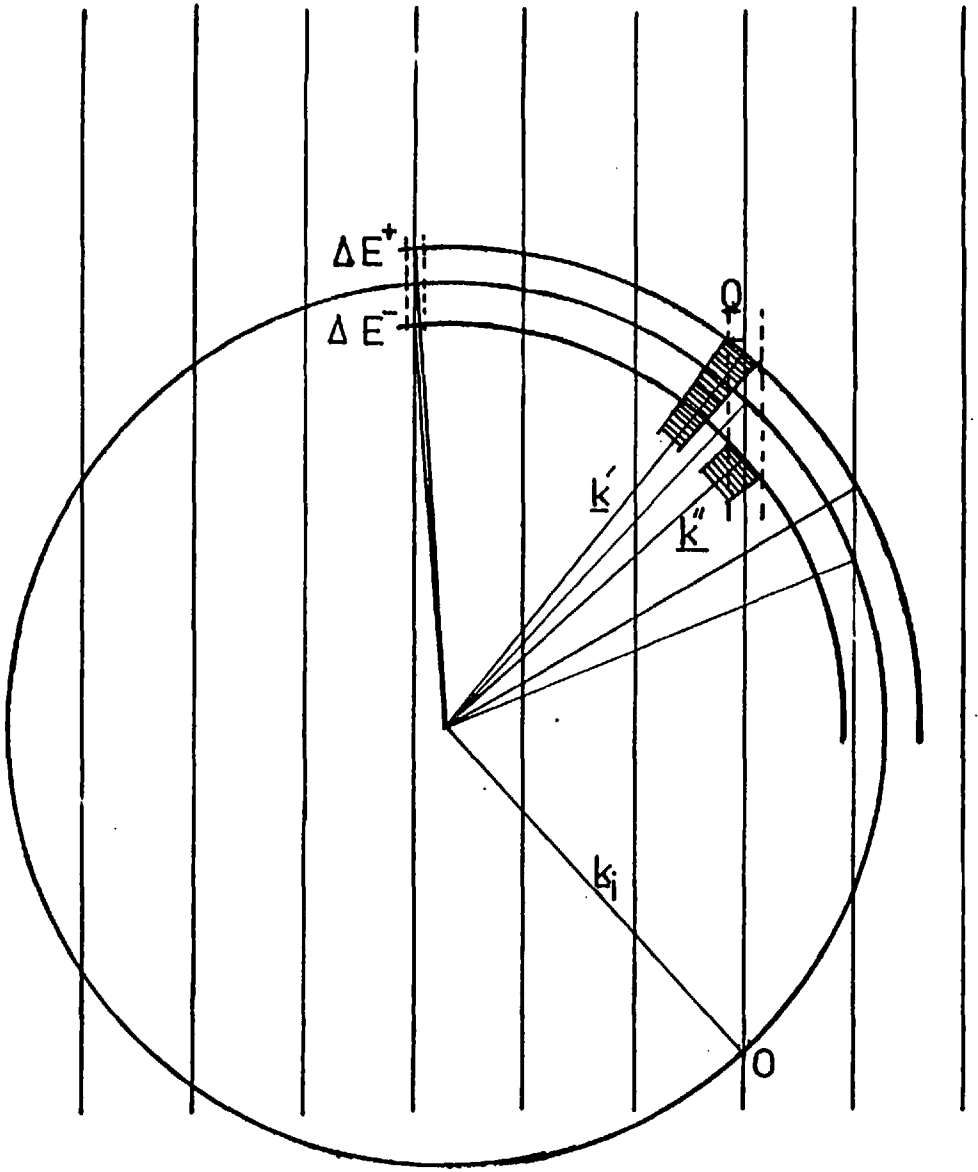


FIG. 8.2

EWALD DIAGRAM SHOWING THE CHANGE IN EXIT ANGLES FOLLOWING INELASTIC INTERACTIONS

$\theta_i = 43°$

$\lambda_i = 0.56$ Å corresponding to $E_i \approx 65$meV

$\Delta E \approx 10$meV

For $Q = 0$ scattered beams are given by k', k''

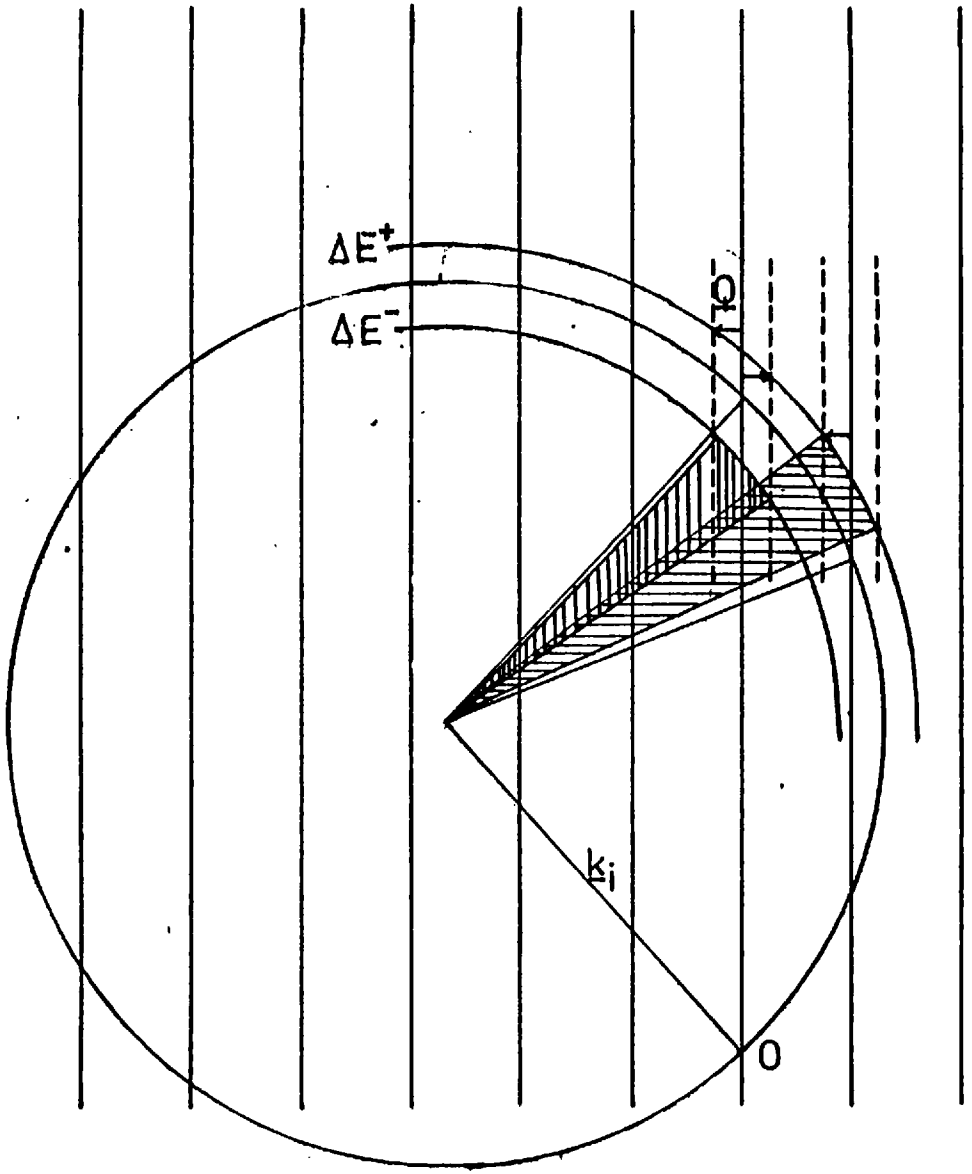
For small $|Q|$'s range of scattered angles is indicated by the hatched areas.

At exit angles near to the surface normal there is overlap between elastic and inelastic beams for small $|Q|$'s

loss and gain processes increases. The possibility also exists, as is shown in Fig. (8.3), that overlap will occur between beams from different diffraction channels. For an elastic peak which lies close to the surface normal Fig. (8.2) shows that the energy gain and loss processes will overlap the elastic peak even for wavevectors having small $|\underline{Q}|$.

The preceeding discussion has indicated that although angular scattering distributions of molecular beams do contain information that is apparently related to inelastic scattering processes it is difficult to extract any quantitative information. This difficulty arises primarily because no energy analysis of the scattered gas is performed so that energy exchange has to be deduced from in plane scattering Despite the complexity of the situation more detailed investigations of helium scattering would appear to be worthwhile because the inelastic interactions studied are likely to involve surface vibrational modes that cannot readily be studied by alternative techniques.

Although inelastic features are difficult to quantify the general shape and intensity of helium scattering distributions from oxygen covered surfaces clearly indicate that inelastic interactions are much more significant than they are on the clean surface. It has long been known that energy accommodation coefficients for gas covered surfaces are much higher than for clean surfaces (Thomas 1953) and the angular scattering distributions support this observation.



EWALD DIAGRAM SHOWING THE OVERLAP IN SCATTERING ANGLES THAT CAN ARISE BECAUSE OF INELASTIC INTERACTIONS

Incident data as Fig. 8.2

FIG. 8.3

(vi) Inelastic Scattering of Molecular Deuterium

The interaction of deuterium with a surface may involve one or more of the following processes:-

(i) Energy transfer between the surface vibrational modes and the rotational modes of the molecules.

(ii) Energy transfer between the surface vibrational modes and the translational modes of the molecules.

(iii) Energy transfer between the rotational and translational modes of the molecules.

Processes (ii) and (iii) may be investigated in molecular beam studies as the resultant change in the momentum of the incident particle causes changes in the angular scattering distributions. Process (ii), in fact, is identical with the inelastic scattering discussed previously for helium. The kinematic scattering relations for process (iii) are:-

$$\begin{aligned} \underline{K}_f &= \underline{K}_i + \underline{G} \\ E_f &= E_i \pm \Delta E_{rot} \end{aligned} \qquad (8.2)$$

It should be noted that, unlike the equivalent relationships for process (ii) (see Equations 8.1a, 8.2b) these equations do not include wavevector term Q. This type of process may therefore be represented on an Ewald diagram, as in Figs. (8.2) and (8.3), with

$\underline{Q} = 0$. It may be possible to distinguish between interactions of type (ii) and (iii) when analysing angular scattering distributions. Rotational-translational energy transfer processes involve only a limited set of discrete energies, determined by the rotational energy levels of the molecule, whereas energy transfer involving vibrational modes of a solid involve a continuous band of allowed energies. In addition the phonon wavevector term in Equation (8.1) will cause further broadening of the inelastic features of type (ii) processes. These arguments suggest that process (iii) will result in much sharper features in the angular scattering distributions than would process (ii).

The angular scattering distributions shown in Fig. (7.23a,b) demonstrate conclusively that diffraction is observed for deuterium scattered from oxygen covered surfaces. The diagrams also show a considerable amount of structure that might possibly be due to rotational-translational energy transfer processes. Confirmation of this is difficult due partly to the limited data available and also to uncertainties in the parameters defining the incident beam.

The uncertainties associated with the incident beam are two-fold. First the theory of isoentropic expansion of polyatomic gases is not well developed and it is difficult to estimate the incident beam using formulae of the type which are applicable to monatomic beams. In the case of helium it should be remembered that the

experimentally determined wavelength seemed to indicate almost complete conversion of the enthalpy of the gas to forward motion rather than the partial conversion calculated from the theoretical formulae. In the case of diatomics complete conversion of gas enthalpy to forward motion would result in the incident molecules having an energy of 7/2 kT. Complete conversion of rotational energy does not occur, however, and this gives rise to the second problem in defining the incident beam parameters; namely finding the population of rotational states. An estimate of the beam energy can be made from the positions of the elastic diffraction peaks. The table below shows the results for data relating to Fig. (7.23a,b).

Fig.	ANGULAR POSITION OF PEAK	θ_i	λ_{exp}/Å
7.23a	53.5^o	35^o	0.513
	19.5^o	35^o	0.535
	6.0^o	35^o	0.522
7.23b	65.5^o	42.5^o	0.523
	26.0^o	42.5^o	0.529
	11.5^o	42.5^o	0.530

These values of λ_{exp} are in good agreement especially when one considers that uncertainty of $\pm 1^o$ in the scattering angle gives rise to a variation in λ of 0.05 Å. This method of determining λ will only be valid if the intensity of scattered beams shows no strong dependence on the incident wavelength and if the incident beam has a fairly narrow velocity distribution.

The average value of λ_{exp} in the above table is 0.525Å. This compares with expected wavelengths of 0.565Å and 0.478Å respectively for beams in which there is (a) no transfer of rotational energy into forward motion and (b) complete conversion of rotational energy into forward energy.

With the limited data available it is not possible to determine the extent to which rotational-translational energy exchange occurs during the gas-solid interaction. An attempt to explain the structure associated with diffraction features in Fig. (7.23) in terms of energy exchange with the rotational states of deuterium was rather inconclusive. Allowing for the appropriate selection rule ($\Delta J=\pm 2$) the most likely energy changes of the incident beam are ±22meV and -37meV. Such energy changes would produce some peaks in approximately the correct positions as observed in Fig. (7.23) but much of the structure remains unexplained. Hence no firm conclusions can be made on the basis of the available evidence.

A summary of the results of the approach outline above is given in the table below

ANGLE OF INCIDENCE	Elastic Peak	$\Delta J(1\rightarrow 3)$	$\Delta J(3\rightarrow 1)$	$\Delta J(0\rightarrow 2)$	$\Delta J(2\rightarrow 0)$
4.25°	65.5°	-	48.0°	-	53.5°
	42.5°	72.3°	33.4°	52.9°	36.6°
	26.0°	38.3°	21.0°	31.2°	22.3°
3.5°	53.5°	-	41.3°	72.8°	45.5°
	35.0°	54°	28°	42.6°	30.4°
	19.5°	25.5°	16°	23.4°	17.3°

It should be noted, however, that there are many similarities in the general shape of the scattering distributions of helium and deuterium. Since the helium scattering can only involve inelastic interactions that arise due to interaction with surface vibrational modes the relative importance of rotational-translational energy transfer and inelastic interaction with surface vibrational modes is difficult to estimate for deuterium molecular beams.

Summary

The results given in Chapter Seven indicate that a great deal of information may be extracted from the angular distributions of low molecular weight gases scattered from chemisorbed layers on metal single crystals. It has been shown that diffraction of molecular beams can give information on surface geometries and thus compliment data obtained from LEED studies. In some instances (e.g. low temperature studies where electron beam desorption effects may be important) it may prove more useful than LEED. The data should also be more susceptible to analysis since the scattering process is confined to the topmost layer of atoms. There also seems little doubt that by studying the details of the scattering distribution information concerning energy transfer processes may be obtained, thereby providing details of the vibrational modes of the surface layer.

In order to achieve the full potential of the technique considerable improvements in the present experimental system are undoubtedly required, but even with the present system more detailed studies could yield useful information. The most critical factor in the experiment is the energy spread within the incident beam. Although the present beam arrangement is an improvement on the oven source used previously in this laboratory, a marked improvement in beam performance would result from the use of substantially higher reservoir pressures. It may well be that the rather broad diffraction peaks observed with the present apparatus obscure a great deal of detail connected with energy transfer processes and that the use of a more monoenergetic beam would allow a quantitative assessment of these energy transfer processes without requiring energy analysis of the scattered beams. Although energy analysis is an extremely desirable feature of any molecular beam system, the increased size and complexity of the apparatus does not, at the present time, justify the rather limited energy analysis that is obtained.

It should, perhaps, be emphasised that although evidence has been presented for considering atom scattering as a technique complimentary to LEED it is fully appreciated that the technique can never replace LEED as the routine technique in establishing surface symmetry properties because of the larger scale apparatus required. LEED clearly has the great advantage of providing rapid direct

display of information and there is considerably less difficulty in providing a monoenergetic incident beam of electrons than one of atoms. It should be noted, however, that in order to extract all the information available in a LEED experiment it is necessary to resort to angular profiles and energy profiles thus making the time-scale of the LEED and atom scattering techniques more comparable.

REFERENCES

Abuaf, N., Anderson, J.B., Andres, R.P., Fenn, J.B. and Miller, D.R., (1966), R.G.D. 5th. Symp. 2, 1317.

Alldredge, G.P., Allen, R.E., and de Wette, F.E., (1971), Phys. Rev., B4, 1682.

Anderson, J.B., (1974),'Molecular Beams and Low Density Gas Dynamics', Ed. Peter P. Wegener. p.1-93. Marcel Decker INC (New York).

Anderson, J.B., Andres, R.P., Fenn, J.B. and Mause, G. (1964), R.G.D. 4th. Symp. 2, 106.

Anderson, J.B., Andres, R.P. and Fenn,J.B., (1965), Advances in Atomic and Molecular Physics, 1, 345.

Anderson, J.B. and Fenn, J.B., (1965), Phys. Fluids, 8, 780.

Armand, G., Dobrzysnski, L., Masri, Y., (1972), J. Vac.Sci. Technol., 9, 705.

Avery, N., (1974), Surface Sci., 41, 533.

Bas, E.B. and Bänninger, U., (1974), Surface Sci., 41, 1.

Bauer, E., (1966), Surface Sci., 5, 152.

Bauer, E. and Engel, T., (1978), Surface Sci., 71, 695.

Becker, E.W. and Bier, K., (1954), Z. Naturforsch., 92, 975.

Beder, E.,(1964) Surface Sci., 1, 242.

Beeby, J.L., (1971), J. Phys. C. (Solid St. Phys.), 4, 1359.

Beeby, J.L., (1972a), J.Phys. C. (Solid St. Phys.), 5, 3438.

Beeby, J.L., (1972b), J.Phys. C. (Solid St. Phys.), 5, 3457.

Bernasek, S.L. and Staudt, G.E., (1976), J. Catal., 45, 372.

Bird, G.A., (1970), AIAA, 8, 1908.

Bledsoe, J.R. and Fisher, S.S., (1974), Surface Sci., 46, 129.

Boato, G., Cantini, P. and Mattera, L., (1974), Japan. J. Appl. Phys. Suppl.2, Part 2, 553.

Boato, G., Cantini, P. and Mattera, L., (1976b), Surface Sci., 55, 141.

Boato, G., Cantini, P. and Taturek, R., (1976b), J. Phys. F.(Metal Phys.), 6, L237.

Brook, J.W. and Oman, R.A., (1964), R.G.D. 4th. Symp., 1, 125.

Buchholz, J.C., Wang, G-C. and Lagally, M.G., (1975), Surface Sci., 49, 508.

Cabrera, N., Celli, V., Goodman, F.O. and Manson, R., (1970), Surface Sci., 19, 67.

Chappell, R.,(1971), Ph.D. Thesis, University of London.

Chung, M.F. and Jenkins, L.H., (1970), Surface Sci., 22, 479.

Coad, J.P. and Riviere, J.C., (1971), Surface Sci., 25, 607.

Chow, H. and Thompson, E.D., (1976a), Surface Sci., 54, 269.

Chow, H. and Thompson, E.D., (1976b), Surface Sci., 59, 225.

Comsa, G., Comsa, G.H., and Fremererey, I.K., (1974), Z. Naturforsch, 29a, 189.

Duke, C., (1974), Advances in Chemical Physics, XXVII, 1.

Engel, T., Niehaus, H. and Bauer, E., (1975), Surface Sci., 52, 237.

Estermann, I. and Stern,O. (1930), Z. Physik, 61 95.

Estermann, I., Frisch, R. and Stern,O. (1931), Z. Physik, 73, 348.

Evans, E. and Mills, D.L., (1972), Phys. Rev., B5, 4126.

Fenn, J.B. and Deckers, J., (1963), R.G.D. 3rd. Symp., 1, 516.

Fisher, S.S. and Bledsoe, J.R., (1972), J. Vac. Sci. Technol., 9, 814.

Fleundy, M.A.D. and Lawley, K.P., (1973) in 'Chemical Applications of Molecular Beam Scattering', Chapman and Hall.

Frank, H., Hoinkes, H. and Wilsch, H., (1977), Surface Sci., 64, 362.

Frisch, R. and Stern,O., (1933), Z. Physik, 84, 1930.

Frotzheim, H., Ibach, H. and Lehwald, S., (1976), Phys. Rev. Lett., 36, 1549.

Garcia, N., (1976), Phys. Rev. Letters, 37, 912.

Garibaldi, U., Levi, A.C., Spandini, R. and Tommei, G.E., (1975), Surface Sci., 48, 649.

Goodman, F.O., (1971), Surface Sci., 24, 667.

Goodman, F.O., (1974), Surface Sci., 46, 118.

Goodman, F.O., (1976), J. Chem. Phys., 64, 1051.

Goodman, F.O., (1977), Surface Sci., 65, 37.

Goodman, F.O. and Wachman, H.Y., (1976), 'Dynamics of Gas Surface Scattering' (Academic Press, New York).

Goodman, F.O. and Tan, W.K., (1973), J. Chem. Phys., 59, 1805.

Haas, T.W., Grant, J.T. and Dooley, G.J. III, (1972a), in 'Adsorption Desorption Phenomena', Ed. F. Ricca (Academic Press), p.359.

Hamel, B.B. and Willis, D.R., (1966), Phys. Fluids, 9, 829.

Hayward, D.O. and Walters, M., (1974), Proc. 2nd Int. Conf. on Solid Surfaces (1974), Japan J. Appl. Phys. Suppl. 2, Part 2 (1974), 587.

Horne, J.M. and Miller, D.R., (1977), Surface Sci., 66, 365.

Ho, W., Willis, R.F. and Plummer, E.W., (1978), Phys. Rev.Lett., 40, 1463.

Howsmon, A.J., (1966), R.G.D. 4th. Symp. 2, 417.

Howsmon, A.J.,(1967), R.G.D. 5th. Symp. 1, 67.

Ibach, H.,(1977), Surface Science, 66, 56.

Jackson, J.M. and Howarth, A., (1933), Proc. Roy. Soc. (LONDON), A142, 447.

Johnson, T.H. (1928), Phys. Rev., 31, 103.

Johnson, T.H., (1930), Phys. Rev., 35, 650.

Johnson, T.H., (1931), Phys. Rev., 37, 847.

Joyner, R.W., Rickman, J. and Roberts, M.W., (1975), Surface Sci., 39, 445.

Kantrowitz, A. and Grey, J., (1951), Rev. Sci. Instru., 22, 328.

Kittel, C., (1971), 'Introduction to Solid State Physics', 4th Edition (Wiley, New York).

Kristiakowsky, G.B., and Slichter, W.P. (1951), Rev. Sci. Instru., 22, 333.

Lapujoulade, J. and Lejay, Y. (1977), Surface Sci., 69, 354.

Lennard-Jones, J.E. and Devonshire, A.F., (1936), Nature, 137, 1969.

Lennard-Jones, J.E. and Devonshire, A.F., (1937), Proc. Roy. Soc., (LONDON), A158, 253.

Liva, M.P. and Frankl, D.R., (1976), Surface Sci., 59, 643.

Mason, B.F. and Williams, B.R., (1972), J. Chem. Phys., 57, 872.

Mason, B.F. and Williams, B.R., (1974), Surface Sci., 45, 141.

Mason, B.F. and Williams, B.R., (1978), Surface Sci., 77, 385.

Mazumdar, A.R. and Wassmuth, H.W., (1972), Surface Sci., 30, 617.

Merrill, R.P. and Smith, R.L., (1970), J. Chem. Phys., 52, 5861.

McLure, J.D., (1970), J. Chem. Phys., 52 2712.

Miller, D.R. and Andres, R.P., (1967), J. Chem. Phys., 46, 3418.

Moran, J.P., (1970), AIAA, 8, 539.

O'Keefe, D.R., Smith, J.N. Jnr., Palmer, R.L. and Saltzburg, H., (1970a), J. Chem. Phys., 52, 4447.

O'Keefe, D.R., Smith, J.N. Jnr., Palmer, R.L. and Saltzburg, H., (1970b), Surface Sci., 20, 27.

Owen, P.L. and Thornhill, C.K., (1948), Aeronautical Research Council, (UK), R&M No: 2616.

Palmer, R.L., Smith, J.N. Jnr., Saltzburg, H. and O'Keefe, D.R., (1970), J. Chem. Phys., 53, 1666.

Pendry, J.R., (1974) 'Low Energy Electron Diffraction' Academic Press, New York.

Redhead, P.A., Hobson, J.P. and Kornelsen, E.V., (1968), The Physical Basis of Ultra High Vacuum., London, Chapman and Hall.

Rowe, G. and Ehrlich, G., (1975), J. Chem. Phys., 63, 4648.

Roundy, V. and Mills, D.L., (1972), Phys. Rev. B5, 1347.

Saltzburg, H. and Smith, J.N. Jnr., (1966), J. Chem. Phys., 45, 2175.

Sau, R. and Merrill, R.P., (1973), Surface Sci., 34, 268.

Scott,J.E.and Phipps,J.A.(1966), 5th RGD, Vol. 2, 1337.

Shapiro, A.H.,(1953) in 'The Dynamics and Thermodynamics of Compressible Fluid Flow', The Rolald Press Co., (New York).

Smith, J.N. Jnr., O'Keefe, D.R. and Palmer, R.L., J. Chem. Phys., 52, (1970), 315,

Smith, J.N. Jnr., Palmer, R.L., and O'Keefe, D.R., J. Chem. Phys., 55, (1971), 4572.

Smith, J.N. Jnr., (1973), Surface Sci., 34, 613.

Somojai, G.A. and Brumbach, S.B., (1974), CRC Critical Rev.in Sol. State. Sci., 4, 429.

Stern,R.M.,(1964), Appl. Phys. Letters, 5, 218.

Subbaras,R.B. and Miller D.R., (1972), J. Vac. Sci. Technol., 9, 808.

Szmerska, I. and Lipska, M., (1976), J. Catal., 41, 107.

Szmerska, I. and Lipska, M. (1977), J. Catal., 47, 144.

Tendulkar, D.V. and Stickney, R.E.,(1971), Surface Sci., 21, 516.

Thompson, P.A., (1972), Compressible-Fluid Dynamics, (McGraw-Hill, New York).

Toennies, J.P., (1974), Appl. Phys., 3, 91.

Tong, S.Y., (1975), Prog. in Surface Science, 7, 1.

Tsuchida, A. (1969), Surface Science, 14, 375.

Walters, M. (1973), Ph.D. Thesis, University of London.

Weinberg, W.H. and Merrill, R.P., (1972a), J. Chem. Phys., 56, 2881.

Weinberg, W.H. and Merrill, R.P., (1972b), J. Chem. Phys., 56, 2893.

Williams, B.R., (1971a), J. Chem. Phys., 55, 1315.

Williams, B.R., (1971b), J. Chem. Phys., 55, 3220.

Wolken, G. Jnr., (1973), J. Chem. Phys., 58, 3047.

Wolken, G. Jnr., (1974), J. Chem. Phys., 61, 456.

Wood, B., Mason, B.F. and Williams, B.R., (1974), J. Chem. Phys., 61, 1435.

Yamamoto, S. and Stickney, R.E., (1967), J. Chem. Phys., 47, 1091.

In the above references R.G.D. has been used as an abbreviation for Rarefied Gas Dynamics.